Design, characterization and application of layered double hydroxide-based colloidal systems

PhD Thesis

Zoltán Somosi

SUPERVISORS: Dr. István Pálinkó

Dr. István Szilágyi

Doctoral School of Chemistry

Department of Physical Chemistry and Materials Science

MTA-SZTE 'Momentum' Biocolloids Research Group

Faculty of Science and Informatics

University of Szeged

Szeged

2021

Table of contents

1. Introduction 6

2. Literature overview 8

2.1. Layered Double Hydroxides 8

2.2. Preparation of LDH 10

2.2.1. Coprecipitation method 10

2.2.2. Rehydration method 11

2.2.3. Preparation of porous LDH materials 11

2.3. Colloids 12

2.3.1. Charging and aggregation 12

2.3.2. Polyelectrolytes 14

2.3.3. LDH colloids 15

2.4. Applications of LDH 15

2.4.1. LDH-based antioxidants 16

2.4.1.1. Oxidative stress and antioxidants 16

2.4.1.2. LDH-based antioxidants 18

2.4.2. Wastewater treatment 20

3. Aim of the study 22

4. Experimental 23

4.1 Materials 23

4.2 Preparation of bare LDH 24

4.3. Preparation of LDH-PSS-PDADMAC hybrid 25

4.4. Preparation of PSS-Cu(Bpy)$_2$-PDADMAC-Fe(Cit)$_2$ 25

4.5. Preparation of mesoporous LDH 25

4.7. Measurement techniques 28

4.7.1. XRD 28

4.7.2. Spectroscopy 28

4.7.3. BET (Brunauer-Emmett-Teller) 29

4.7.4. Microscopy 29

4.7.5. Electrophoretic mobility 29

4.7.6. Dynamic light scattering 30

4.7.7. Adsorption experiments 31

4.7.8. Antioxidant assays 31
4.7.9. Sedimentation experiments 32
5. Results 33
5.1. LDH-polyelectrolyte bilayer hybrid 33
5.1.1. Characterization of substrate LDH 33
5.1.2. PSS layer 36
5.1.3. PDADMAC layer 39
5.2. Antioxidant composite material 42
5.2.1. [Cu(Bpy)$_2$] layer 42
5.2.2. PDADMAC layer 43
5.2.3. [Fe(Cit)$_2$] layer 44
5.2.4. Salt-induced aggregation 46
5.2.5. Characterization of the LDH-PSS-Cu(Bpy)2-PDADMAC-Fe(Cit)2 composite 47
5.2.5.1. Characterization by SEM 47
5.2.5.2. Electron paramagnetic resonance spectroscopy 48
5.2.5.3. Antioxidant activity 50
5.3. Hierarchically ordered mesoporous LDH 53
5.3.1. Characterization 53
5.3.1.1. Stability of SDS-LDH dispersions 53
5.3.1.2. XRD study 56
5.3.1.3. Characterization by IR 58
5.3.1.4. Electron microscopy investigation 60
5.3.1.5. Porosity of the LDHs 62
5.3.2. Removal of anions from aqueous samples 65
5.4. Wastewater treatment with LDH colloids 71
5.4.1. Characterization 71
5.4.2. Separation of LDH materials by flocculation agents 75
5.4.3. Sedimentation by dilution 77
6. Conclusions 81
7. Acknowledgement 83
8. References 84
9. Summary 94
10. Tartalmi összefoglaló 98

Abbreviations

ASP – Adsorption Saturation Plateau

BET theory – Brunauer–Emmett–Teller theory

CCC – Critical Coagulation Concentration

CMC – Critical Micelle Concentration

CSIRO – Commonwealth Scientific and Industrial Research Organisation

CUPRAC – CUPric Reducing Antioxidant Capacity

DLS – Dynamic Light Scattering

DLVO theory – Derjaguin–Landau–Verwey–Overbeek theory

DPPH – 2,2-diphenyl-1-picrylhydrazyl

DXS – Dextran-Sulfate

EDX – Energy-Dispersive X-ray spectroscopy

EPM – Electrophoretic Mobility

EPR – Electron Paramagnetic Resonance

IEP – Isoelectric Point

IR – Infrared Spectroscopy

LDH – Layered Double Hydroxide

LDO – Layered Double Oxide

PDADMAC – Poly(diallyldimethylammonium chloride)

PSS – Poly(sodium 4-styrenesulfonate)

ROS – Reactive Oxygen Species

SDS – Sodium Dodecyl Sulfate

SEM – Scanning Electron Microscopy

SOD – Superoxide Dismutase

TEM – Transmission Electron Microscopy

UV-Vis – Ultraviolet–Visible

XRD – X-ray Diffraction

Structure of organic compounds

Poly(sodium 4-styrenesulfonate) (PSS)

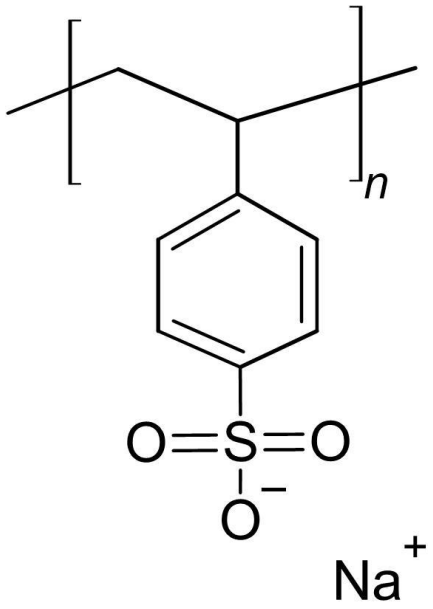

Poly(diallyldimethylammonium chloride)

(PDADMAC)

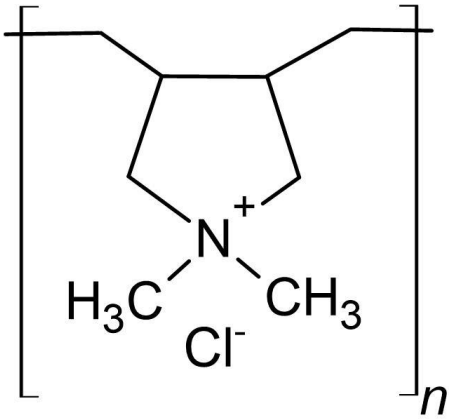

Dextran-Sulfate (DXS)

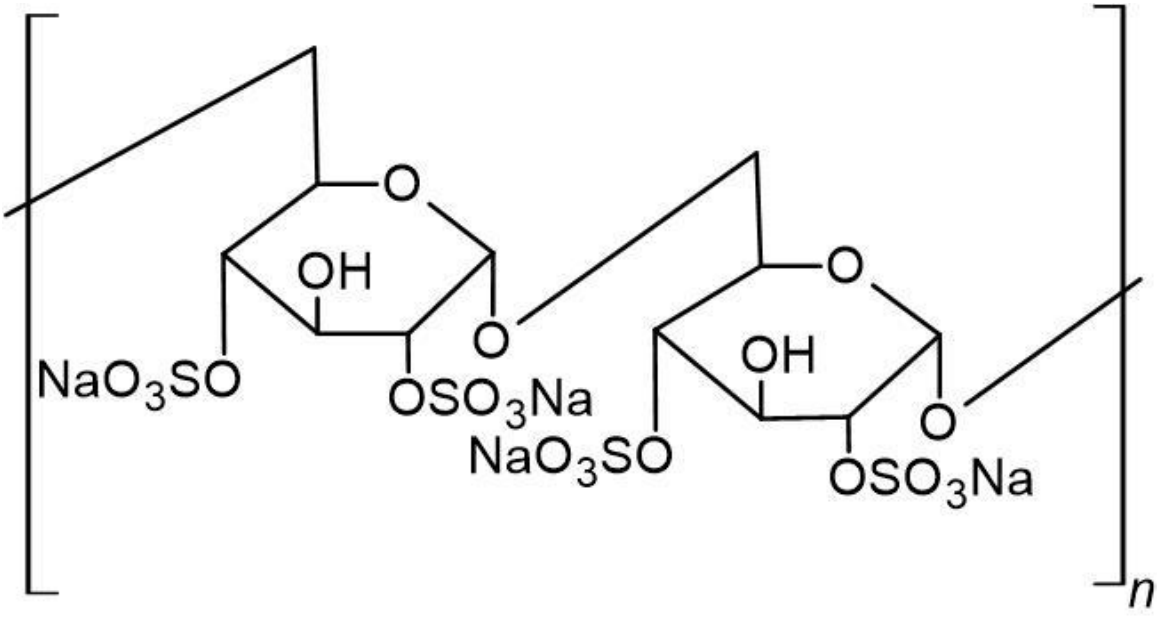

Sodium Dodecyl Sulfate (SDS)

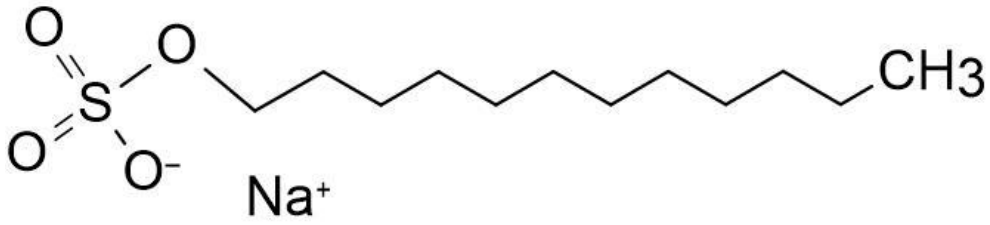

1. Introduction

Colloidal state exists when molecules in a medium have at least one dimension between approximately 1 nm and 1 μm, or that in system discontinuities are found at distances of this order of magnitude. Colloidal dispersions play a pivotal role in various industrial fields and are in the interest of researchers for a long time. Dispersed particle systems are present for instance in the manufacturing of cosmetics or textiles, the preparation of pharmaceutical products and even in wastewater treatment processes. The colloidal stability of such dispersions is crucial, particle aggregation must be controlled in order to achieve the desired properties.

The material discussed in the present dissertation is layered double hydroxide (LDH), a naturally occurring anionic clay. The lamellar structure of the material is composed of metal hydroxide layers of positive charge and interlayer space with charge compensating hydrated anions. LDHs are applied in various fields due to the low cost and ease of synthesis, the high variability in structure and biocompatibility.

Layered double hydroxide colloids are present in many different research and applications. Accordingly, during applying LDH colloids in drug or gene delivery, the carried compound is either transferred in the interlayer space or adsorbed on the outer surface of the particles. For instance, LDHs of intercalated or adsorbed biomolecules such as enzymes or nucleic acids were in the focus of research groups dealing with various biomedical therapies and/or prevention of diseases. Tuning colloidal properties in this case is crucial to successfully apply these materials in living organisms.

In case of catalysis, where LDH may act as catalyst or catalyst support, both the interlayer space and outer surface can be utilized. Colloidal properties play an important role since aggregated particles lose active site and will be less efficient in the catalytic process, therefore, stability of the system is a key parameter to maintain.

Due to being one of the few natural materials possessing positive structural charge, LDH is a promising candidate as adsorbent for various anionic compounds. Thus, there is an increasing number of studies concerned with the development of LDH-based composite colloids applied in wastewater treatments, as adsorbents for contaminants. In these works, the destabilization of the colloidal system is the goal to aggregate (or flocculate) the particles for easier separation of the adsorbent leading to subsequent water remediation. Due to the high ionic (usually metals and inorganic anions) content of some wastewaters, *in situ* preparation of LDH colloid in the

wastewater is also possible giving rise to even more efficient contaminant removal. Another considerable topic is the usage of LDH colloids after modification of these materials by intercalation, surface modification or templating. The latter one can lead to more defined pores with high specific surface area, which are advantageous for specific and efficient ion adsorption, while the low cost of material production making it a promising candidate for water remediation even at larger scales.

The above examples indicate the importance of colloidal stability in various LDH applications. Therefore, systematic studies on LDH colloids are needed and this topic attracts widespread contemporary interest in the scientific communities. Previous pioneering works mostly characterized LDH colloids in a qualitative fashion, however, some recent contributions also reported aggregation rates and surface charge parameters determined with good precision. Due to their irregular shape and various compositions, it is challenging to predict the behaviour of LDHs in different colloid systems, therefore, comprehensive studied must be carried out prior to their applications.

In the present thesis, LDH particles are applied in aqueous colloidal dispersions. First, LDH nanoparticles were synthetised and functionalized to develop antioxidant composites of high colloidal, structural and functional stability. Second, the effect of surfactant adsorption was investigated on LDH particles considering the charging and aggregation properties, which were key features to synthesize mesoporous LDH materials used for removal of toxic anions. Third, *in situ* synthesized LDH samples were used in water remediation processes for mine wastewaters of high ionic content. The LDH particles used in these applications were fully characterized in both dispersions and solid states by numerous experimental techniques and the structure-efficiency relations were revealed based on these findings. The antioxidant activities and the anion adsorption capacities were compared to previously reported systems.

2. Literature overview

2.1. Layered Double Hydroxides

Layered double hydroxides (LDHs) are anionic clays with lamellar structure. The composition of LDH can be various and it can be also found in nature. The first discovered LDH was hydrotalcite in 1842, but it's chemical composition was only defined in 1915 by Ernesto Manasse as $Mg_6Al_2(OH)_{16}(CO_3)\times 4\ H_2O$.[1] Since the first discovered LDH was the hydrotalcite, the group of LDH-like materials are commonly named in this way. Their structure is similar to another mineral called brucite ($MgOH_2$) owning the same lamellar structure, in which Mg(II) ions are coordinated by OH^- ions in an octahedral fashion. This geometry is valid also in case of LDH materials.[2] The charge of the LDH layers develops as follows. In the case of brucite, the layers charge is neutral, but for LDHs/hydrotalcites, partial substitution of the divalent metal ions for trivalent ions leads to a positive net charge in the layers. This charge is compensated by anions in the interlayer area (Figure 1).[3] The generic composition of a typical LDH composed of divalent and trivalent metal cations with the consideration of intercalated anions being hydrated is the following:

$$[M^{2+}_{1-x}M^{3+}_{x}(OH)_2][A^{n-}_{x/n}\times m\ H_2O],\ 0< x< 1$$

The ratio of the divalent and the trivalent ions is limited, too high ratio of trivalent cations leads to the electrostatic destabilization of the layers and low ratio gives rise to contamination.[4] The +2 and +3 oxidation state metal ions are not the only possible ones to build-up an LDH compound. For instance, Li^+ as the only monovalent ion and various +4, +5 or even +6 oxidation state metal ions can form LDH too, once appropriate preparation methods is used.[5] +4 oxidation state Zr ion was substituted into ZnAl/MgAl-LDH[6] and from +6 oxidation state molybdenum CoMo-LDH was prepared via coprecipitation method.[7]

Among the composition, the structural feature of LDHs is an interesting topic of research and especially the morphology can be tuned during synthesis. From simple templating of the LDH material leading to hierarchical porous materials[8], through the development of LDH-based spherical architectures[9] or core-shell LDH-based composites[10] to flower-like structures,[11,12] a wide range of morphologies was achieved via different synthesis and treatment methods to meet the requirements in the desired applications.

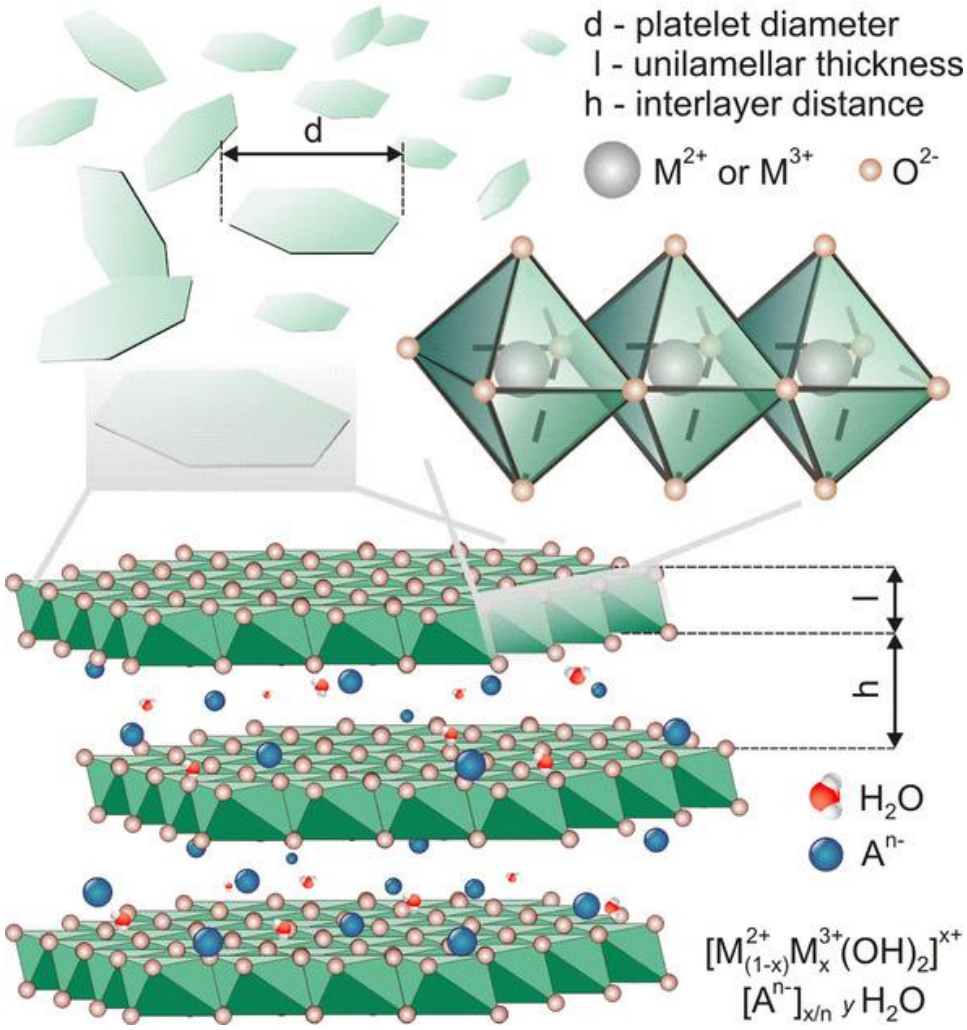

Figure 1. Schematic structure of layered double hydroxide.[13]

In the interlayer space, due to the positive charge of the layers, charge compensating anions can be found. Such an intercalated anions can be replaced by various negatively charged compounds. Different anions show different affinity to the layers, this can be described partly with the Hofmeister series.[14] Briefly, anions of higher valence or the ones, which can make hydrogen bonds with the layers are attached stronger as follows:

$$CO_3^{2-} >> SO_4^{2-} >> OH^- > F^- > Cl^- > Br^- > ClO_4^- > NO_3^- > I^-$$

Carbonate is one of the strongest adsorbing anion, it's presence can be problematic in many processes and it's removal from the layers can only be carried out with special techniques.[15] Accordingly, preparation of most LDHs is carried out in inert atmosphere to avoid the dissolution of the carbon dioxide from the air under the favourable basic conditions present during the synthesis, as discussed below.

Upon heating, the LDH loses water first, which is the water adsorbed on the outer surface. Reaching 400-500 °C, it loses more water by breaking up the chemical bonds of hydroxides leading to an amorphous mixed metal oxide, called layered double oxide (LDO).[16] This amorphous material can be reversed into LDH with the rehydration process utilizing the so-called 'memory effect'.[17] At higher temperatures between 600-1000 °C the LDH turns into a spinel phase.[18] This cannot be rehydrated like LDOs, no 'memory effect' exists anymore. Such spinel can lead to the formation of various nanostructures composed of different metals and can be used in catalysis due to the large amount of metal centers.[18]

2.2. Preparation of LDH

The preparation of LDH can be performed through various methods. These methods may lead to a huge variety of LDHs of different compositions, particle sizes, shapes, materials properties, yielding etc. Detailed description will only be given in case of the preparation techniques used in our work and other unrelated methods will not be discussed. An overall enumeration of the synthesis methods can be given as follows: coprecipitation method,[19] hydrothermal synthesis,[20] sol-gel method,[21] urea hydrolysis,[22] mechanochemical synthesis[23] and electrochemical synthesis.[24]

2.2.1. Coprecipitation method

The most common and simple way of LDH synthesis is the coprecipitation method. During this process, the solution of mixed of metal salts are added to a basic solution (generally the pH is set with NaOH or Na_2CO_3) leading to the formation of the LDH. The properties of the product depend on the temperature and the pH during the precipitation. The speed of the addition of the metal salt solutions to the basic solution is important as well. The stirring time after the reaction and temperature during that also play a role in the 'aging' of the LDH, which tunes the final properties.[25] The speed of the pouring of the solutions is a primary factor. If this process is slow, performed in a dropwise fashion, the nucleation process is also slow, the LDH particles are larger and the degree of crystallinity is higher. If the process is quick, it is called the flash coprecipitation method. The synthesized crystallites in this case are smaller sized, have lower degree of crystallinity and possess the most advantageous colloid features such as moderate polydispersity.[5]

The size and crystallinity of the product can be tuned with post treatments. Aging treatment consisting of stirring at elevated temperature for different times can lead to better crystallinity. Post-hydrothermal treatment can further improve the polydispersity.[20] Lyophilization is also a possible post-treatment method, it can help tuning the size of the particles.[26] Anions are being

present in the solution along with the mixed salts and the base leading to their intercalation between the layers. The nature of the interlamellar space can be influenced by the overall concentration of the desired anion in the solution as well as by their affinity to the LDH surface. The intercalated anions enable the fine tuning of the interlayer distance.[27]

2.2.2. Rehydration method

Dehydration-rehydration method is commonly used one to prepare LDHs. Layered double hydroxides are calcined throughout the process leading to mixed metal oxides and the structure is restored by hydration utilising the earlier mentioned 'memory effect'. During the rehydration process, the properties of the LDH can be tuned, the addition of other solvents, time, temperature can lead to different crystallinity, morphology and surface area.[28] Also the interlayer anion can be changed if the LDO is rehydrated in an aqueous salt solution containing the desired anion since during the rehydration process, the calcined layered structure is exposed to water and anions. Inert nitrogen atmosphere is a must in this procedure due to the high sensitivity of the layers to atmospheric carbon dioxide.[5]

2.2.3. Preparation of porous LDH materials

The porosity of the LDH can be an important aspect during the synthesis. Porous LDHs are used in various fields including wastewater treatment, catalytic reaction, energy storage and others. The final porosity and pore characteristics are important parameters, larger active sites and higher selectivity can be achieved with the proper synthesis of the material.[16]

Numerous methods are present in the literature to develop porous LDH compounds. Three general methods are the soft, hard and self-sacrificial templating. In case of soft templating, organic materials are used such as surfactants or block copolymers leading to well-defined mesoporous structures.[29] The formation of this porous substance is a result of interactions between the soft templating material and inorganic species, what builds up the mesoporous final product. Zhang et al. prepared a hierarchical three-dimensional LDH in a one-step soft-template synthesis with sodium dodecyl sulfate (SDS) for removal of ionic dyes.[30] Hard templating uses a solid material as a template such as polymers, silica or carbon derivatives. An exciting study considering hard templating was carried out by Tokudome et al. In their study, the synthesis of LDH nanoclusters was carried out in a one-pot route. Combining this method with hard templating with polystyrene spheres, they could produce well-defined microporous structure with a pore diameter of 80 nm.[31] Hard templating has some advantages compared to soft templating. For instance, it does not need

controlled conditions, such as control of hydrolysis and condensation of guest species during the templating process. One can even better control the final product's porosity.[29] Considerable disadvantages are smaller number of available hard templates and the procedure is more complicated due to the removal of the hard template after the reaction, which usually happens in multiple steps. Self-sacrificial method is advantageous in tuning the materials porosity, pore size distribution and pore morphology with the appropriate choice of the conditions and the sacrificial template.[32] Moreover in self-sacrificial templating processes, the removal of the template is not needed resulting in a less complicated protocol than the other two. One of the first advances in this field was carried out by Géraud et al. with 'inverse opal' method developing three-dimensional macroporous LDH using polystyrene colloidal crystal as the template for self-assembly.[33]

2.3. Colloids

Colloidal systems and their stability play an important role during industrial, environmental or biomedical applications of LDHs. While in wastewater treatment unstable systems are desired for sedimentation, in drug delivery, stable non-aggregating systems are advantageous to achieve high efficiency. In catalytic processes both stabilization and destabilization can be desired, as in stable systems one prevents the loss of active sites, while destabilization of the system can lead to the removal of the catalyst after the reaction is terminated.

2.3.1. Charging and aggregation

The theoretical basics of processes taken place in colloidal systems are important to understand the present work. First, the theory developed by Derjaguin, Landau, Vervey, and Overbeek (also known as DLVO theory) is a cornerstone in colloid science.[34,35] The basis of the theory can be used to predict particle aggregation and stability in colloidal dispersions through describing interparticle forces concerning attractive van der Waals forces and repulsive electrical double layer forces. The theory treats separately the van der Waals forces and electrostatic double layer forces but the two types of interaction can be superimposed at each distance to calculate the force interacting between the particles. The theory was originally developed for identical particles (homoaggregation) but with appropriate extensions, asymmetric systems and heteroaggregation can also be interpreted.[36] The van der Waals forces are weak, distance dependent forces between atoms, molecules or particles. They are always present and originating from the interactions of rotating and fluctuating dipoles. On the other hand, there are electrostatic double layer forces responsible for interparticle repulsion for charged particles (Figure 2).

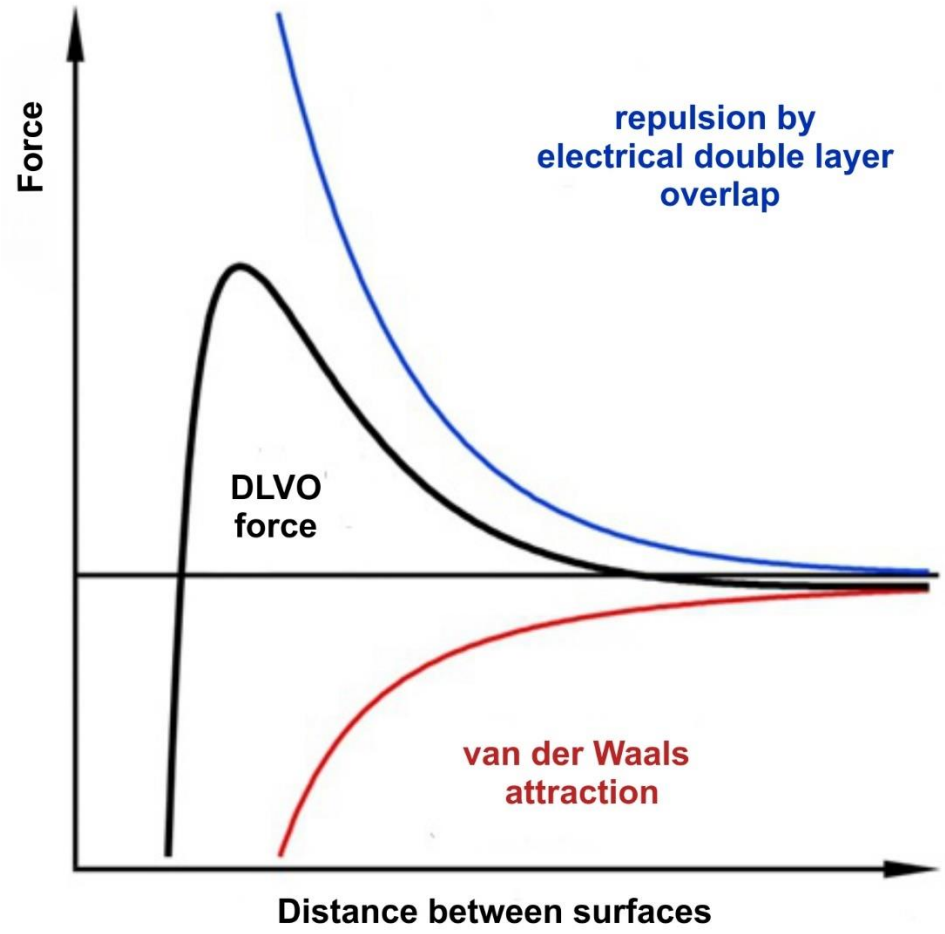

Figure 2. Presentation of the surface forces described by the DLVO theory.

The charge of the surface can originate from the dissociation of surface functional groups, structural charge (like LDH) and by the adsorption of charged species (e.g., simple ions or larger molecules). This latter one is considered the first so called Stern layer. It can be also divided into inner and outer Helmholtz planes. Near the layer, there are counterions compensating and screening the charge of this first layer. Unlike the Stern layer, where charges are tightly bound, in case of the second layer the distribution of charges are loosely associated and called diffuse layer building up the electrical double layer in this way. The electrical double layers repel each other upon approach of two particles. The thickness of the electrical double layer can be estimated by the Debye length and depends on the ion concentration in the solution.[37] Increasing the ion concentration, the electrical double layer shrinks. The overall charge of the particles can be described with the zeta potential, which is the potential at distance from the surface, where a hydrodynamically stagnant

layer composed of ions and solvent molecules exist. This can be measured directly, but appropriate theoretical models must be used for data interpretation.

Particles approaching each other in dispersions due to Brownian motion must overcome a potential energy barrier in order to aggregate. This is only possible if repulsive double layer forces are not stronger than attractive van der Waals forces. To achieve this situation, we can manipulate the charge of the Stern layer or increase the ionic strength in the dispersion leading to the decay of the electrical double layer forces. The manipulation of the Stern layer may occur through adsorbing species like polyelectrolytes.[38] Indeed, surface charge has a really important role in colloidal stability, high charges lead to stabilizing strong electrical double layer repulsion, while neutralizing the charge leads to unstable dispersions. Tuning the amount of charged adsorbents on the surface or changing the ionic strength can lead to dispersions of different stabilities. Increasing the ionic strength leads to the shifting of the dispersion from the stable regime to slow aggregation and at high concentrations unstable dispersions and fast aggregation take place.[39] These regimes are usually separated with the so-called critical coagulation concentration (CCC).[40] Fast aggregation is only diffusion controlled meaning every collision between the particles leads to aggregate formation. Aggregating dispersions can be described with the use of stability ratio, which can be measured by different techniques including light scattering.[41]

2.3.2. Polyelectrolytes

Polyelectrolytes are commonly used materials to tune aggregation processes in particle dispersions. They are macromolecules with repeating units possessing a charged group. In aqueous solutions, these groups can be ionized leading to the formation of charged polymers. Polyelectrolytes can be classified as cationic or anionic according to the sign of the carried charge and can be divided into two groups, namely, strong and weak ones. Strong polyelectrolytes are fully dissociated at a wild scale of pH, while weak polyelectrolytes are not fully charged in solution and their line charge density can be modified by the pH.[42] Another way to differ polyelectrolytes is their origin, there are both synthetic and natural ones. Nucleic acids, proteins and some polysaccharides are good representations of natural polyelectrolytes.[43]

Polyelectrolytes have various applications. For instance, multilayers and thin films attract the interest of many research groups.[44] They can be composed with layer-by-layer technique. This process takes place on a suitable substrate with sequential adsorption of positively and negatively charged polyelectrolytes from solutions allowing controlled build up. These films and coatings can

have the benefit of anti-corrosive and[45] anti-reflective properties[46] as well as controlled drug release[47] leading to various applications.

Adsorption of polyelectrolytes on oppositely charged particles occurs due to electrostatic attraction, hydrogen bonding, ion correlation and entropy effects. There are many attachment points between the surface and the polyelectrolyte segments. The possibility of all segments detaching at the same time is highly unlikely and for this reason, the adsorption is considered irreversible in most of the cases.[48] Tuning the charge of particles in colloidal suspensions can lead to both stabilizing and destabilizing effects depending on the applied polyelectrolyte dose. Stable colloidal dispersions are required for industrial and medical processes. Destabilization and flocculation play an important role in wastewater treatment for instance.[49] The destabilization occurs due to charge neutralization, bridging effects, depletion forces and polyelectrolyte patching. During bridging, long polyelectrolyte chains form tails and loops on the surface allowing the adsorption on multiple particles. Polyelectrolyte patching is the property of both short and long polyelectrolyte chains adsorbing in an island fashion on particles leading to polyelectrolyte patches on the surface and to aggregation through local charge inversion.[50]

2.3.3. LDH colloids

Due to its importance, LDH colloids were investigated in numerous studies.[51, 52] Colloidal routes are used for a long time to prepare various LDH materials since it is an excellent way to tune the final materials properties.[53] In the last years the interaction between LDH particles and their interaction with different ions and compounds got more and more attention. The ion specific effect on LDH particles was discussed in a comprehensive study considering mono-, di-, tri- and tetravalent ions in a wide range of concentration.[14] A similar study was carried out with LDH-polyelectrolyte systems investigating also the effect of ionic strength on the charging and aggregation of LDH particles, which is essential for further applications.[13] The earlier mentioned polyelectrolyte sequential adsorption method may be applied to LDH particles using as a substrate. This gives rise to adsorption of different species on the surface leading to the development of drug carriers, sensors or catalysts. Furthermore, via covalent linkage, LDH-nucleic acid nanocomposites can be obtained in colloidal system leading to possible gene delivery.

2.4. Applications of LDH

The flexibility in the composition of the layers, the exchangeable interlayer anions, the ease of synthesis, the biocompatibility and the low cost promoted LDH into a widely researched and

applied material in diverse fields such as catalysis, water treatment, energy storage, sensing, drug delivery, flame retardants, corrosion inhibition or development of multifunctional smart-coatings.[24,54] Traditionally, the main point of interest of LDH application is the interlayer space due to the versatility of the possibly intercalated compounds.[55] Nevertheless, we focus here on 2 topics, which are related to the topic of the present dissertation, namely, LDH applications in free radical scavenge and in water remediation.

2.4.1. LDH-based antioxidants

2.4.1.1. Oxidative stress and antioxidants

Oxidative stress is the consequence of the imbalance between production and decomposition of reactive oxygen species (ROS) in the body. Oxidative stress and elevated level of ROS is the result of various factors such as environmental stressors (pollutants, UV light and ionizing radiation), high levels of stress as well as harmful habits (alcoholism and smoking).[56] The presence of free radicals leads to unwanted disorders in living organisms. Generally, radical is an atom, molecule or ion owning an unpaired valence electron. Due to this unpaired electron, they are highly reactive and unstable leading to short lifetimes.[57] The exceptions are some organic radicals that are stable due to effects like delocalization or steric hindrance among others.

ROS can be deduced from the flair for electron acceptability of O_2 being in partially reduced or excited form. They include superoxide, peroxides, hydroxyl radicals and others and play an essential role in our life functioning as signalling molecules in cells and maintaining the normal operation of living creatures. Accordingly, a basal level of ROS is essential for life. However, because of the high reactivity, the elevated level of ROS is toxic and can lead to many problems. Development of various diseases such as different types of cancer, chronic inflammation, neurological disorders and male infertility can be originated from the increased oxidative stress and thus, the high level of ROS.[58] Moreover the presence of these species can lead to reduced-quality commercial products in case of food, textile and cosmetic industries. The increased level of ROS in our life puts the food industry into a challenge to produce products with higher antioxidant content to prevent negative effects of ROS. This can be achieved through antioxidant additives.[59,60, 61] Besides, the cosmetic industry is facing a similar challenge due to the increased UV-light explosion of skin and inflammation problems, novel products are needed there too.[61] Summarily, controlling the level of ROS is crucial in both biomedical and industrial processes.

The regulation of ROS level is naturally carried out by molecular antioxidants (flavonoids, vitamins, etc.) and enzymatic antioxidants (superoxide dismutase, peroxidases, etc.) with the latter ones being way more effective. Molecular antioxidants face the problem of limited solubility in water.[62] Enzymes are highly active and soluble in most cases, however, they are very susceptible to circumstances like pH, temperature or ionic strength, which are negatively affecting their activity during combatting oxidative stress. This makes the application of enzymes as antioxidant additive difficult, especially in the industry.[59, 61]

Various materials were developed by research groups to answer this challenge. Nanomaterials possessing antioxidant activity (nanozymes) or the ones with immobilized natural or artificial enzymes can be successful antioxidants in either biomedical or industrial processes. Nanozymes usually contain redox active metals (iron(III) or manganese(II)), which are responsible for the enzymatic activity. On the other hand, artificial enzymes are constructed of transition metal complexes being similar to the active centre of antioxidant enzymes.[63] Complexes with the appropriate structure can mimic the antioxidant and ROS scavenging abilities of the native antioxidant enzyme.[64,65] Despite these promising properties, there are various drawbacks are present such as tendency for aggregation, toxicity of the nanoparticles or the metal ion leakage of the complexes. Due to these reasons the choice of the suitable nanoparticle support is crucial to develop wildly applicable antioxidant nanomaterials.

Assessing the antioxidant activity of the developed materials is important. Immobilized enzymes can lose their activity during the adsorption process, while proving the antioxidant property of newly developed materials is also necessary. For such reasons, different assays were used to determine the antioxidant activity. One type of assays are enzymatic ones using enzymically generated ROS. A well-known example is the Fridovich method, where superoxide dismutase (SOD) activity can be probed.[66]

The non-enzymatic assays are also possible to perform with free radicals like 2,2-diphenyl-1-picrylhydrazyl (DPPH) or 2,2'-azino-bis(3-ethylbenzthiazoline-6sulfonic acid) ($ABTS^{+}$) which are free radicals, but they can still be reduced by antioxidants to determine their activity.[67] Redox activity of antioxidants can be tested with redox active metal complexes too. The 2,4,6-tris(2-pyridyl)-*s*-triazine ligand with Fe^{3+} centre is the basis of ferric reducing antioxidant power assay (FRAP) and 2,9-dimethyl-1,10-phenanthroline ligand coordinated with Cu^{2+} is the main reagent for cupric reducing antioxidant assay (CUPRAC).[68]

2.4.1.2. LDH-based antioxidants

Layered double hydroxides were widely used as a base for antioxidant materials, where the radical scavenging activity was achieved by intercalating redox active compounds between the layers or adsorbing them on the outer surface.[69] Among the intercalated ones, the mostly applied guest molecules are phenolic compounds like ascorbic acid and gallic acid. Gallate, the anionic form of gallic acid, was intercalated by exfoliation-reassembly process by Choy et al.[70] Kong et. al prepared a MgAl-LDH intercalated with carnosine via ino-exchange method, the obtained material showed remarkably high activity in scavenging of DPPH radicals.[71] Due to the limited solubility, ellagic acid was not in the interest of the scientific community for some time, however, a recent study reports intercalation of this compound into LDH, while maintaining antioxidant activity and improving water solubility. The material showed great activity in DPPH scavenging that could be further improved with the treatment of the ellagic acid-LDH hybrid with organic solvents leading to comparable activity to Trolox, which is a comprehensively used model antioxidant.[72] An interesting concept was the development of LDH-olanzanpine (2-methyl-4-(4-methylpiperazin-1-yl)-10H-thieno[2,3-b][1,5]-benzodiazepine) hybrid. This drug molecule has low solubility, however, it can be used in various pharmaceutical applications like treatment of mental diseases (bipolar disorder or schizophrenia) or brain damage, which are related to oxidative stress. If the substrate was CaAl-LDH for olanzanpine, it showed antioxidant activity in three different antioxidant assays namely with DPPH (40,83%) and nitric oxide (16,73%) radical scavenge. Moreover, as the third assay, inhibition capacity of lipid peroxidation by thiobarbituric acid with a result of 16,73% was demonstrated. These findings could lead to the use of LDHs in the pharmaceutical industry for bipolar disorder and schizophrenia therapy.[73]

The positively charged outer surface of LDH can also be utilized to adsorb antioxidant active materials, but in many cases, surface modification is needed prior immobilization due to the limited colloidal stability of LDH particles and to prevent the loss of antioxidant activity. Immobilization on the outer surface is important since larger molecules cannot be intercalated due to the limited interlayer space. These materials are different in the type of immobilized antioxidant compounds, they can be molecular antioxidants, enzymes or mimicking metal complexes. For instance for metal complex immobilized on LDH, a highly stable antioxidant colloid was developed with Cu^{2+}-histamine complex stabilized by poly(vinylpyridine-b-methacrylic acid) copolymer. The developed material showed high activity in scavenging superoxide radical ions even at higher

temperatures.[74] Hemin was immobilized on CuAl-LDH by Qiao et al. to mimic the active site of HRP. The material showed excellent peroxidase activity in scavenging peroxynitrite radicals ($ONOO^-$). The composite showed higher activity than hemin alone. The reason behind can be the electrostatic attraction between the anionic radical and the LDH particles as well as the π electron donor property of the LDH to the iron centre of hemin (Figure 3). The composite was tested in the reaction between tyrosine and $ONOO^-$ with inhibition up to 80%.[75]

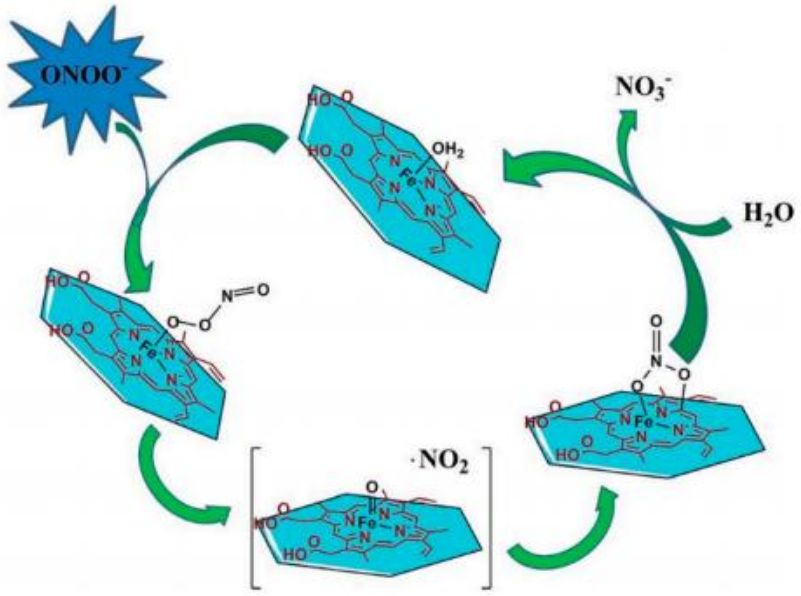

Figure 3. The mechanism of the hemin-LDH hybrid induced isomerization and reduction of ONOO- and scavenging of NO_2.[75]

Horseradish peroxidase (HRP) enzyme was immobilized on MgAl-LDH particles coated by heparin by Pavlovic et al. The developed hybrid owned similar activity to the native HRP, with the advantage of high stability of the composite in aqueous dispersions. Also the adsorption of HRP was strong on the surface due to electrostatic and hydrophobic interactions along with hydrogen bonding preventing the enzyme leakage from the material.[76]

A novel direction in LDH-based antioxidant research is the development of nanozymes. Nanozymes are nanomaterials with enzyme-like properties while possessing improved stability compared to natural enzymes.[77] These enzyme mimicking materials can not only be used in catalytic reactions but also can be incorporated highly sensitive sensor. One of the earliest reported LDH with intrinsic nanozyme activity was published by Zhang et al. The developed CoFe-LDH

nanoplatelets were effective mimetics to peroxidases owing to the activity by the redox active metal ions composing the layers. This was proven with the oxidation of 3,3',5,5'-tetramethylbenzidine in the presence of H_2O_2. The material had efficiency similar to native HRP and also regarding the optimal properties like pH and temperature. The activity regime in H_2O_2 dose was even higher for the LDH material. The developed compound was used as an H_2O_2 and glucose sensor.[78] Another interesting concept was the synthesis and growth of CuAl-LDH on carbon fibers. The developed composite possessed peroxidase mimicking ability making it a promising sensing element material for H_2O_2 and glucose detection.[79]

2.4.2. Wastewater treatment

Hydrotalcite-type materials are often used in treatment of wastewaters of different origin. The application in this field varies in a large scale exploiting different properties of LDH such as composition and structure. The anion exchange capacity is used for the removal of toxic or undesirable anions. The removal of selenate with CaAl-LDH[80] and Zr doped LDH for the removal of phosphate[81] were both exciting progresses in this field. Also complexing agents can be intercalated into the interlayer space for the removal of cations including toxic metal ions. Such interaction is reported in the removal of lead with glutamate intercalated LDH.[82] Surfactant modified LDH can be an appropriate host for the co-intercalation of guest molecules with the interlayer surfactant leading to the possibility to remove different organic species. Lei et al. carried out synthesis of dodecylbenzene sulfonate intercalated ZnAl-LDH with efficient removal of 2,4,6-trichlorophenol from wastewater.[83]

Layered double hydroxide-based nanocomposites and hybrid materials gained considerable interest of many researchers due to their improved ability in removal of hazardous and toxic pollutants. The modified LDH-containing materials showed enhanced adsorption capacities due to various reasons like improved surface area and better stability. Tian et al. developed an epitaxially grown LDH on a natural mineral called vermiculite leading to enhanced Cr(VI) removal due to the hierarchical porous three dimensional framework leading to high surface area and enhanced transfer channels.[84] Also if the LDH is hybridized with magnetic particles, the ease in separation and reusability is a lot better. A great example for this is the study of Shan et al. developing Fe_3O_4/MgAl-LDH composite, what was an effective adsorbent for 3 different red dyes in aqueous dispersions between pH 2-10. After the adsorption process, the adsorbent particles could be easily removed with an external magnet.[85] Various factors can play role in the effectivity of the adsorption

process such as pH, competitive anions, dosage of adsorbent and temperature.[86] These factors must be considered before remediation experiments on wastewaters especially in the case of oxyanions to be removed.[87]

Bioremediation is also a possible way to utilize LDHs. Attaching a bacterium to a solid support can enhance their metabolic activity. Encapsulation of bacteria is also possible into the interlayer space while preserving activity. The immobilization and encapsulation of bacteria Pseudomonas sp. strain ADP was achieved with coprecipitation method leading to LDH bionanocomposites with improved activity in atrazine degradation in both cases.[88,89]

In situ synthesis of LDH from wastewater containing metal ions is an interesting concept. This way the forming of the material consumes some of the pollutants from the wastewater with the removal of the layer forming metal cations and also removing polluting species by intercalation into the interlayer space or surface adsorption on the LDH layers facilitating the further wastewater treatment by these processes.[90] A recent article reports this approach using *in situ* formation of ZnFe-LDH, while efficiently removing As(III) ions from aqueous samples.[91] Literature data concerning wastewater treatment method takes place generally in model systems, there are only few publications using real wastewater systems.[92]

3. Aim of the study

We aimed at the design of LDH particles of different compositions and structures for environmental and antioxidant applications. The systems were fully characterized and used in colloidal dispersions, in which either stabilization or destabilization of the particles were utilized to maximize their efficiency.

First, LDH substrates were synthesized and functionalized with polyelectrolytes and metal complexes of antioxidant activities using the sequential adsorption method. Our goal was also the optimalization of the polyelectrolyte doses and amount of adsorbed of metal complexes to achieve the desired properties such as high colloidal and functional stabilities. The bottom line of these experiments was to build LDH-based novel composites of remarkable antioxidant activity and to probe them in radical scavenging assays to test their efficiency and selectivity. Besides, our purpose was also to clarify the structure-activity relations.

Second, we aimed to gain a better understanding of the role of *in situ* prepared LDHs in wastewater treatment within a cooperative project using mine wastewaters from Australia. Our goals included characterization of the received and synthesized materials as well as working out an economic way to separate the *in situ* formed LDH from the aqueous samples, as they showed high stability preventing water remediation. We aimed to understand the reasons behind the unexpectedly high stability of the system and to optimize the separation methods.

Third, the effect of sodium dodecyl sulfate (SDS) adsorption on the colloidal stability of the LDH systems was comprehensively investigated. Various measurements were carried out to assess aggregation features and surface charge parameters in a wide range of SDS concentrations. Based on the results, the SDS treated LDHs were dehydrated and rehydrated to obtain mesoporous LDHs of high specific surface area. We aimed to characterize the structure and morphology of the novel materials developed. Moreover, anion exchange capacity was determined for toxic anions and compared to existing adsorbents.

With the above studies, our overall goal was to gain a comprehensive knowledge on the applicability of LDH dispersions in different areas, namely, to exploit them as antioxidants and water remediation agents. We also aimed to combine colloid and materials chemistry to get insights in both dispersion and structural properties. These fields were rarely combined in the past and thus, we believe that the findings generated by the doctoral work will attract significant interest in the scientific and technological communities.

4. Experimental

4.1 Materials

The following analytical grade chemicals were used for the experiments without further purification:

- Magnesium(II) chloride hexahydrate ($MgCl_2 \cdot 6H_2O$), VWR International
- Iron(III) chloride hexahydrate ($FeCl_3 \cdot 6H_2O$), VWR International
- 4 M sodium hydroxide solution (NaOH), VWR International
- Tri-sodium citrate dihydrate ($C_6H_5Na_3O_7 \cdot 2H_2O$), VWR International
- Ammonium acetate (NH_4OAc), VWR International
- Trisodium phosphate ($Na_3PO_4 \cdot 12H_2O$), VWR International
- 2,2-diphenyl-1-picrylhydrazyl radical (DPPH), VWR International
- Copper(II) chloride dihydrate ($CuCl_2 \cdot 2H_2O$), VWR International
- 2,9-dimethyl-1,10-phenanthroline (neocuproine), VWR International
- Aluminum(III) chloride hexahydrate ($AlCl_3 \cdot 9H_2O$), Alfa Aesar
- Xanthine ($C_5H_3O_2$), Alfa Aesar
- Dextran sulfate sodium salt ($C_{12}H_{22}O_{25}S_5$, 8 kg/mol), Alfa Aesar
- 2,2'-Dipyridyl (99%) ($C_{10}H_8N_2$), ACROS Organics
- Nitro blue tetrazolium chloride monohydrate ($C_{40}H_{30}Cl_2N_{10}O_6 \cdot H_2O$), ACROS Organics
- Xanthine oxidase from bovine milk, Sigma-Aldrich
- Magnesium(II) nitrate hexahydrate ($Mg(NO_3)_2 \cdot 6H_2O$), Sigma-Aldrich
- Aluminum(III) nitrate nonahydrate ($Al(NO_3)_3 \cdot 9H_2O$), Sigma-Aldrich
- 0.1 M and 3 M sodium hydroxide solutions (NaOH), Sigma-Aldrich
- Sodium dodecyl sulfate ($NaC_{12}H_{25}SO_4$), Sigma-Aldrich
- 96 m/m% ethanol (C_2H_5OH), Sigma-Aldrich
- Potassium dichromate ($K_2Cr_2O_7$), Sigma-Aldrich
- 25 m/m% ammonia solution (NH_4OH), Sigma-Aldrich

- Sodium nitrate ($NaNO_3$), Sigma-Aldrich
- Sodium chloride (NaCl) Sigma-Aldrich
- Poly(sodium 4-styrenesulfonate) $(C_8H_7NaO_3S)_n$, 10 kg/mol), Sigma Aldrich
- 20 weight % aqueous poly(diallyldimethylammonium chloride) (PDADMAC) (275 kg/mol molecular mass)
- Nitrogen (N_2, 99,995%), Messer

All measurements were carried out and samples were prepared with ultrapure water produced by a Puranity TU 3 UV/UF+ (VWR) device. The ultrapure water and the salt solutions were filtered using a Millex syringe filter of 0.1 μm pore size to remove insoluble impurities. The experiments were performed at room temperature unless otherwise indicated.

4.2 Preparation of bare LDH

The substrate particle used for immobilization of metal complexes was Mg_2Al-Cl LDH with narrow particle size distribution. The synthesis was carried out with the flash coprecipitation method.[93] A solution of mixed metal salts of $MgCl_2$ (0.2 M) and $AlCl_3$ (0.1 M) with a total volume of 10 mL and 60 mL of 0.15 M NaOH solution was prepared. The two solutions were placed in a glovebox being under nitrogen atmosphere to prevent carbonation of the base and the later forming LDH. The mixed salt solution was quickly added to the vigorously stirred NaOH solution and the pristine LDH was formed. The obtained raw LDH was kept under N_2 atmosphere for 30 minutes, while was continuously stirred. After this, the LDH slurry was separated with centrifugation and washed 5 times with water. The LDH was dispersed into 50 mL water, sonicated for 10 minutes in an ultrasonic bath and transferred into a stainless-steel autoclave with a Teflon lining (Col-IntTech, Irmo, SC, USA). An oven was preheated to 120 °C and the autoclave was placed in it for 24 hours for a post hydrothermal treatment. After the removal of the autoclave from the oven and the cool down to room temperature, the LDH dispersion was centrifuged and washed 5 times again with water. The obtained dispersion was then dried into powder at 40 °C in oven. The powder sample was redispersed into a 10 g/L stock dispersion for further experiments, while some of the powder was kept for solid state characterization.

4.3. Preparation of LDH-PSS-PDADMAC hybrid

On the LDH substrate discussed above, a bilayer polyelectrolyte coating was developed to achieve improved colloidal properties for further processing. Accordingly, 50 μL of 10000 mg/L LDH suspension was dispersed into 2950 μL of water and 50 μL of 0.005 mg/L poly(sodium 4-styrenesulfonate) (PSS) solution. After mixing of the components, the sample was equilibrated overnight. The next day, 1000 mL of 0.005 mg/L poly(diallyldimethylammonium chloride) (PDADMAC) solution was added. The overall concentration in the final composite for the PSS was 100 mg/g and for the PDADMAC was 300 mg/g. These concentrations were selected on the basis of extensive charging and aggregation measurements to optimize the colloidal stability of the systems, as discussed later.

4.4. Preparation of PSS-$Cu(Bpy)_2$-PDADMAC-$Fe(Cit)_2$

On the basis of the previous experiments, a multilayered composite was developed on the LDH particles using polyelectrolytes and metal complexes. The process was similar like in the case of LDH-PSS-PDADMAC. In the first step, 50 μL of 10000 mg/L LDH suspension was dispersed into 2884 μL of water and 1000 μL of 0.005 mg/L PSS. The second layer was $Cu(Bpy)_2$ by adding 33 μL of 15 mM $Cu(Bpy)_2$ solution. The third layer was PDADMAC by adding 1000 μL ml of 0.005 mg/L stock solution. The final layer was $Fe(Cit)_2$ adding 33 μL of 15 mM $Fe(Cit)_2$ solution. The concentrations for the final composite was 100 mg/g for PSS, 0.1 mM for $Cu(Bpy)_2$, for PDADMAC was 100 mg/g and for $Fe(Cit)_2$ was 0.1 mM. In all steps, the samples were equilibrated overnight and the pH of the overall solution was around 7.

4.5. Preparation of mesoporous LDH

MgAl-LDH was prepared by a combined coprecipitation-rehydration method using SDS as sacrificial template. 72 mL of 1.5 M NaOH solution was added drop by drop to 100 mL solution of mixed metal salts containing 0.3 M $MgCl_2$ and 0.1 M $AlCl_3$ at room temperature. The solution was stirred and heated at 60 °C for 12 hours before filtering and washing. The gained LDH was slurry was dispersed in 100 mL of 30 mM SDS solution and stirred for two days at 60 °C to allow the adsorption of the surfactant at pH ~ 8.5. Thereafter, the dispersion was filtered, washed several times and dried. The SDS content of the gained material was removed by calcination at 510 °C for 12 hours and this process resulted in the formation of LDO. Due to the memory effect,[17] the LDH

structure was reconstructed by rehydration, during which the LDO was redispersed in 100 mL of 10 mM NaCl dissolved in a mixture of H_2O, EtOH and 0.015 NaOH with a volume ratio of 85:5:10 under N_2 protection. The slurry was stirred at 60 °C for two days followed by filtration, several washing steps with water and drying in a desiccator under N_2 atmosphere. The final product was named as SDS_3-LDH, SDS_{10}-LDH and SDS_{30}-LDH referring to the used surfactant dose during the synthesis. The mesoporous structure was characterized with various experimental techniques, as discussed later.

4.6. Preparation of *ex* and *in situ* LDH

Three different samples were received from Commonwealth Scientific and Industrial Research Organisation (CSIRO), Australia as part of a cooperation and a fourth one was synthesized in our lab by a slightly modified coprecipitation method.

Sample 1 was prepared in demineralized water with the addition of $Mg(OH)_2$ and $NaAlO_2$ in a 3:1 ratio, dissolved in NaOH at a final pH of 9.7.

Sample 2 was prepared in mine wastewater (pH 4.5, see composition in Table 1). The synthesis occurred by dissolving $NaAlO_2$ in NaOH, which was added to the wastewater sample to reach a final pH of 8.5.

Sample 3 was prepared using the acidic mine water as medium too. The synthesis was the same as in the case of Sample 2 ($NaAlO_2$ dissolved in NaOH) but $Mg(OH)_2$ was also added to the wastewater to induce the LDH formation.

Sample 4 was prepared as follows. $MgCl_2 \cdot 6H_2O$ was dissolved in water followed by the addition of $NaAlO_2$ dissolved in NaOH while being stirred. To set the final pH to 9.8, 1 M NaOH was added dropwise. The dispersion was then aged at 80°C for two days to facilitate higher crystallinity, centrifuged and washed with demineralized water. Finally, the 3:1 Mg:Al molar ratio LDH was obtained.

Overall sample 1 and 4 were prepared by an *ex situ* method, while sample 2 and 3 were prepared in an *in situ* way. All of the obtained materials were stored in 10 g/L stock dispersions. In further experiments, they were diluted with electrolyte solutions of the same ionic strength and pH as in the original mine wastewater samples.

Table 1. Ionic composition of acidic (pH 4.5) mine wastewater obtained from Boddington Gold Mine, Western Australia.

Ion	mg/L	mM
Na^{+}	7.3×10^{2}	3.2×10^{1}
K^{+}	3.2×10^{1}	8.2×10^{-1}
Mg^{2+}	3.5×10^{2}	1.5×10^{1}
Ca^{2+}	3.0×10^{2}	7.5
Al^{3+}	1.0×10^{1}	3.7×10^{-1}
Fe^{3+}	1.7×10^{1}	3.0×10^{-1}
Mn^{2+}	1.7×10^{1}	3.1×10^{-1}
Cl^{-}	1.5×10^{3}	4.2×10^{1}
SO_4^{2-}	5.8×10^{2}	6.0
Cd^{2+}	6.2×10^{-2}	5.5×10^{-4}
Ce^{3+}	1.5	1.0×10^{-2}
Co^{2+}	3.4	5.8×10^{-2}
Cu^{2+}	3.0×10^{1}	4.8×10^{-1}
La^{3+}	7.2×10^{-1}	5.2×10^{-3}
Nd^{3+}	6.0×10^{-1}	4.2×10^{-3}
Ni^{2+}	7.3	1.2×10^{-1}
Sr^{2+}	1.1	1.2×10^{-2}
Y^{3+}	2.5×10^{-1}	2.8×10^{-3}
Zn^{2+}	9.6	1.5×10^{-1}
CO_3^{2-}	2.1	3.4×10^{1}

4.7. Measurement techniques

4.7.1. XRD

The formation of the layered structure was confirmed by XRD using a PW 1830 diffractometer (Philips, Amsterdam, The Netherlands), which applies Cu-K radiation (L = 0.1542 nm) and operates in Bragg-Brentano geometry with Ni filter at a voltage of 40 kV and a current of 30 mA. The diffractograms were recorded in the 4-80 2-Theta range with a step size of 0.02. The powder samples were placed on a glass zero background holder for the acquisition of the XRD patterns.

4.7.2. Spectroscopy

Infrared (IR) spectra were measured on a BIO-RAD Digilab Division FTS-65A/896 apparatus, equipped with a diffuse reflectance spectroscopy (DRS) accessory. In a typical measurement, 256 scans were collected with 4 cm^{-1} resolution in the 4000-600 cm^{-1} wavenumber range.

The antioxidant assays and the sedimentation tests were carried out by recording the UV-Vis spectra with a Genesys 10S spectrophotometer (Thermo Scientific). The wavelength range used was 190-1100 nm with 0.1 nm scaling.

EPR spectra were recorded with a BRUKER EleXsys E500 spectrometer (microwave frequency 9.54 GHz, microwave power 13 mW, modulation amplitude 5 G, modulation frequency 100 kHz). To record frozen solution spectra, 0.20 mL samples were mixed with 0.05 mL methanol to avoid crystallization of the water and transferred into quartz EPR tubes and the spectra were recorded in Dewar containing liquid nitrogen (77 K). The spectra were simulated with the "epr" program.[94] The spectra of $Fe(Cit)_2$ was measured separately and for the iron containing samples, this broad singlet background signal was eliminated in order to be able to simulate the copper(II) spectrum components. The anisotropic EPR spectra were analysed considering axial or rhombic g-tensors (g_x, g_y, g_z) and copper hyperfine tensors (A_x, A_y, A_z). The nitrogen superhyperfine structure was determined taking into account with a rhombic hyperfine tensor (a_x^N, a_y^N, a_z^N) were the x,y,z directions referred to the g-tensor orientations. Orientation dependent linewidth parameters (α, β, and γ) were used to fit the linewidths through the equation $\sigma MI = \alpha + \beta M_I + \gamma M_I^2$, where M_I denotes the magnetic quantum number of copper(II) ion. Since a natural copper(II) chloride was used for the measurements, the spectra were calculated by the summation of spectra ^{63}Cu and ^{65}Cu weighed

by their natural abundances. The hyperfine and superhyperfine coupling constants and the relaxation parameters were obtained in field units (Gauss = 10^{-4} T).

4.7.3. BET (Brunauer-Emmett-Teller)

N_2-sorption experiments were carried out on a NOVA3000 (Quantachrome) instrument. The samples were degassed with N_2 at 100°C for 5 h under vacuum to clean the surface of the adsorbent materials. The measurements were performed at the temperature of liquid N_2. The specific surface area was calculated from the adsorption isotherms. The pore size distribution was calculated from the desorption part of the sorption isotherms.

4.7.4. Microscopy

The morphology of the solids was characterized by a Hitachi S-4700 scanning electron microscope (SEM). The surface of the samples was covered with gold via physical vapor deposition before the measurements, which were conducted with 10 kV accelerating voltage.

Energy dispersive X-ray analyser (EDX, Röntec QX2 system) was coupled to the microscope to provide the occurrence of elements in the samples. For these measurements, accelerating voltage was set to 20 kV and noble metal deposition was omitted.

Transmission electron microscopy (TEM) was used to obtain more detailed pictures of the materials. For these measurements, a FEI Tecnai^{TM} G2 20 X-Twin type instrument was used, which operates at an acceleration voltage of 200 kV. The materials were imaged in dried state by both electron microscopy techniques.

4.7.5. Electrophoretic mobility

Electrophoretic mobility values were measured with a LiteSizer 500 (Anton Paar, Graz, Austria) light scattering device using the phase analysis technique. Omega-shaped plastic capillary cuvettes (Anton Paar) were used for the electrophoretic experiments. The sample preparation process included the adding of calculated amount of ultrapure water, polyelectrolyte and NaCl stock solutions, which were mixed in order to adjust the polyelectrolyte concentration and the ionic strength. The total volume of these mixtures was always 1.8 mL. The sample preparation process was finalized by adding 0.2 mL of 100 mg/L LDH stock dispersion. The samples were then allowed to rest for 2 h at room temperature. The capillary cuvettes were flushed with the majority of the dispersions and the last 0.35 mL was used for the actual measurement. The reported electrophoretic mobility values are the average of five individual measurements, the error of these measurements was about 10%.

The electrophoretic mobilities were in some cases converted to zeta potentials using the Smoluchowski equation:[37]

$$\zeta = \frac{u\eta}{\varepsilon_0 \varepsilon} \quad (1)$$

where ε is the relative permittivity of water, ε_0 is the permittivity of vacuum and η is the viscosity of the solvent.

4.7.6. Dynamic light scattering

Time-resolved dynamic light scattering (DLS) measurements were carried out with the above Litesizer 500 instrument equipped with a 40 mW semiconductor laser (658 nm wavelength) operating in the backscattering mode at a scattering angle of 175°. To determine the hydrodynamic radii, the correlation functions were collected for 20 s and the decay rate constants were calculated using the Cumulant method.[95] The sample preparations were the same as in the case of electrophoretic mobility measurements with the exception that the measurements were commenced after addition of the LDH stock. The particle concentration was constant at 10 mg/L. The fluctuating intensity of the scattered light was correlated by the intensity autocorrelation function to obtain the translational diffusion coefficient (D_t), from which the hydrodynamic radius (R_h) of the particles was calculated using the Stokes-Einstein equation:[96]

$$R_h = \frac{k_B T}{6\pi\eta D_t} \quad (2)$$

where k_B is the Boltzmann constant, T is the absolute temperature.

The size of the particles in a time-resolved manner corresponds to the stability of the colloidal system. Apparent rate of the particle aggregation was calculated from the increase in the size data recorded in aggregating dispersions and colloidal stability was expressed in terms of stability ratio (W) with the following equation:[97]

$$W = \frac{k_{app}^{fast}}{k_{app}} = \frac{dR_h(t)/dt|_{t\to 0}^{fast}}{dR_h(t)/dt|_{t\to 0}} \quad (3)$$

k_{fast} is the diffusion-controlled aggregation rate, which can be measured at high salt concentrations. This value is one or close to one in the case of unstable, quickly aggregating dispersions, while higher stability ratios refer to slower aggregation and more stable systems. Reaching the fast aggregation region happens through the critical coagulation concentration (CCC) where the potential energy barrier preventing the aggregation disappears. The DLVO theory can describe

quantitatively the aggregation processes and the interparticle forces, but in this work, it will be only used for qualitative comparison to identify the predominant interparticle forces in LDH dispersions.

4.7.7. Adsorption experiments

For the nitrate adsorption study, 50 mg of LDH samples were suspended in 10 mL solutions containing 5-625 mg/L nitrate anions at room temperature. The samples were continuously stirred at pH 7.0 for 120 h. After the reaction terminated, 1 mL aliquots were filtered with a 0.22 μm membrane filter and the concentrations of nitrate ions in the filtrate were determined by UV-Vis spectrophotometry (Shimadzu UV-1650). For the dichromate adsorption, appropriate amount of $K_2Cr_2O_7$ was dissolved in 100 mL of water and the pH was adjusted to 5.0 by adding appropriate amount of NH_4OH solution. Thereafter, 100 mg of LDH material was dispersed into the solution. The reaction time (5-240 min) and the initial concentration of dichromate ion (5-1400 mg/L) were altered. An aliquot of the sample was filtered after 120 h and the concentration of the dichromate in the filtrate was measured by UV-Vis spectrophotometry (Shimadzu UV-1650). The error of this method is about 3%. The absorbents were regenerated by dispersing the used LDH compounds in 3 M NaCl aqueous solutions, which were vigorously stirred for 12 h. The slurry was then filtered by 0.45 μm membrane filter, washed with water several times and dried at 65 °C overnight.

4.7.8. Antioxidant assays

SOD assay: The SOD assay (or Fridovich method) is based on xanthine and xanthine oxidase generated superoxide radical anions, which can be scavenged by superoxide dismutase or the model antioxidants. The test is followed by the reduction of nitro blue tetrazolium chloride (NBT) indicator molecules by the superoxide anion leading to colour change from yellow to blue. In case of complete inhibition, no colour change occurs. The colour change was measured at 565 nm. A probe reaction contained 0.1 mL of 3 mM xanthine, 0.1 mL of 3 mM NBT and 0.1-2.5 mL of the composite stock dispersion followed by the addition of 0.3 mL of 3 mg/mL xanthine oxidase, the compound initiating the test reaction. The above solutions were all prepared in phosphate buffer at pH 7.5 applying a total phosphate concentration of 1 mM.

DPPH assay: The DPPH radical scavenging activity of the catalytic composites was measured. DPPH is a relatively stable radical, what can be reduced by redox active antioxidant materials. In a typical test, 60 μM of DPPH was dissolved in 3500 μL of methanol and 100 μL of the catalytic material was added into the system followed by quick homogenization. During the reaction, the change in the concentration of violet-coloured DPPH was followed by measuring the

absorbances at 517 nm wavelength with a spectrophotometer. The decreases in the absorbances corresponded to the decrease in the radical concentration. The remaining DPPH percentage was then calculated to quantify the activity of the composite material.

CUPRAC assay: In the CUPric Reducing Antioxidant Capacity (CUPRAC) assay the redox activity of the material is measured. Cu(II) forms a complex with neocuproine through chelating. In the presence of redox active materials, Cu(II) is reduced to Cu(I) in the neocuproine complex. During the test, solutions of $CuCl_2$ (10 mM), neocuproine (7.5 mM in ethanol) and NH_4OAc (pH=7.1) (500 μL each) was mixed in a cuvette. Thereafter, 550 μL of the redox active material was added and mixed. The cuvettes were placed in dark environment for 30 minutes and the absorbance of the yellow-coloured Cu(I) neocuproine complex was measured at 450 nm wavelength with a spectrophotometer.

Guaiacol assay: Guaiacol assay measures the peroxidase-like activity of materials. The assays contain 240 μL of the antioxidant material, 240 μL of guaiacol with concentration varied between 2-40 mM and 1872 mL of 12.9 mM phosphate buffer (pH=7) mixed in a cuvette. Then, 48 μL (135 mM) hydrogen peroxide solution was added to the mixture as the final step to initiate the test. The measurement started immediately after mixing the components followed by placing the cuvette in a UV-Vis spectrophotometer to measure absorbances at 470 nm wavelength to follow the formation of the guaiacol oxidation products.

4.7.9. Sedimentation experiments

The sedimentation experiments including the determination of dilution factors and the half time of sedimentation was based on the UV-Vis measurements at 450 nm because LDH do not have a specific absorbance at that wavelength. The absorbance values measured were indicator of the turbidity of the dispersions. In the first period of the measurements after the dilution, a slight increase can be observed in the absorbance due to the enrichment of the LDH in the light path. This was chosen as maximum absorbance. Half of this absorbance value was chosen as the indicator of sedimentation rate, namely, ‘half time of sedimentation’ plotted as a function of the dilution factor, which was the ratio of added water volume and the volume of the original sample. The diluting water had the same electrolyte concentration and pH as the original wastewater. The sedimentation experiments were carried out on the samples as they were received, at 10g/L concentration.

5. Results

5.1. LDH-polyelectrolyte bilayer hybrid

As discussed before, the main objective of the doctoral work was the applications of LDH particles in colloidal systems along different aspects. Since colloidal stability is an important factor during biomedical, industrial and environmental applications, particular attention was paid to comprehensively study the charging and aggregation of the particles throughout the work. In the first part of the research, a stable colloidal LDH system was developed by adsorbing polyelectrolyte layers and was used as a basis to build up a functional antioxidant nanocomposite with the sequential adsorption method. To the best of our knowledge, this is the first report on polyelectrolyte bilayer formation on nanoparticulate supports, however, such a process was published earlier using planar substrates. The preparation of the LDH-based hybrid can be described as follows.

5.1.1. Characterization of substrate LDH

The LDH substrates used for the polyelectrolyte bilayer material was prepared with coprecipitation, as discussed earlier. Being composed of Mg(II) and Al(III) metal ions, one of the most common LDH type, the confirmation of the successful synthesis was rather straightforward. Accordingly, the formed lamellar structures were verified with XRD as one of the most powerful technique to investigate LDH structure.[1]

In Figure 4, one of these diffractograms is shown as an example. The diffraction pattern confirms that the obtained material is LDH due to the location of the diffraction peaks since the assigned Miller indices show a good agreement with the literature data.[98] The *003* and *006* reflections are sharp indicating a good crystallinity of the compound. In addition to the qualitative investigation of the material structure, quantitative analysis took place on the diffractogram using the Bragg and the Scherrer equations. From the Bragg equation, one can determine the *d*-spacing values as:[99]

$$n\lambda=2d\sin\theta_B \quad (4)$$

where n used as an integer (generally it is 1), λ the wavelength of the incident wave, d the lattice spacing, what is the distance between the atom planes giving rise to the diffraction peaks and θ_B is the Bragg angle.

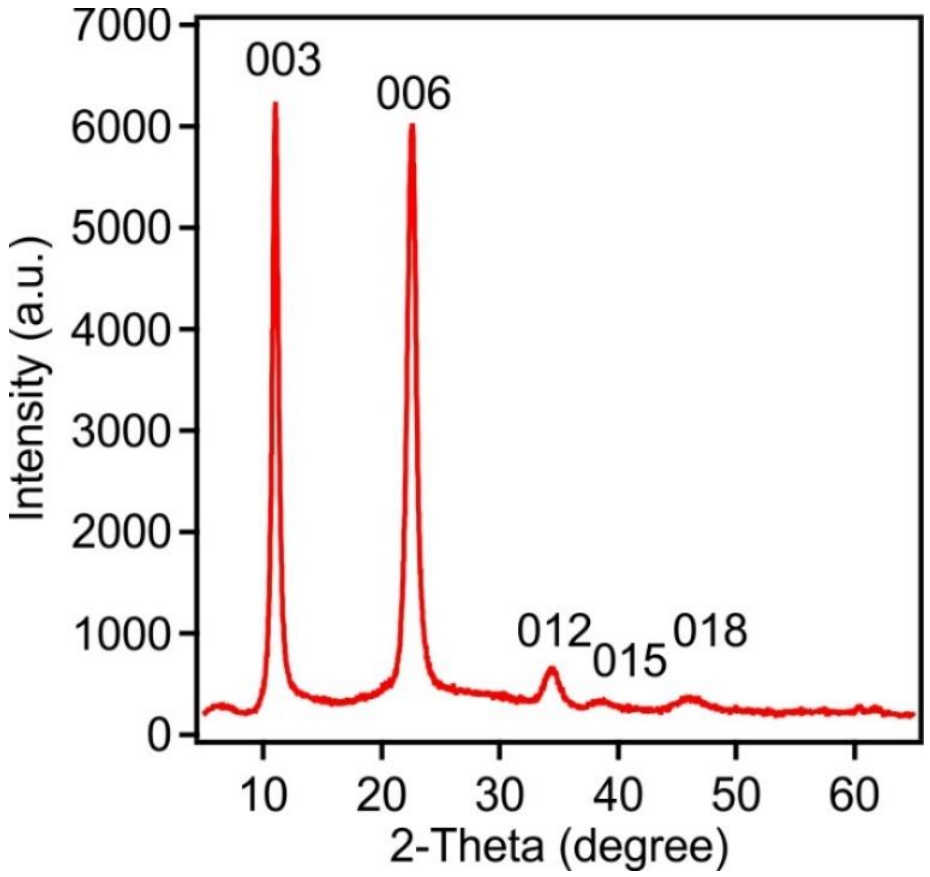

Figure 4. XRD pattern of Mg_2Al-LDH with chloride interlayer anion.[100]

From the *003* peak, the d003 parameter can be determined, which is the distance of one layer and the interlayer space together. This was found to be 0.8 nm and the interlayer space was calculated to be 0.33 nm. These data is similar to the ones previously reported in the literature.[93] The Scherrer equation gives us information of the ordered domain (υ) as

$$\upsilon = K\lambda/\beta\cos\theta_B \quad (5)$$

where K is the shape factor and β is the line broadening at the full widths at half of the intensity of the diffraction peak. The calculation yielded an average thickness of the particle as 30 nm meaning that it is composed of about 38 layers.

IR spectroscopy was used as part of the characterization techniques. The IR spectrum in Figure 5 showed good correlation with the literature data.[26] Accordingly, the peak at 3400 cm^{-1} reflects the O-H stretching vibration, the band at 1620 cm^{-1} is assigned to O-H scissoring, while

the peak at 1340 cm^{-1} is O-C stretching group referring to the presence of carbonate ions despite our most cautious efforts to avoid it. These findings also confirm the successful formation of the LDH material.

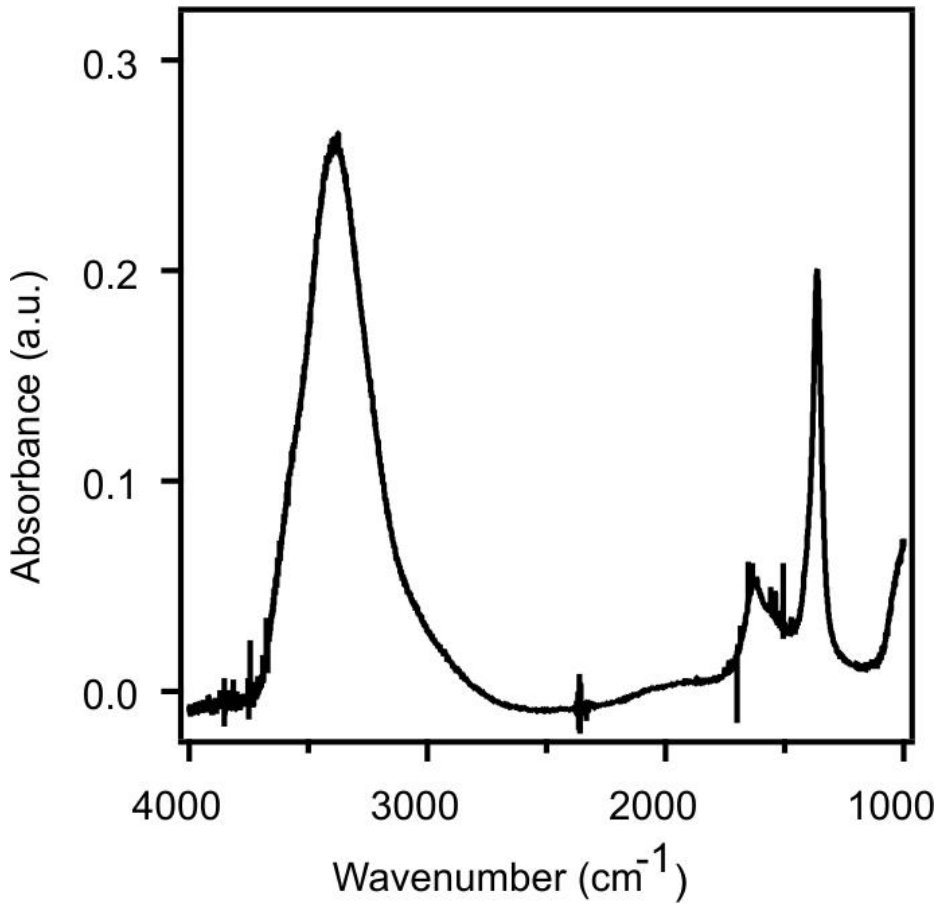

Figure 5. FT-IR spectrum of Mg_2Al-LDH with chloride interlayer anion.

The substrate LDH was characterized with dynamic and electrophoretic light scattering techniques in stable dispersions, where the colloidal properties of single particles can be assessed. The hydrodynamic radius measured for the LDH particles was (167±6) nm, while the polydispersity index was (0.23±0.03).

These data indicate pretty narrow particle size distribution, which was our goal to achieve during the synthesis. Electrophoretic mobility of the particles was measured and found to be $(1.0\pm0.5)\times10^{-8}$ m^2/Vs due to the positive structural charge of the LDH, which was utilized in the sequential adsorption process later.

The preparation of the polyelectrolyte bilayer material (and the antioxidant composite later) was performed with the sequential adsorption process[101] with separate immobilization steps on the LDH surface applied. The experimental conditions were optimized in each step by assessing the electrophoretic mobilities and the aggregation properties. Determining the dose of the different substances is crucial in order to prepare stable particle dispersions in each individual steps for further processing as well as to obtain homogeneously distributed hybrid particles at the end of the preparation process.

5.1.2. PSS layer

As mentioned before, the LDH substrate particles possessed a positive surface charge. This gave rise to the possibility of adsorbing an oppositely charged polyelectrolyte through electrostatic attraction. The chosen polyelectrolyte for this purpose was polystyrene sulfonate (PSS) possessing a negative charge due to the ionized sulfonate side groups. The PSS was expected to adsorb only on the positive outer surface and no intercalation takes place due to the narrow interlayer spacing (see interpretation of the XRD results above). The polyelectrolyte concentration was varied in a wide range, while particle concentration (10 mg/L) and the ionic strength (10 mM) was kept constant.

One can see in Figure 6 that the electrophoretic mobility (EPM) values were still positive at low doses of the PSS due to the naturally possessed structural charged of the substrate. The data decreased with increasing the dose of PSS indicating the adsorption on the surface. This process led to a charge neutralization at the isoelectric point (IEP), where the overall charge of the particles at this point is zero. Further increase in the dose led to charge reversal due to various effects such as electrostatic attraction, ion correlation, entropy effect (gained from release of solvent molecules and counterions upon adsorption)[102] and continued to the negative regime until the onset of the adsorption saturation plateau (ASP) was reached. The surface was saturated with the adsorbing compound at this dose meaning that this is the maximum amount of PSS that can adsorb and further added polyelectrolyte remained dissolved in the solution. From the intercept of the linear fits on the plateau and the decreasing mobility regime, the dose corresponding to the onset of ASP can be calculated and it corresponds to surface saturation. 100 mg/g was the determined value. No change occurred in the EPM data by further increasing the PSS dosage. This dose was used in our further experiments.

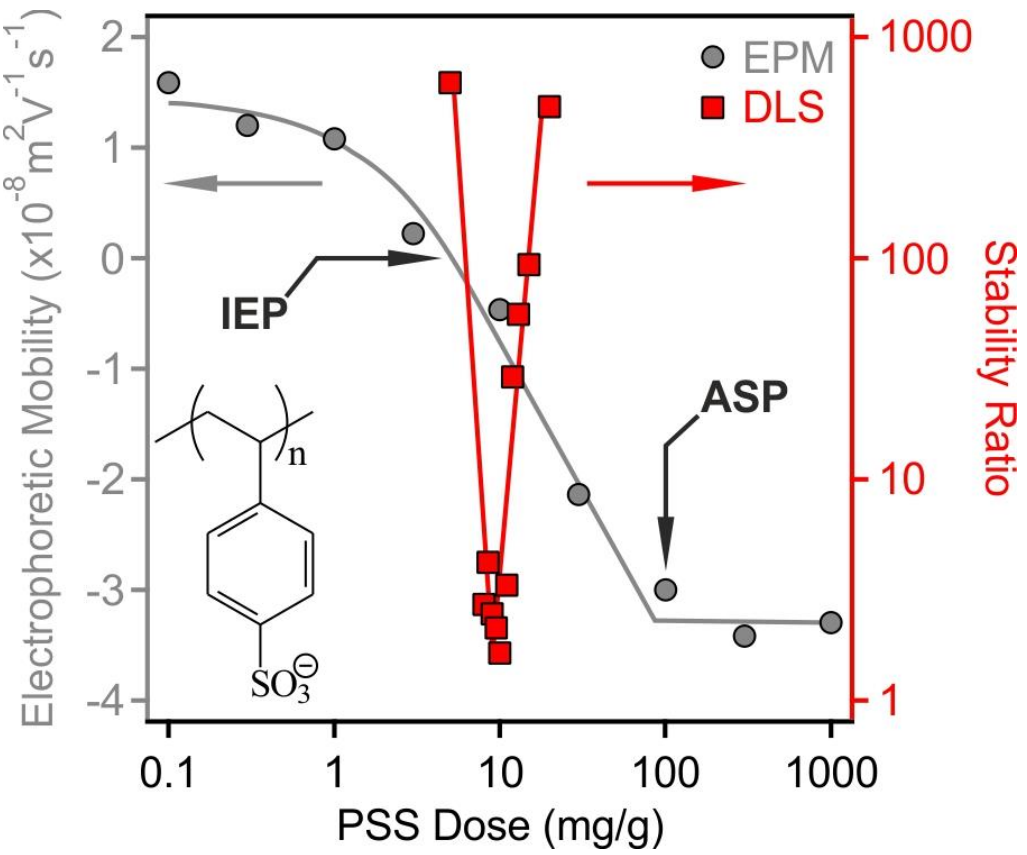

Figure 6. Electrophoretic mobility (circles, left axis) and stability ratio (squares, right axis) values of Mg_2Al-LDH particles in the presence of PSS polyelectrolyte. The PSS dose in mg/g unit on the x-axis refers to mg PSS per one gram of LDH. The structure of PSS can be seen in the inset and the solid lines are just to guide the eyes.[100]

The EPM values were measured in the same PSS concentration range at different ionic strengths shown in Figure 7 aiming to probe the effect of the ionic environment on the charging properties. The changes in the salt level did not lead to any major change in the shape of the EPM curves, as they follow the same tendencies and the majority of the data remained within the experimental error. It can be concluded that the system is rather insensitive to the ionic strengths. The reason behind this can be assumed as a result of the counterion condensation into the adsorbed polyelectrolyte chains (so-called Manning condensation), which prevents the effective screening of the surface charge by the salt constituents.[103]

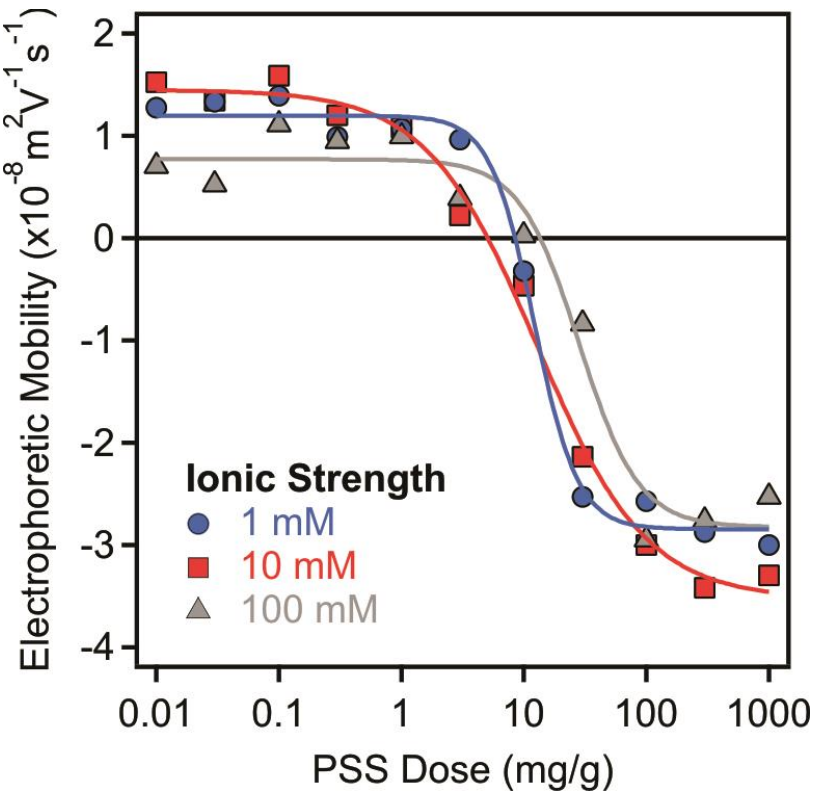

Figure 7. Electrophoretic mobilities of LDH particles as a function of the PSS dose at different ionic strengths adjusted with NaCl. The lines serve as guidelines for the eye.[100]

DLS is an excellent technique to determine the hydrodynamic radius of the particles in a time-resolved fashion, from which assessing the colloidal stability of the dispersions is possible. Such a colloidal stability was expressed in terms of stability ratio, as detailed in the experimental part. Note that stability ratio of unity refers to fast particle aggregation, while higher values indicate more stable dispersions.[41] During these measurements, the same experimental conditions were applied as in the EPM study.

At high and low polyelectrolyte concentrations, where the particles still possess a relatively high magnitude of charge, the stability ratio is high or immeasurable (Figure 6). In the proximity of the IEP, rapid aggregation occurred (stability ratios are low and close to one) indicating an unstable regime for the dispersions. More importantly, highly stable samples were observed at the onset of ASP at a PSS dose of 100 mg/g (denoted as LDH-PSS later).

This can be qualitatively explained with the DLVO theory.[39] Accordingly, particles do not possess charge at the charge neutralization point and thus, electrical double layers are absent. Above and below this point, the charged particles are stabilized by the repulsion induced by the

overlap of the electrical double layers, while at IEP, attractive van der Waals forces predominate. In Figure 8, this is demonstrated by the hydrodynamic radii in a time-resolved fashion at three different concentrations at (9.5 mg/g), below (8.5 mg/g) and above (12.0 mg/g) the IEP. Proving the system is the least stable at the isoelectric point.

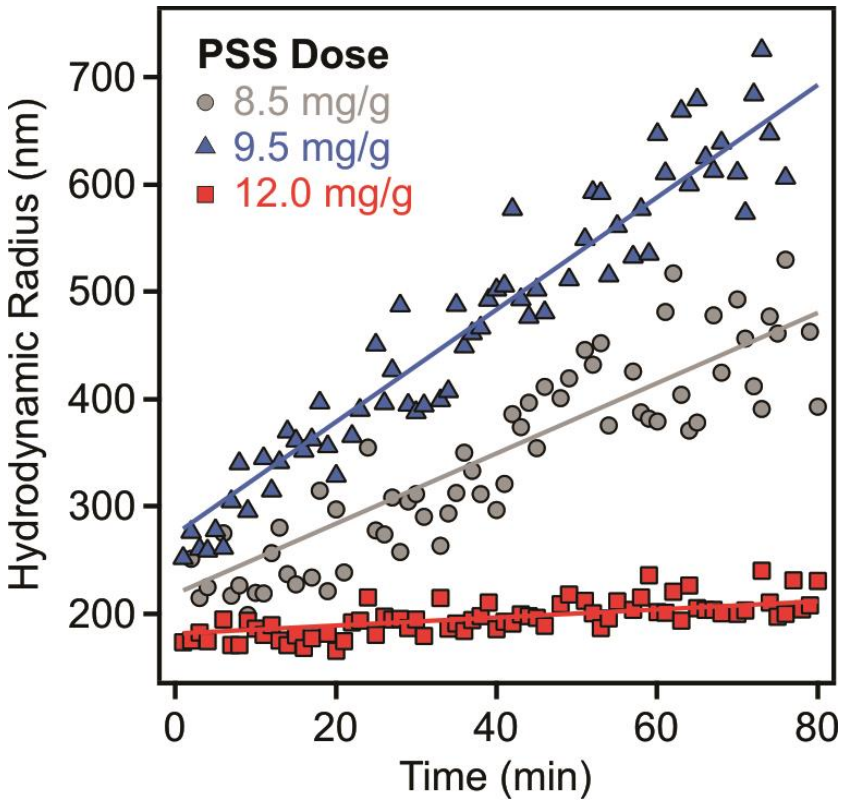

Figure 8. Hydrodynamic radii of LDH particles at different PSS doses as a function of the measurement time. The solid lines are linear fits used to calculate the stability ratios as it can be seen in equation (3). The slope of dose 9.5 mg/g was used for k_{app}^{fast}.[100]

5.1.3. PDADMAC layer

A second polyelectrolyte layer was developed on the negatively charged LDH-PSS hybrid, with the use of positively charged PDADMAC. The conditions of the measurement were similar to the ones in the experiments during building up the first layer, i.e., the particle concentration (10 mg/L) and the ionic strength (10mM adjusted by NaCl) were kept constant. Electrophoretic mobilities and stability ratios were determined to investigate the influence of the PDADMAC adsorption on the surface charge and aggregation properties of the LDH-PSS particles (Figure 9).

Tendencies in the electrophoretic mobilities in case of PDADMAC adsorption were similar to previous experiences in case PSS, although the charge balance was the opposite. Increasing the

polyelectrolyte dose led to charge neutralization due to the adsorption of the positively charged PDADMAC on the negative LDH-PSS surface. The IEP was located at 100 mg/g. Further increase of the PDADMAC dose led to charge reversal and the ASP what was found to be at 300 mg/g.

Concerning stability ratios, unstable dispersions were observed at the IEP, while the particles were stable away from this point, also at 300 mg/g, therefore, this dose was chosen as the loading dose of PDADMAC. Under these conditions, the obtained LDH-PSS-PDADMAC hybrid is positively charged and forms stable colloid.

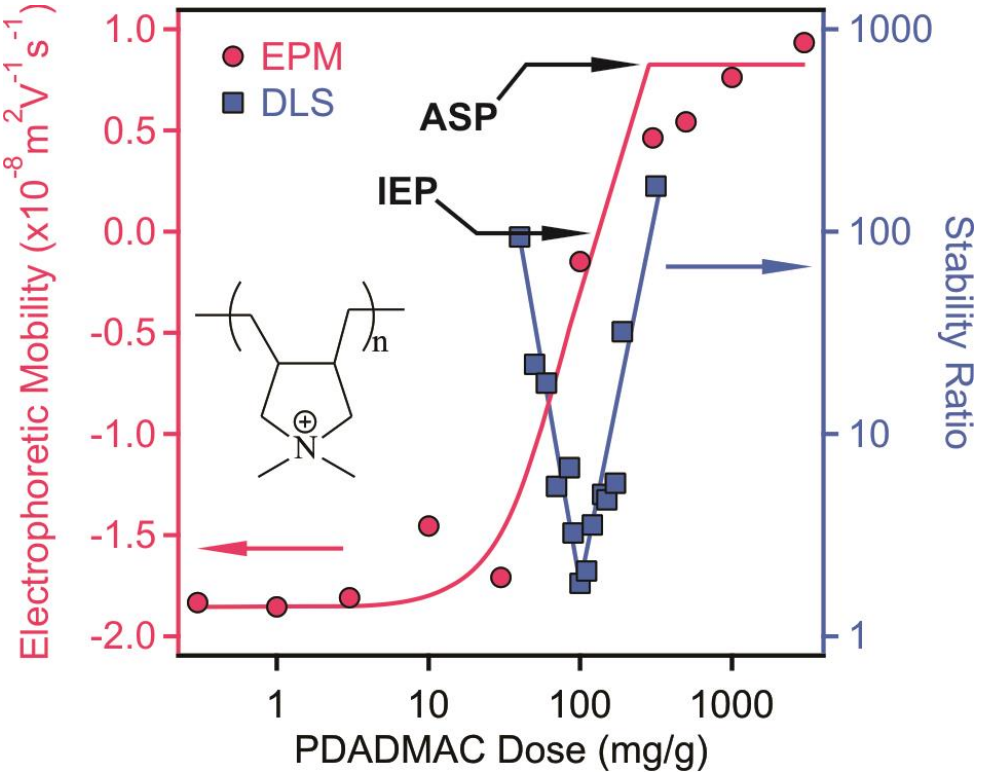

Figure 9. Electrophoretic mobility and stability ratio values of LDH-PSS hybrid in the presence of PDADMAC polyelectrolyte. The structure of PDADMAC can be seen in the inset.[100]

The bare LDH particle possessed a relatively low charge as mentioned before (1.0×10^{-8} m^2/Vs in EPM). This means that destabilization of the particles may occur at rather low ionic strengths. To address this issue, the CCC, which separates the stable and unstable regimes in salt-induced aggregation, was determined and found to be 80 mM for bare LDH (Figure 10).

The same experiments were performed for all three systems (bare LDH, LDH-PSS, LDH-PSS-PDADMAC) and thus, EPM and stability ratio values were measured at different ionic strengths. In this way, the effect of polyelectrolyte layer formation on the colloidal stability of the particles could be investigated. The EPM values indicate that the charge approaches zero with

increasing the ionic strength due to the screening effect of the salt constituent ions on the surface charges. Bare LDH particles and LDH-PSS-PDADMAC system possessed a relatively low positive charge, while the LDH-PSS system is of a high negative surface charge (Figure 10).

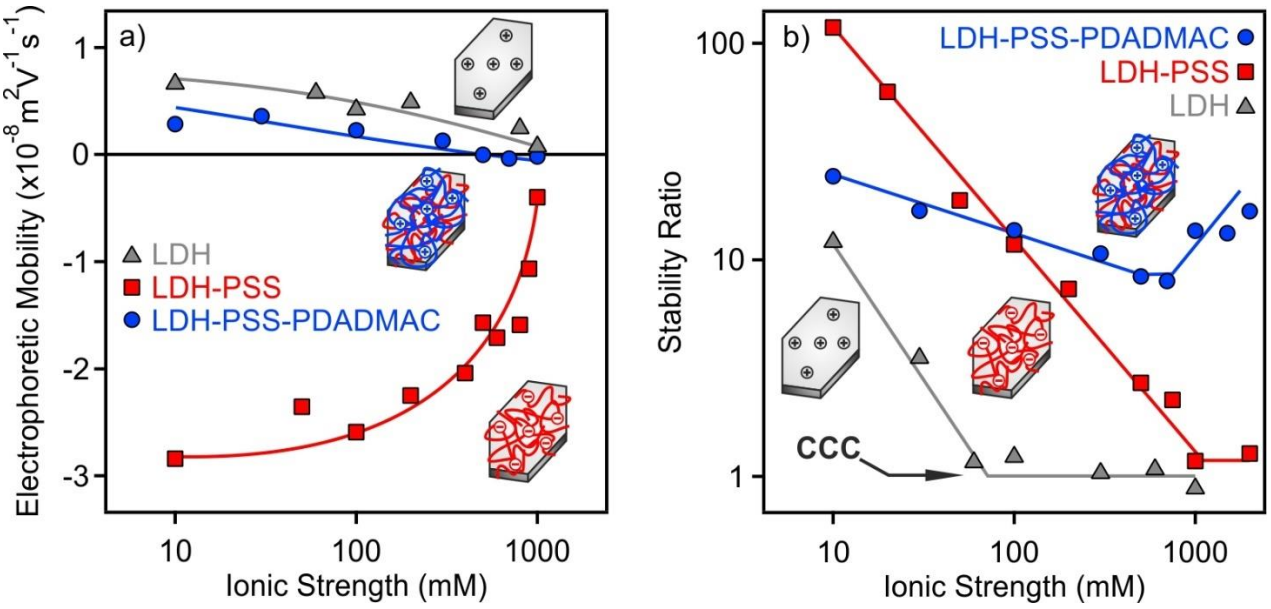

Figure 10. Electrophoretic mobility (a) and stability ratio (b) of bare LDH (triangles), LDH-PSS (squares) and LDH-PSS-PDADMAC (circles) particles versus the ionic strength adjusted by NaCl.[100]

Concerning the stability ratios measured at different ionic strengths, the bare LDH and the PSS-LDH particles followed the tendency predicted by the DLVO theory. At low salt concentrations, the system was stable and increasing the salt concentration the system was destabilized. The CCC for the bare particle was 80 mM while for the PSS-LDH system 1000 mM was recorded. The low CCC of the bare particle is common,[14] while the lot higher CCC value for the PSS-LDH system can be explained by the stabilizing force of the polyelectrolyte. The electric double layer forces just themselves are rather unlikely to lead to such stabilization, steric interactions from the overlapping of the polyelectrolyte chains on the particle surfaces can lead to further, so called electrosteric, stabilization.[104]

The case of the LDH-PSS-PDADMAC system is rather unique. The data show progressive destabilization with the increase of the ionic strength, but the diffusion-controlled regime was not reached, i.e., the stability ratios remained higher than unity in the entire ionic strength range investigated. A minimal stability ratio at 1000 mM was observed and by further increasing the salt level, slight restabilization occurred. The EPM data of LDH-PSS-PDADMAC do not show good

correlation with this finding, since the overall surface charge is low and it is approximately zero at higher ionic strengths. Therefore, electrical double layer forces do not play a significant role and particles should aggregate.

The reason behind this phenomenon can be explained with steric forces again, which originates from the adsorbed polyelectrolyte chains. It has been reported earlier that polyelectrolyte layers swell at higher ionic strengths giving rise to the formation of loops and tails on the surface.[105,106] These conformational changes may lead to stronger steric stabilization due to the overlap of the extended polyelectrolyte chains.[107,108]

Overall, both the built-up of mono- and bilayer hybrid had higher stability than the bare LDH particle. With the first layer, the hybrid possessed a negative charge and became an excellent adsorbing site for positively charged compounds. With the second layer, the overall positive charge of the substrate was regained, while lot higher stability was obtained and promoted itself into a potential candidate as an excellent substrate to negatively charged compounds. These results were utilized for the next part of the work, in which a multilayer antioxidant material was developed as follows.

5.2. Antioxidant composite material

As stated before, one of the goals was to develop a stable dispersion of a multilayer composite material possessing antioxidant properties. Stabilization of the dispersions was carried out with the adsorption of polyelectrolyte layers on LDH substrate, while tuning the surface charge and the colloidal properties, in a similar fashion as in the previous chapter. The developed composite material contained four different layers, namely, two polyelectrolytes and two metal complexes: PSS, $[Cu(Bpy)_2]$, PDADMAC and $[Fe(Cit)_2]$. The first adsorbed layer was PSS, in this process there was no change from the protocol used in chapter 5.1.2. The applied PSS dose was 100 mg/g.

5.2.1. $[Cu(Bpy)_2]$ layer

The second layer introduced was $[Cu(Bpy)_2]$ in order to achieve the antioxidant properties as Cu(II) ions in the metal complex working as an active metal centre similar to metalloenzymes such as SOD. The 1:2 metal to ligand ratio implies that the copper(II) ions are coordinated by four nitrogen atoms of the ligands in solutions, however, Cu(Bpy) complexes may also be present in smaller extent. Due to this fact, the overall charge of the $[Cu(Bpy)_2]$ can be considered as positive. This was proven by the observation that the addition of the metal complex to the negatively charged

LDH-PSS hybrid changed the electrophoretic mobility values (Figure 11) significantly. Charge neutralization and slight charge reversal were observed at high complex concentrations, the ASP region was not reached due to the solubility limit of the metal complex. The stability ratios decreased by increasing the dose of the [$Cu(Bpy)_2$] reaching the unstable regime, where the stability ratios were close to one. Unlike in the case of polyelectrolytes, the typical U-shape curve could not be achieved and thus, stability ratios remained unity at high complex concentration. Since the goal was to prepare stable dispersions, the dose was chosen from stable domain with the exact concentration of 0.1 mM [$Cu(Bpy)_2$]. The obtained composite was named as LDH-PSS-$Cu(Bpy)_2$. The overall charge of the material was negative.

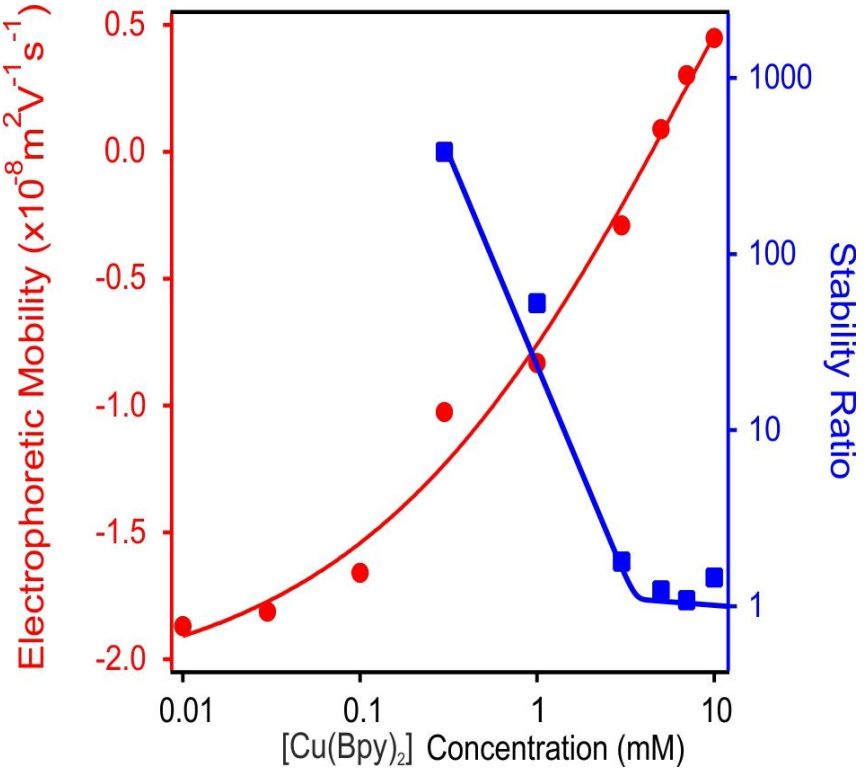

Figure 11. Electrophoretic mobilities (circles) and stability ratios (squares) determined in the LDH-PSS-$Cu(Bpy)_2$ system at constant LDH-PSS and varied [$Cu(Bpy)_2$] concentration at 10 mM ionic strength adjusted by NaCl.[109]

5.2.2. PDADMAC layer

Since the overall charge of LDH-PSS-$Cu(Bpy)_2$ remained negative, it gave the opportunity to adsorb PDADMAC via electrostatic interaction, as the third layer. Similar tendencies could be observed to the ones shown in the case of the bilayer material. The trend in case of the EPM values were indeed very similar, the data was nearly exactly the same, even though the location of the IEP

shifted to lower doses of polyelectrolyte. The consequence of this shift can be observed in the stability ratios. In the case of the LDH-PSS-PDADMAC hybrid stability ratio of unity was observed at 100 mg/g dose of PDADMAC, while in case of the LDH-PSS-Cu(Bpy)$_2$-PDADMAC composite the unity value of stability ratio occurred at 40 mg/g PDADMAC dose. Such a change in the IEP value and the unstable region is a result of the adsorption of the [Cu(Bpy)$_2$] in the previous step. Charge reversal occurred at appropriately high PDADMAC doses and the adsorption process continued until surface saturation leading to a plateau in the mobility values. The onset of the ASP was around 100 mg/g dose (Figure 12). Due to these results, a PDADMAC dose of 100 mg/g was applied in the composite, at which the dispersion was stable, i.e., the stability ratios were extremely high under these experimental conditions.

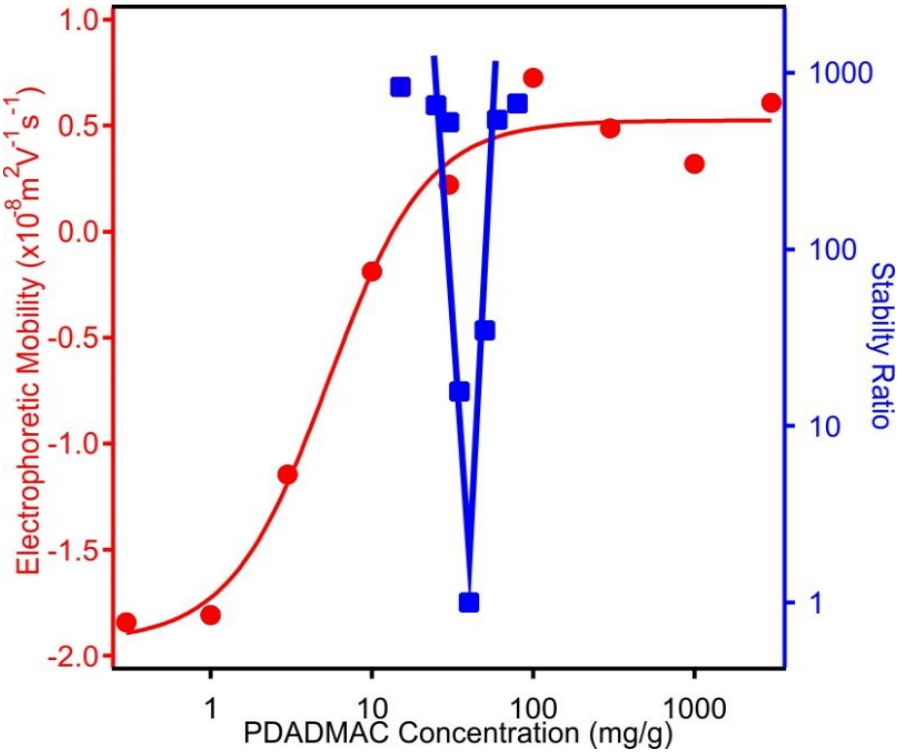

Figure 12. Electrophoretic mobilities (circles) and stability ratios (squares) determined in the LDH-PSS-Cu(Bpy)$_2$-PDADMAC system as a function of PDADMAC dose at 10 mM ionic strength adjusted by NaCl.[109]

5.2.3. [Fe(Cit)$_2$] layer

The fourth and final layer was the metal complex [Fe(Cit)$_2$]. According to literature data, aqueous solutions containing iron(III) and citrate ions was frequently investigated. The published results indicate that mixed hydroxo-citrate complexes may also form in the system, however, the species are all negatively charged.[110,111]

Since the overall charge of the LDH-PSS-Cu(Bpy)$_2$-PDADMAC composite was positive, these complexes adsorbed on the surface due to the opposite charge. The goal of the addition of Fe(Cit)$_2$ was to create another active centre due the redox properties of the metal ion and thus, to enhance the antioxidant activity. Similarly to the trends seen before for the polyelectrolyte adsorption, charge neutralization occurred even at very low [Fe(Cit)$_2$] loadings indicating that the metal complex has a strong affinity to the surface (Figure 13). Stability ratios followed the tendency observed before in case of PSS and PDADMAC meaning that close to the charge neutralization point, the stability ratios were low, i.e., the system was unstable and fast aggregation occurred. Stable dispersions formed at [Fe(Cit)$_2$] doses away from the IEP. This is in qualitative agreement with the DLVO theory, as discussed above. The final concentration of [Fe(Cit)$_2$] was chosen as 0.1 mM since at this concentration, the multilayer composite material possessed a highly negative charge and a highly stable dispersion was obtained.

The composition of the final composite was LDH-PSS-Cu(Bpy)$_2$-PDADMAC-Fe(Cit)$_2$ as the dose of the polyelectrolytes were 100 mg/g and the concentration of metal complexes were 0.1 mM. The obtained hybrid is denoted as COMP in this work.

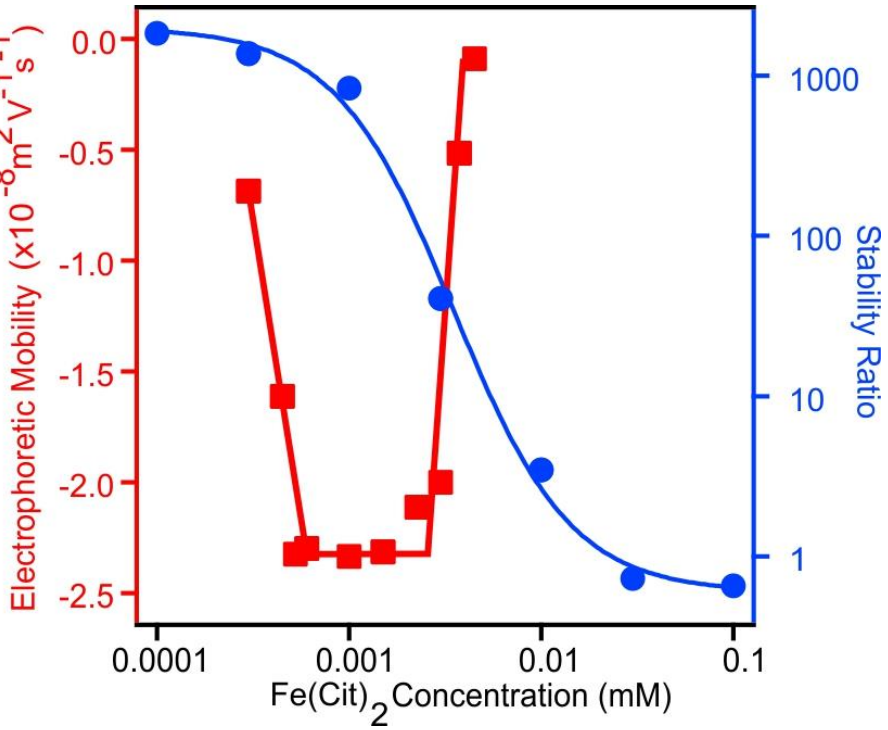

Figure 13. Electrophoretic mobilities (circles) and stability ratios (squares) determined in the LDH-PSS-Cu(Bpy)$_2$-PDADMAC-Fe(Cit)$_2$ system versus the [Fe(Cit)$_2$] concentration at 10 mM ionic strength adjusted by NaCl.[109]

5.2.4. Salt-induced aggregation

As a final probe of the colloidal properties, the resistance of COMP against salt-induced aggregation was determined. This is an important parameter during use in catalytic processes like medical treatments and industrial manufacturing ones, where the antioxidants are in contact with various dissolved electrolytes. The behaviour of COMP was compared to the bare substrate LDH particle by measuring both EPM values and stability ratios at different NaCl concentrations.

The increase in salt concentration resulted in decreasing EPM values in magnitude and in EPM close to zero due to the screening effect of the salt constituents on the surface charges (Figure 14 (a)). This is a typical behaviour of dispersions containing charged particles and indifferent salts as it was shown for the case of the mono- and bilayer hybrid material earlier too. While the bare particle possessed relatively low positive charge at low ionic strength, the COMP material had a significant negative charge as a result of the adsorbed molecules.

This data is in close relation with measured stability ratios (Figure 14b), which can be described by the DLVO theory. Accordingly, higher charges led to higher stability, while increased ionic strengths results in weaker electrical double layer forces and to lower stability. The bare particle shows relatively low stability in the 10-100 mM NaCl concentration regime while the composite shows much higher stability indicated by high stability ratio values also in this regime. As the stability ratios decrease with the increasing NaCl concentration the CCC was reached and the values remained unity thereafter. The CCC value of the composite is around 200 mM NaCl being higher than the one for the bare particle.

Interestingly, the colloidal stability of the composite is lower than the stability of the LDH-PSS-PDADMAC hybrid without metal complexes immobilized. This can be explained as the LDH-PSS-PDADMAC hybrid stability ratio values at high salt concentration were atypical due to steric effects most probably caused by the overlapping side chains detailed above. The disappearance of such effect and the return to pure DLVO-type interactions can be described as the effect of the adsorption of metal complexes on the polyelectrolyte layers, which gave rise to a more compact structure preventing the formation of polyelectrolyte tails and loops on the surface. As a conclusion of the build-up process, a multilayer composite was successfully developed with the sequential adsorption method leading to high stability. Metal complexes immobilized inside the structure should provide considerable antioxidant activity.

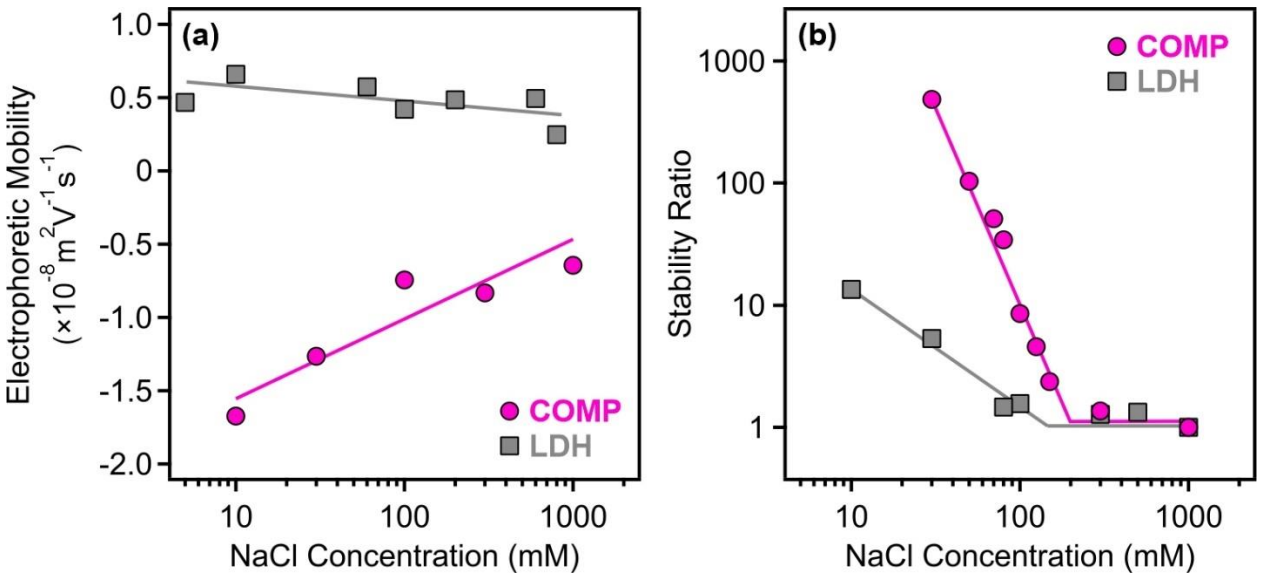

Figure 14. Electrophoretic mobility (a) and stability ratio (b) values determined for the bare LDH (squares) and for COMP (circles) at different NaCl concentrations. The breakpoint in the lines in (b) indicate the location of the CCC.[109]

5.2.5. Characterization of the LDH-PSS-Cu(Bpy)2-PDADMAC-Fe(Cit)2 composite

5.2.5.1. Characterization by SEM

SEM images were taken after dying the composite material. The final COMP (LDH-PSS-Cu(Bpy)$_2$-PDADMAC-Fe(Cit)$_2$) showed the typical morphology of Mg$_2$Al-LDH materials meaning the appearance of rounded edged platelets unlike some other LDH type of sharp edges.[112] The lateral size of the particles was in the 150-200 nm range (Figure 15). The individual particles can be observed on the images, no huge aggregates appeared despite the drying process proving the remarkable colloidal stability of the COMP claimed earlier. The COMP dispersions concentration was 10 mg/L and were sonicated for 10 minutes before the drying process.

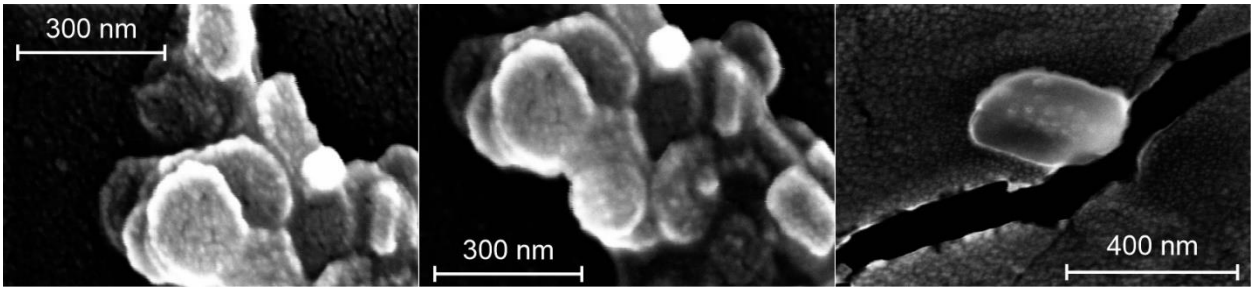

Figure 15. SEM images of COMP. The measurements were performed after drying the dispersions.[109]

5.2.5.2. Electron paramagnetic resonance spectroscopy

To investigate the coordination geometry around the iron(III) and copper(II) ions, EPR spectroscopy was used before and after immobilization. The EPR spectra of $[Fe(Cit)_2]$ was rather uninformative due to the fast relaxation even at 77 K leading to a broad singlet line. The spectra of copper(II)-bipyridyl systems have already been measured by Garribba et al. and found mono-ligand Cu(Bpy) complex possesses the usual g-tensor values ($g_x \sim g_y < g_z$) showing an elongated octahedral geometry.[113] The $[Cu(Bpy)_2]$ complex showed the opposite trend in g-tensors ($g_x \sim g_y > g_z$), which suggests trigonal bipyramidal geometry (Figure 11A).[113] As a result, the free $[Cu(Bpy)_2]$ complex system could be simulated as the sum of 25% mono and 75% bis-ligand complex spectra (Figure 16a and Table 2).

Table 2. Anisotropic EPR parameters of components obtained in the simulation of the EPR spectra.[a]

Coordination compound	g_x	g_y	g_z	A_x(G)	A_y(G)	A_z(G)	a_x^{N1} (G) a_y^{N1} (G) a_z^{N1} (G)	a_x^{N2} (G) a_y^{N2} (G) a_z^{N2} (G)
$[Cu(Bpy)_2]$	2.177	2.177	2.017	83.7	83.7	75.8		
[Cu(Bpy)]	2.066	2.066	2.274	12.6	12.6	154.7		
[Cu(Bpy)(COMP)]	2.062	2.062	2.280	14.0	14.0	147.8		
$[Cu(Bpy)_2(Cit)]$	2.063	2.063	2.259	23.5	23.5	157.0		
[Cu(Bpy)(Cit)]	2.065	2.051	2.283	4.8	14.6	163.8	11.4. 12.6 10.6	12.7 7.7 13.8

[a]The experimental error were ±0.001 for g, ± 1 G for A and a_N

The mixture of the two complexes ($[Fe(Cit)_2]$ and $[Cu(Bpy)_2]$ systems together) was also measured without the nanoparticle support and significant changes were observed in the spectra. This spectral changes can be assumed as the result of coordination of Cit ligand to the copper(II)-bipyridyl complexes resulting in the mixed ligand complexes [Cu(Byp)(Cit)] and $[Cu(Byp)_2(Cit)]$, both with elongated octahedral geometries (Figure 16 c).

The spectra of the composite was recorded at 100 mg/L concentration shown on Figure 16 d. This spectrum can be fitted with the [Cu(Bpy)(Cit)] component spectra. Accordingly, the adsorption had no significant effect on the EPR parameters (Table 2). The nitrogen superhyperfine

structure clearly confirms the binding of two nitrogen donor atoms in the equatorial plane. Besides, the appearance of the mixed ligand complex on the surface was rather unexpected since the $[Cu(Bpy)_2]$ and $[Fe(Cit)_2]$ complexes were immobilized in different steps during preparation of the COMP.

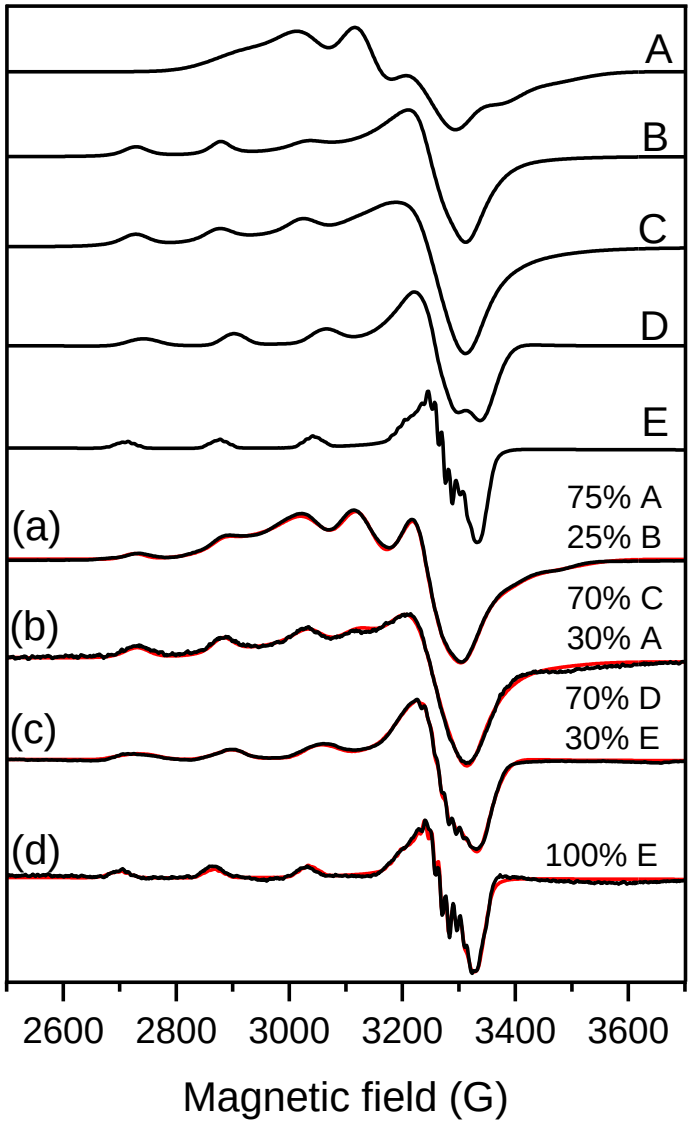

Figure 16. Measured (black) and simulated (red) EPR spectra of samples containing (a) $Cu(Bpy)_2$ solution (b) 100 mg/L LDH-PSS-$Cu(Bpy)_2$, (c) $[Cu(Bpy)_2]$ and $[Fe(Cit)_2]$ in aqueous solution and (d) 100 mg/L composite. The spectra were simulated by the help of component spectra A: $[Cu(Bpy)_2]$, B: [Cu(Bpy)], C: [LDH-PSS-$Cu(Bpy)_2$], D: $[Cu(Bpy)_2(Cit)]$ and E: [Cu(Bpy)(Cit)] described with EPR parameters collected in Table 2.[109]

5.2.5.3. Antioxidant activity

The active centre of antioxidant enzymes contains redox active transitional metal ions coordinated by donor atoms of binding polypeptides.[114] These active centres can be considered as metal complexes. As referred before, due to this consideration, $[Cu(Bpy)_2]$ and $[Fe(Cit)_2]$ complexes were immobilized into the COMP material to serve as active centres upon antioxidant function. The complex environment including the polyelectrolytes, the effect of metal complexes on the overall structure and the immobilization process might lead to the mimicking of the binding and redox properties present in native enzymes. To assess the activities, the composite material was tested in multiple antioxidant tests.

Superoxide dismutase-like activity was tested first as an proper way to observe superoxide radical scavenging ability. As detailed before, superoxide radicals, like all ROS, are responsible for both health problems and for limited quality products in the industry so controlling the level of this radical is crucial in such applications. The oxidation of xanthine to uric acid with xanthine-oxidase leads to superoxide radical production in the assay, which reduces NBT to formazan accompanied with colour change from yellow to blue.[66] In the absence of the superoxide radicals, the reduction of NBT is inhibited and no colour change occurs. The antioxidant activity and inhibition effect of COMP can be measured and calculated from the spectrophotometric data recorded during the colour change in the assays.

The composite showed excellent activity in the test (Figure 17). Accordingly, 100% inhibition could be reached at a concentration around 0.050 mg/L. A usual way to describe the activity of enzymes or enzyme mimics is the so-called IC_{50} value, which is the concentration required for 50% inhibition or to capture 50% of the superoxide radicals forming in the assay. The IC_{50} value for the COMP was found to be 0.026 mg/L. This is a rather high activity and comparable with the activity of the native copper(II)-zinc(II) superoxide dismutase enzyme, whose IC_{50} was found to be 0.069 mg/L earlier, in the same biochemical assay. However, due to structural differences, the concentration of the redox active metal ions is much higher in the composite than in the native enzyme at this mass concentration.[115]

Both the stand-alone $[Cu(Bpy)_2]$ and $[Fe(Cit)_2]$ complexes and also the mixture of the two was applied at the same conditions and equivalent concentration as in the composite in the assay, but inhibition was measured in neither case. These observations indicate a synergistic effect between the complexes upon immobilization, which remarkably improved in the superoxide radical

scavenging activity. The reason behind this can be the beneficial coordination geometry around the metal ions in COMP. The EPR results discussed earlier might be an explanation as the diverse Cu(Bpy)(Cit) complexes form leading to the improved scavenging activity. Overall, COMP showed excellent activity in scavenge of superoxide radical ions.

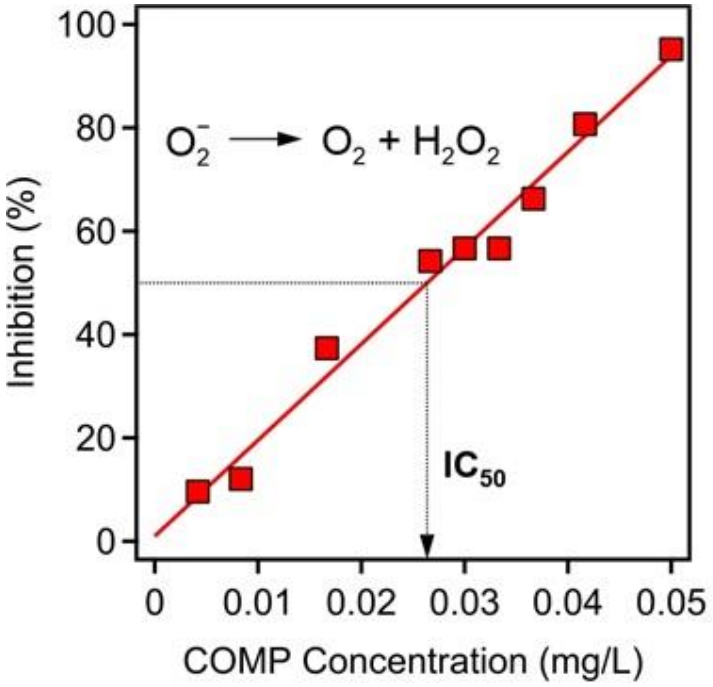

Figure 17. Inhibition of superoxide radical-NBT reaction as a function of the COMP concentration. The dismutation scheme for superoxide radicals is shown in the inset.[109]

As stated earlier, different assays were carried out to assess the broad-spectrum antioxidant activities. Moderate results were gained during the DPPH test. The oxidized form of the DPPH is a radical, which is rather stable and the presence of a radical scavenging material leads to the reduction followed by a colour change from violet (DPHH radical) to yellow (reaction product).[67] The EC_{50} is the quantity used to express the activity in such assays, which is the induced response of the antioxidant at 50% of the maximal possible response to the reaction. The COMP was only able to decompose 55% of the initial DPPH radicals even at high concentrations. The EC_{50} value was found to be 49 mg/L (Figure 18). Similar to the SOD assay, the lone complexes and the mixture of them were also investigated. The $[Cu(Bpy)_2]$ in solution showed only 5.9% scavenging activity, while for $[Fe(Cit)_2]$, 9.7% was measured. In addition, the mixture of the two lone complexes resulted in 11.4% scavenged radicals. These data confirm the advantageous effect of the co-immobilization even though the activity of the composite in this assay is rather moderate.

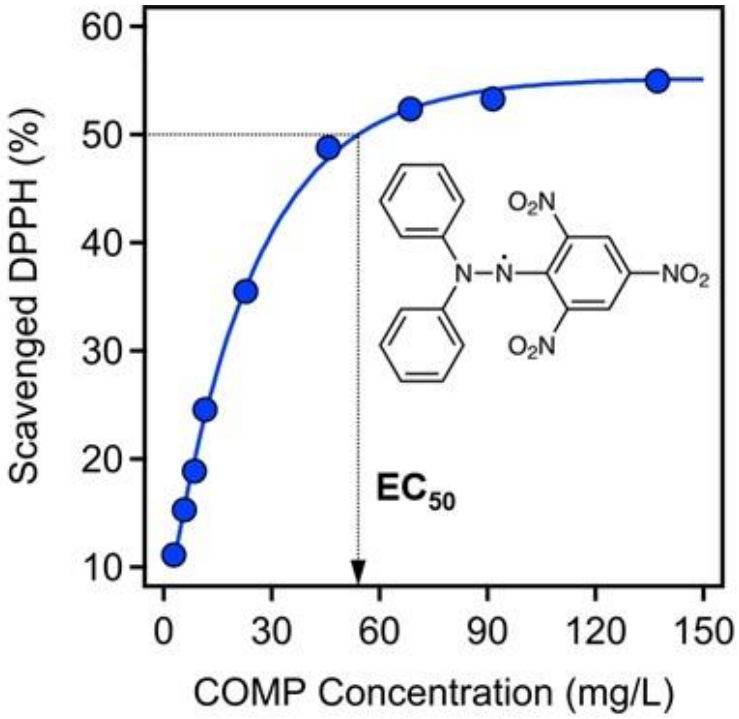

Figure 18. DPPH scavenging ability of COMP as a function of its concentration. The DPPH radical is shown in the inset.[109]

Further assays were applied to probe the antioxidant activity of the material. Namely, CUPRAC[116] and guaiacol-based peroxidase assay.[76] CUPRAC assay measures the redox activity of the antioxidant by reducing Cu(II)-neocuproine complex to Cu(I)-neocuproine. In the CUPRAC assay, the material showed very little to unsignificant activity. The guaicol assay was carried out to measure peroxidase activity of the composite, however no activity was detected.

These findings prove that the novel composite material does not only possess antioxidant activity, but this activity is specific to superoxide radical dismutation. Despite many studies reported complex LDH-based materials with antioxidant activity to date[74], no work reported similar activity and selectivity for SOD-mimicking materials. However, specificity in these studies is usually not probed as they concentrated only on few tests, where the developed materials were successful. Nevertheless, specific material for superoxide dismutation is not reported in case of LDH-based materials to our best knowledge.

Overall we successfully a complex LDH-based composite with high colloidal stability. The composite owned antioxidant activity due to the immobilized metal complexes, which was tested in various assays proving remarkably high superoxide dismutation activity.

5.3. Hierarchically ordered mesoporous LDH

Porous materials with a high specific surface area have always been a point of interest in research due to various potential applications such as water decontamination, catalysis or carrier of larger biomolecules in the pores.[29] Various attempts have been carried out to develop LDH materials with high porosity using different techniques like soft and hard templating[16] or special method like the aqueous miscible organic solvent treatment[117] etc. Surfactant additives are widely used in soft templating as a structure directing agent influencing the interlayer distance, while being intercalated or adsorbed on the outer surface. SDS is one of the most extensively used surfactant for such purpose.[118,119]

While SDS is intercalated between layers in most studies, the surfactant also adsorbs on the outer surface of the lamellae leading to changes in the charging properties and aggregation behaviour, what are important aspects. Even though these circumstances play a relevant role, no systematic study was reported about the charging properties and aggregation behaviour in systems containing SDS modified LDH. Therefore, an attempt was made to combine colloidal and material chemistry approaches to develop a novel high surface area LDH material for applications based on ion adsorption capacity+. The developed material was prepared through coprecipitation of MgAl-LDH what was treated with different concentrations of SDS solution. The treated LDHs were named SDS_3-LDH, SDS_{10}-LDH, SDS_{30}-LDH referring to the SDS dose. The SDS treated materials were calcinated and rehydrated leading to the high surface area LDH materials. These were named as LDH_3, LDH_{10}, LDH_{30} a referring to the SDS dose used during the treatment before the calcination-rehydration.

5.3.1. Characterization

5.3.1.1. Stability of SDS-LDH dispersions

The charging and aggregation of the MgAl-LDH particles were investigated at different electrolyte concentrations. The surface charge density (σ) was estimated from the zeta potential versus ionic strength data using the Debye-Hückel equation (Figure 19):[120]

$$\sigma = \varepsilon_0 \varepsilon \kappa \zeta \qquad (6)$$

where ε is the relative permittivity of water, ε_0 is the permittivity of vacuum and ζ is the zeta potential. A relatively low charge density of +0.5 mC/m^2 was determined.

This is reflected in the stability data and low CCC (7 mM) was obtained in time-resolved DLS measurements. These values are typical for LDH materials containing small inorganic charge compensating anions.[14]

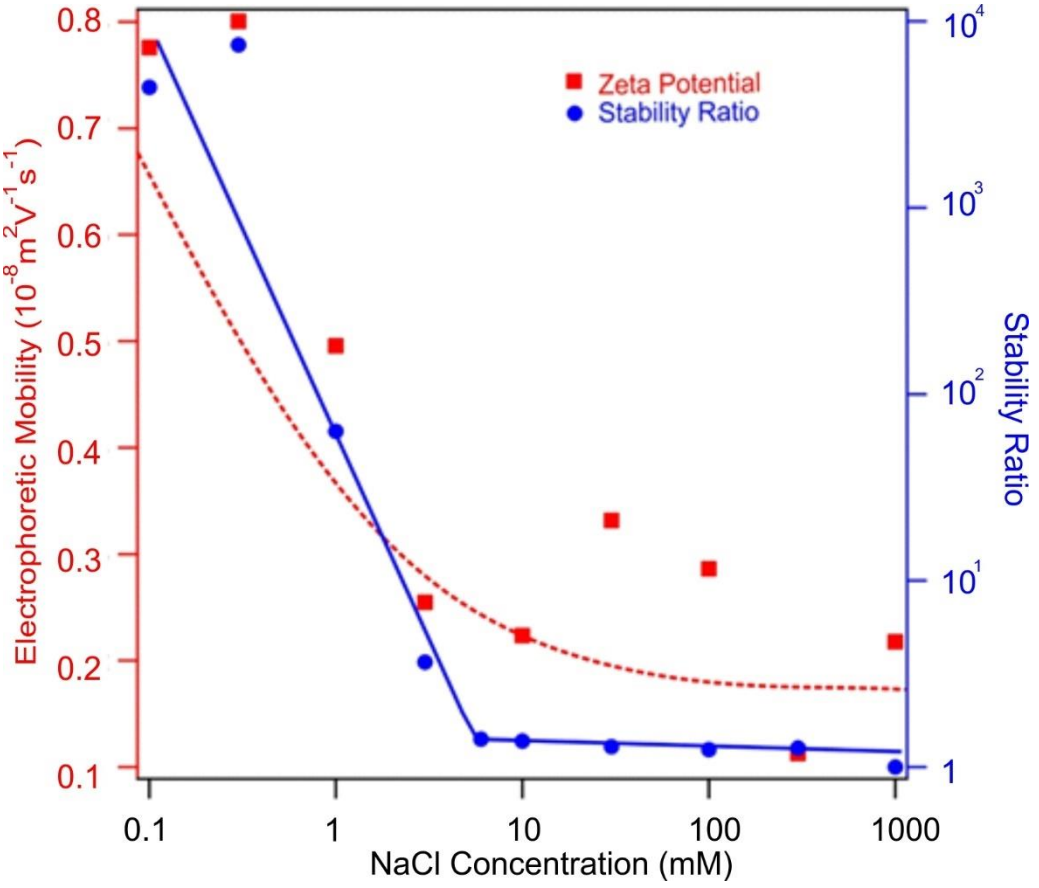

Figure 19. Zeta potential (squares) and stability ratio (circles) values of MgAl–LDH particles as a function of NaCl concentration. The dashed line is the result of calculation using the Debye-Hückel equation.[121]

By knowing these properties of the LDH, a colloidal approach was applied to optimize the SDS concentrations and other synthesis conditions. The aggregation and charging properties were followed as a function of the SDS concentration. At low surfactant doses, the measured zeta potentials were slightly positive due to the structural charge of the particles (Figure 20). As the SDS concentration was increased, the mobility values decreased due to the adsorption of the SDS on the oppositely charged LDH surface leading to charge neutralization at the IEP. For a 10 mg/L LDH particle dispersion, this value was 0.03 mM. Further increase in the surfactant dose led to charge reversal leading to highly negative mobility values.

The colloidal stability was again assessed in time-resolved DLS measurements. At SDS doses around the IEP, unstable dispersions were observed, while at surfactant concentrations far from the IEP value, considerable stability was detected (Figure 20). This trend is in line with the DLVO theory indicating that forces of electrostatic origin are dominating. Accordingly, SDS behaved similarly as seen before in case of polyelectrolytes. Such a strong adsorption of SDS and its corresponding effect on particle aggregation has never been reported in the past.

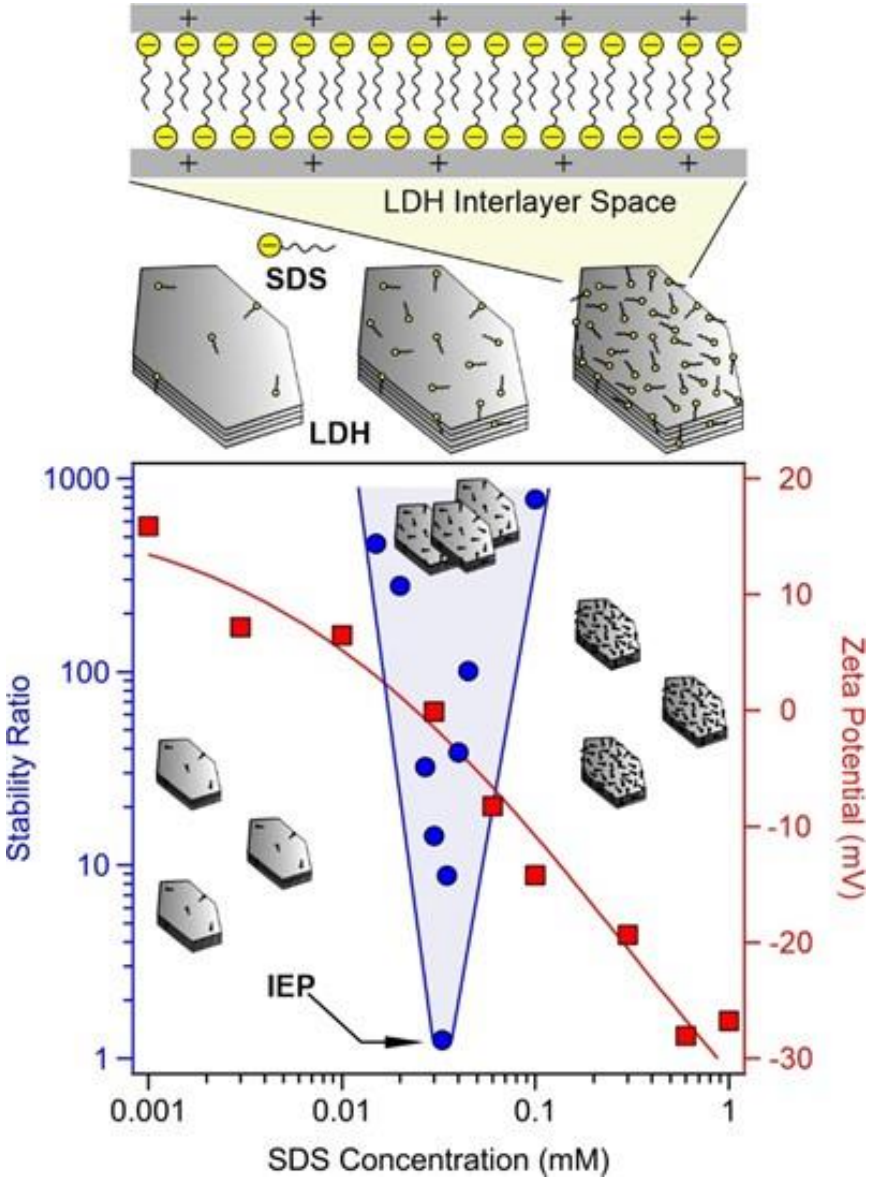

Figure 20. Zeta potentials (squares) and stability ratios (circles) of MgAl–LDH particles as a function of the SDS concentration in aqueous dispersions. The solid lines are eye guides, and the upper scheme illustrates the assumed SDS bilayer formation between the lamellae.[121]

On the basis of these results, three different surfactant concentrations were chosen for the synthesis of the porous LDH material (3.0, 10.0 and 30.0 mM). The zeta potential and stability ratio values were measured at 10 mg/L, however, the concentration of the LDH was enlarged 100 times in the synthesis and since the SDS concentrations were also enlarged accordingly. At 3 mM dose, an unstable dispersion forms due to the SDS concentration close to the IEP. The 10 mM value was chosen owing to the proximity of the critical micelle concentration of the SDS, what is 8 mM.[122] The last chosen dose (30 mM) was at very negative zeta potentials because of the charge reversal by the surfactant adsorption, which led to a highly stable dispersion.

A novel approach was carried out to synthesize mesoporous LDH materials with the help of the surfactant adsorption. The as-prepared LDH was added into three SDS solutions of different concentrations, as indicated above. The SDS-modified products were calcined to remove SDS content and rehydrated to gain LDH structure due to the 'memory effect', discussed earlier.

5.3.1.2. XRD study

As a first step of the structural characterization, XRD patterns of the SDS_3-LDH, SDS_{10}-LDH, SDS_{30}-LDH and the unmodified (prepared without added SDS) MgAl-LDH were recorded (Figure 21). The structure of the MgAl- LDH is regular according to the peak positions. The *003* and *006* reflections appeared in all the materials as a signal of the layered structure. In case of the surfactant treated LDHs, new peaks appeared and pronounced staging effect was observed with increasing the SDS dose. These changes indicated the presence of a new LDH phase. The appearance of the 003' and 006' peaks as well as the disappearance of the 003 one is clearly due to the increasing SDS concentration. Beside the appearance of the 003' and 006' peaks, a new band appeared around 20° at higher surfactant doses, which can be originated from the joint effect of complex multiple staging and different water content.

From the Bragg equation, the interlayer distances were calculated. In case of SDS_3-LDH this value was 0.77 nm, which is similar to other chloride containing MgAl-LDHs.[3] SDS_{10}-LDH is a two-phase material due to the coexistence of the 003 and 003' peaks and the interlayer distances were 0.77 and 2.52 nm, respectively. The interlayer distance could only be calculated from the 003' peak for SDS_{30}-LDH with a value of 2.76 nm. These data clearly show that with increasing the dose of the surfactant, it tends to intercalate between the layers leading to the formation of pillared material.

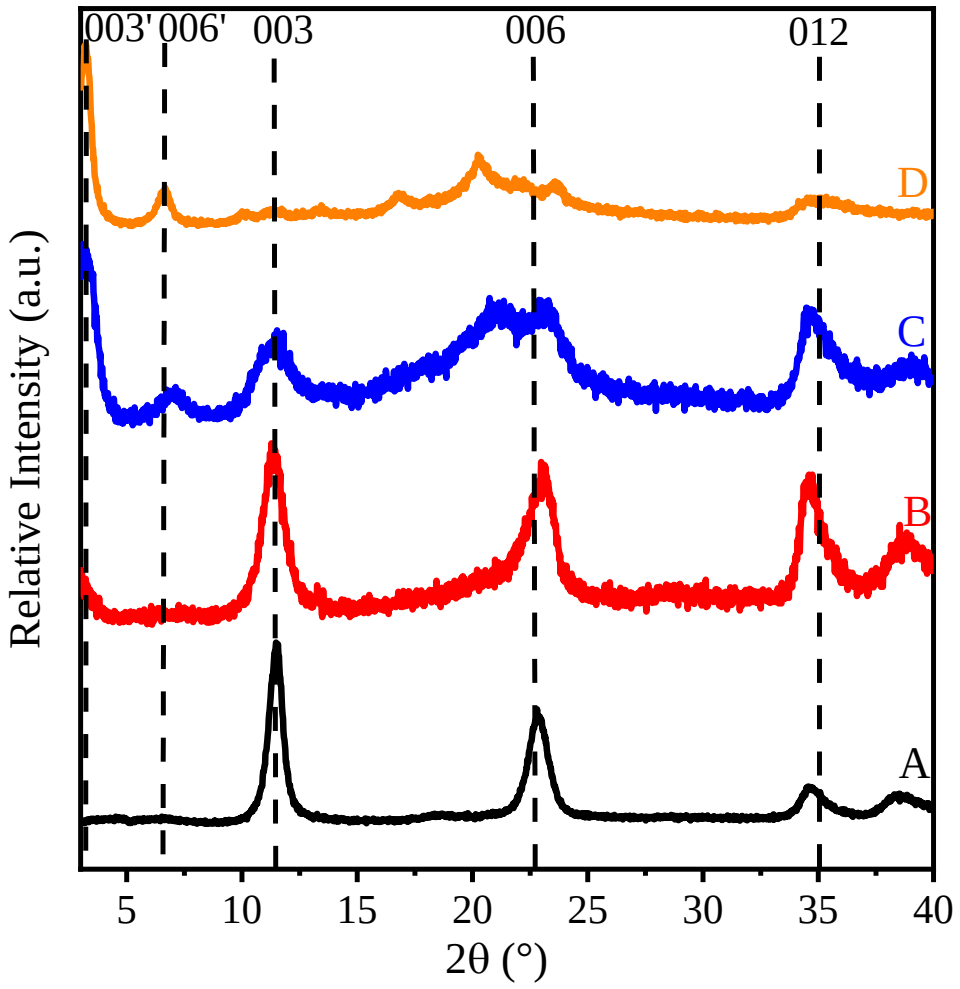

Figure 21. XRD patterns of (A) MgAl–LDH, (B) SDS_3–LDH, (C) SDS_{10}–LDH and (D) SDS_{30}–LDH precursor composites.[121]

The diffractograms of SDS-LDH composites were recorded after the calcination-rehydration treatment as well as the original structure of the LDH before the treatments (Figure 22). According to the results, the reconstruction of the structure was successful. The XRD patterns showed the presence of a single-phase material and the interlayer distances indicated the incorporation of chloride and/or carbonate anions, while the SDS content was eliminated proven by the disappearance of the peaks from the SDS intercalated phase.

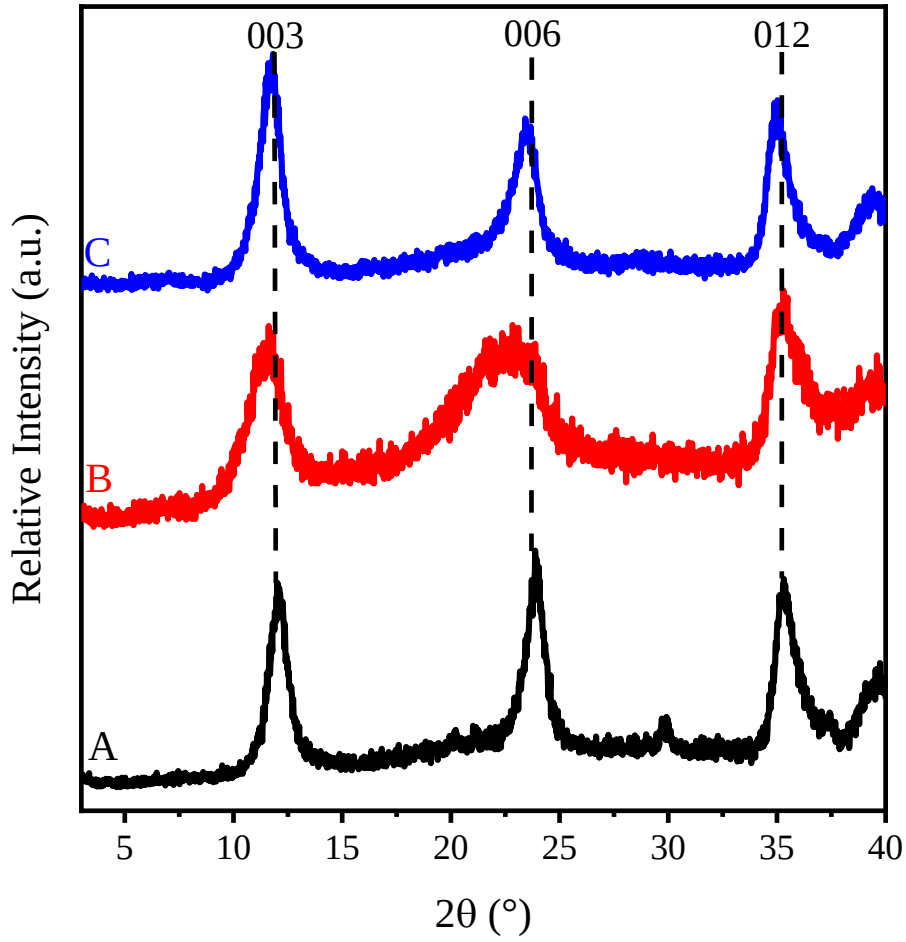

Figure 22. XRD patterns of (A) LDH_3, (B) LDH_{10} and (C) LDH_{30} obtained after rehydration of the corresponding calcinated precursors.[121]

5.3.1.3. Characterization by IR

The IR spectra of the bare and SDS-modified (before calcination) LDH materials and the spectrum of the SDS were recorded (Figure 23). The MgAl-LDH spectrum showed the typical peaks reported earlier for LDH material.[1] Characteristic bands can be observed due to the intercalation and adsorption of the surfactant. The following peaks refer to the surfactant: ν_{as}(CH) 2922 cm^{-1}, ν_{sym} (CH) 2855 cm^{-1}, (CH) (1468/1366 cm^{-1}), ν_{as}(1220 cm^{-1}) and ν_{sym} (S=O) (1071 cm^{-1}). All the characteristic peak assignments can be found in Table 3.

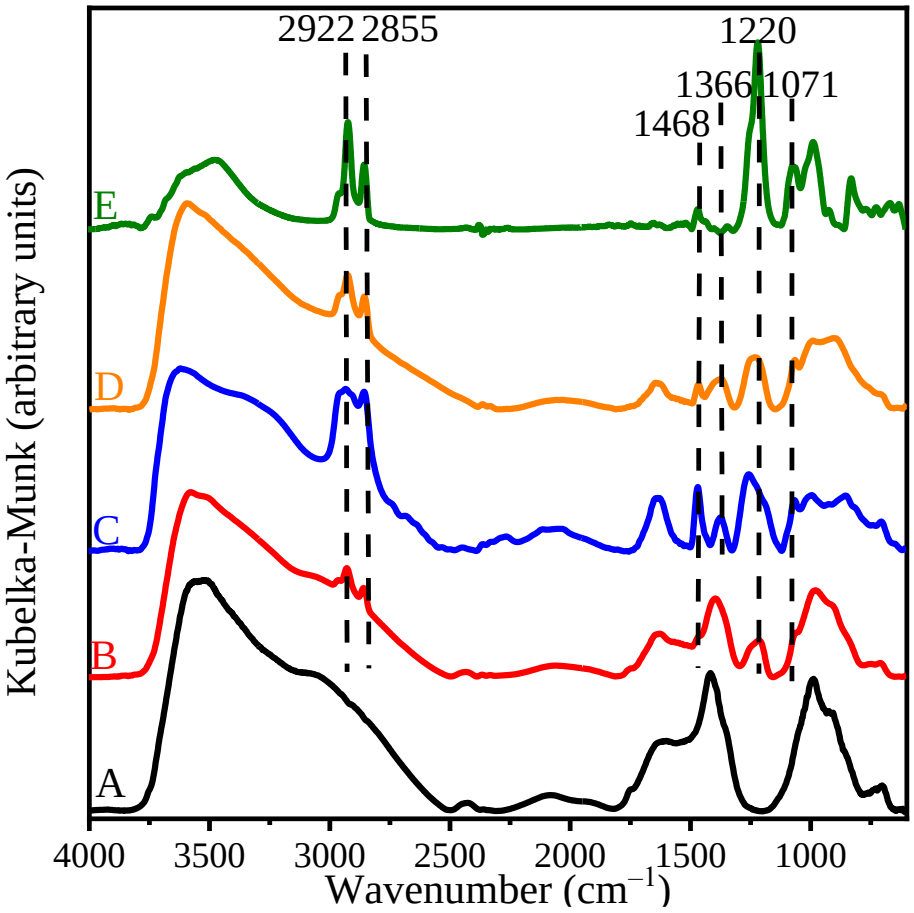

Figure 23. IR spectra of (A) MgAl–LDH, (B) SDS_3-LDH, (C) SDS_{10}-LDH, (D) SDS_{30}-LDH and (E) SDS.[121]

The IR spectra were recorded for LDH materials with restored structure too. In these spectra, only two types of characteristic vibration bands were identified. Namely, the peaks at 992 and 1426 cm^{-1}, which vibrations can be assigned to the surface-adsorbed carbonate ion and peaks at 1638 and 3535 cm^{-1} were assigned to the water content. Comparing these spectra to the ones recorded before the calcination-rehydration process, the peaks referring to organic compounds did not appear proving that the SDS content was eliminated during the calcination process. These results correspond to the findings of the XRD measurements, as a clear proof of the removal of SDS leading to a template-free LDH material.

Table 3. Assignment table of IR peaks present in LDH and SDS-LDH materials

Position (cm^{-1})	Assignment	Component	Reference
3600-3000	H-bonded ν(OH)	water in LDH-SDS	2,123,124,125
2920, 2850	ν_{as}, ν_{sym}(CH)	DS in/on LDH	124,125
1630-1650	β(OH)	water in LDH	2,123
1470-1460 1380-1370	δ(CH)	DS in/on LDH	123,125
1420-1410	$\nu_3(CO_3^{2-})$	surface adsorbed CO_3^{2-}	126
1225-1210	ν_{as}(S=O)	DS in/on LDH	124,125
1060	ν_{sym}(S=O)	DS in/on LDH	124,125
1000-990	$\nu_2(CO_3^{2-})$	surface adsorbed CO_3^{2-}	126

5.3.1.4. Electron microscopy investigation

The LDH samples before and after the calcination-rehydration process were imaged with SEM and TEM. In case of SEM measurements, the LDH_{30} and SDS_{30}-LDH were investigated (Figure 24). The image of the SDS_{30}-LDH sample showed aggregated particles of non-defined structure. LDH_{30} had a detailed structure with smaller particles as a results of the calcination-rehydration process, indicating higher porosity.

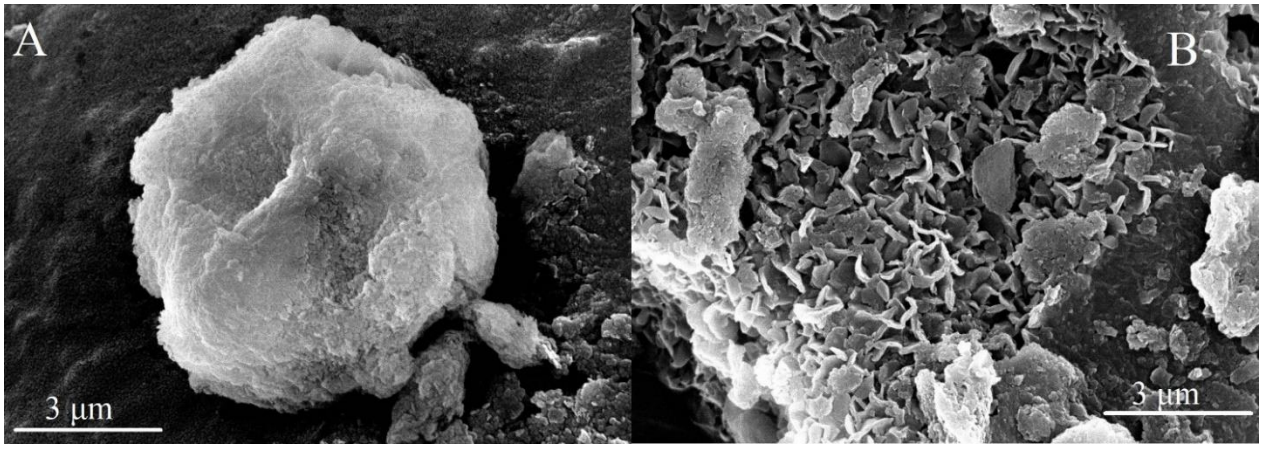

Figure 24. SEM images of (A) SDS_{30}-LDH and (B) LDH_{30} materials.[121]

TEM images were recorded for all three LDH samples after the rehydration process (Figure 25). All samples contained mesoporous holes with different widths. With increasing SDS dose in the samples, the formation of mesopores was more definite. Around the cavities, the LDH sheets were in vertical position, which finding might indicate the location of an LDH shell around the template before calcination. The hierarchical structure appeared in the samples and was also dependent on the SDS dose. In case of LDH_3 there is no sign of such property, while in case of LDH_{10} and LDH_{30} the hierarchical structure was present, however, in a more pronounced way in the latter case. These results shed light on that high colloidal stability of the precursor material play an important role in the formation of the final material.

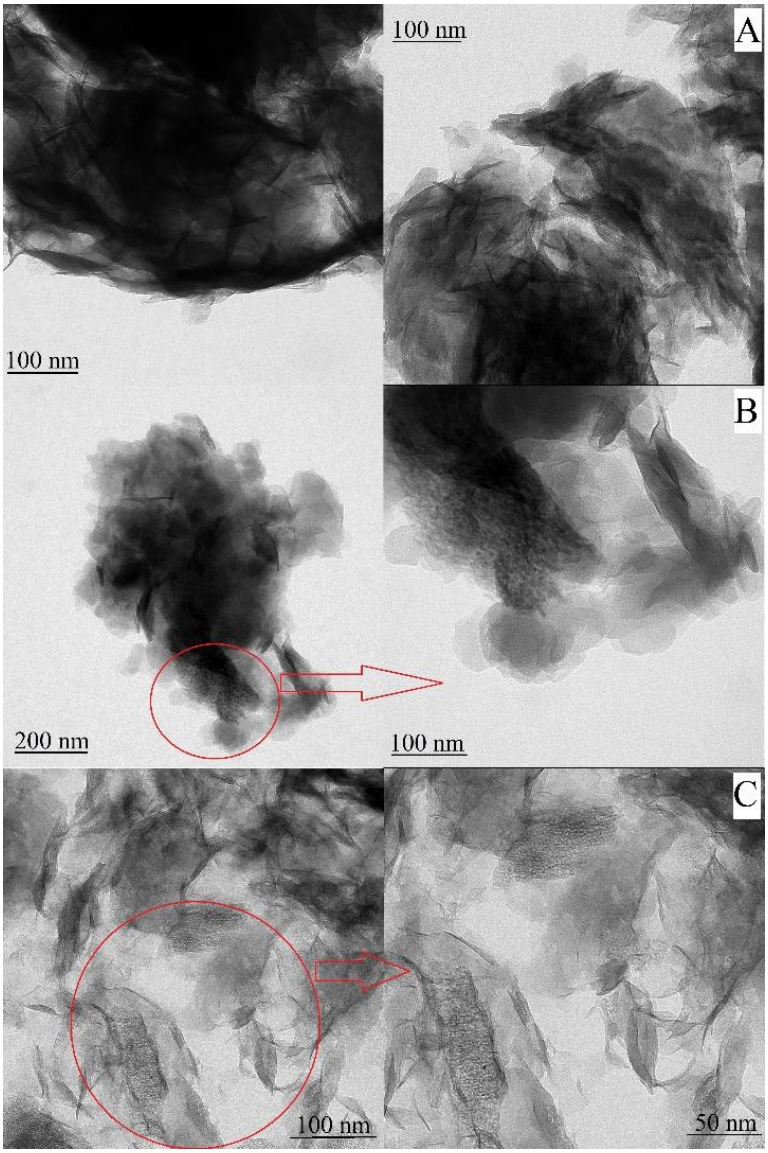

Figure 25. TEM images of (A) LDH_3, (B) LDH_{10} and (C) LDH_{30} rehydrated materials.[121]

5.3.1.5. Porosity of the LDHs

Specific surface area and pore diameter distribution are crucial fundamental information in case of porous materials. BET measurements were carried out to assess these features in N_2-adsorption/desorption experiments. Type IV isotherm was observed in all cases with a H3 type hysteresis loop indicating the presence of mesopores,[127] as shown in Figure 26 for the final materials.

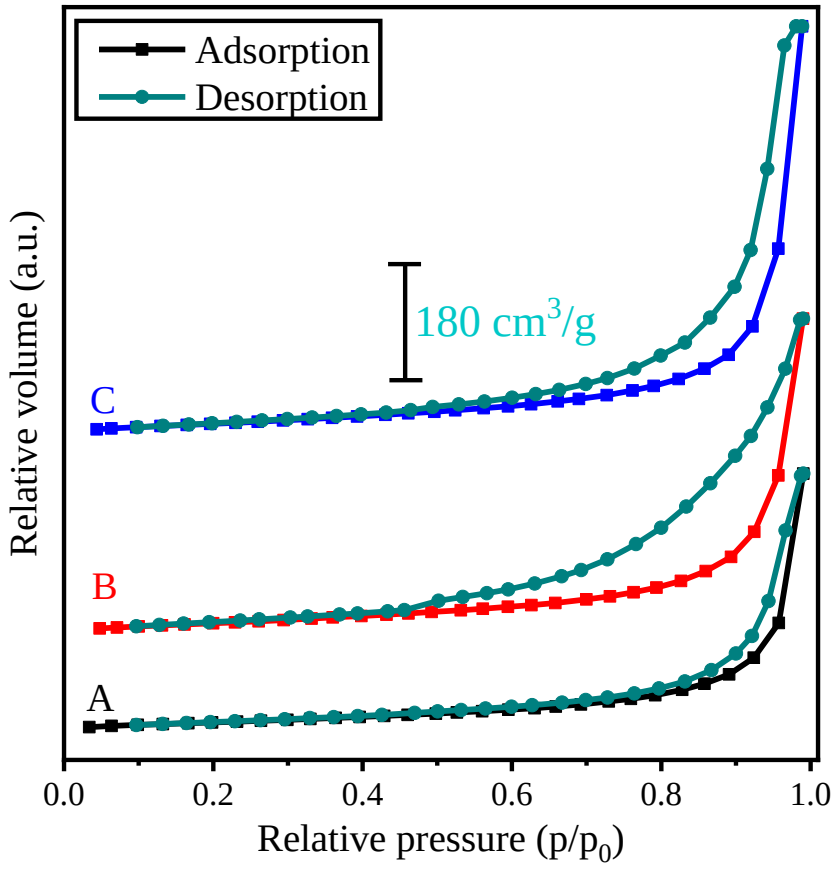

Figure 26. N_2 sorption isotherms of (A) LDH_3, (B) LDH_{10} and (C) LDH_{30} materials.[121]

The surface area and pore volume values increased in the following order: LDH_{30} > LDH_{10} > LDH_3 (Figure 27). This proves that the increasing surfactant concentration during the synthesis leads to higher surface area and more advanced porosity. This is due to the SDS adsorption effect on the LDH surface charge and aggregation properties, i.e., the more stable precursor dispersions lead to more porous materials. Also, the SDS content can go through gaseous thermal decompositions caving well-defined pores and channels during calcination into the LDH and thus, increases the surface area. These results fit the information gained from SEM images.

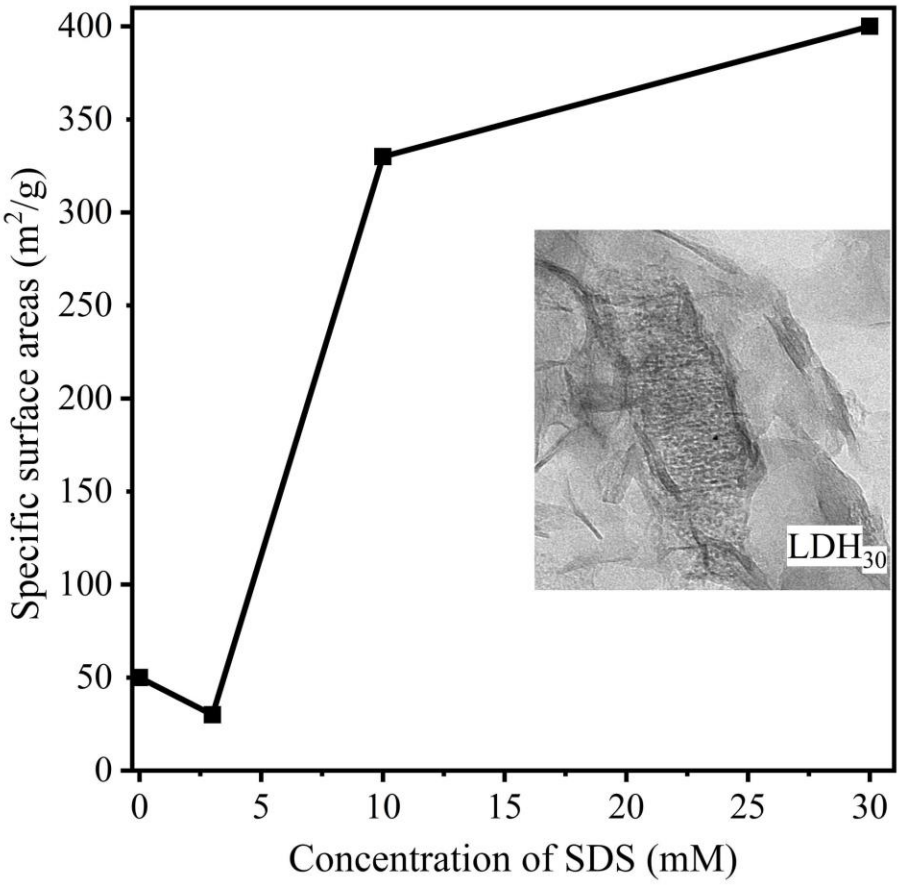

Figure 27. Specific surface area values as a function of SDS concentration applied. The TEM image of LDH_{30} is shown in the inset.[121]

Comparing the base LDH and LDH_{30}, significant differences can be observed, as the surface area is 8 times and the total pore volume is 48 times higher for the latter case (Table 4). Taking a look at previous reports on single phase LDH materials, the determined values for LDH_{30} are close or even higher compared to the earlier reported best values.[128,8,129,12,130,131,132,133,134]

Table 4. Specific surface area and pore diameters of LDH materials

Composites	Main mesopore diameter (nm)	Other mesopore diameter (nm)	Specific surface (BET) area (m^2/g)	Total pore volume (cm^3/g)
MgAl-LDH	–	–	50±23	0.0054
LDH_3	3.5	–	30±16	0.1309
LDH_{10}	3.9	4.5-17.8	330±9	0.2215
LDH_{30}	3.8	5.2-47.8	400±8	0.2553

A complete mesopore distribution was observed in the range of 3.5-50.0 nm. The pore diameters around 4.0 nm can be partially related to the tensile strength effect, which may distort the pore size distribution in that region. High dV/dr values refer to the formation of hierarchically porous structures in all cases (Figure 28).

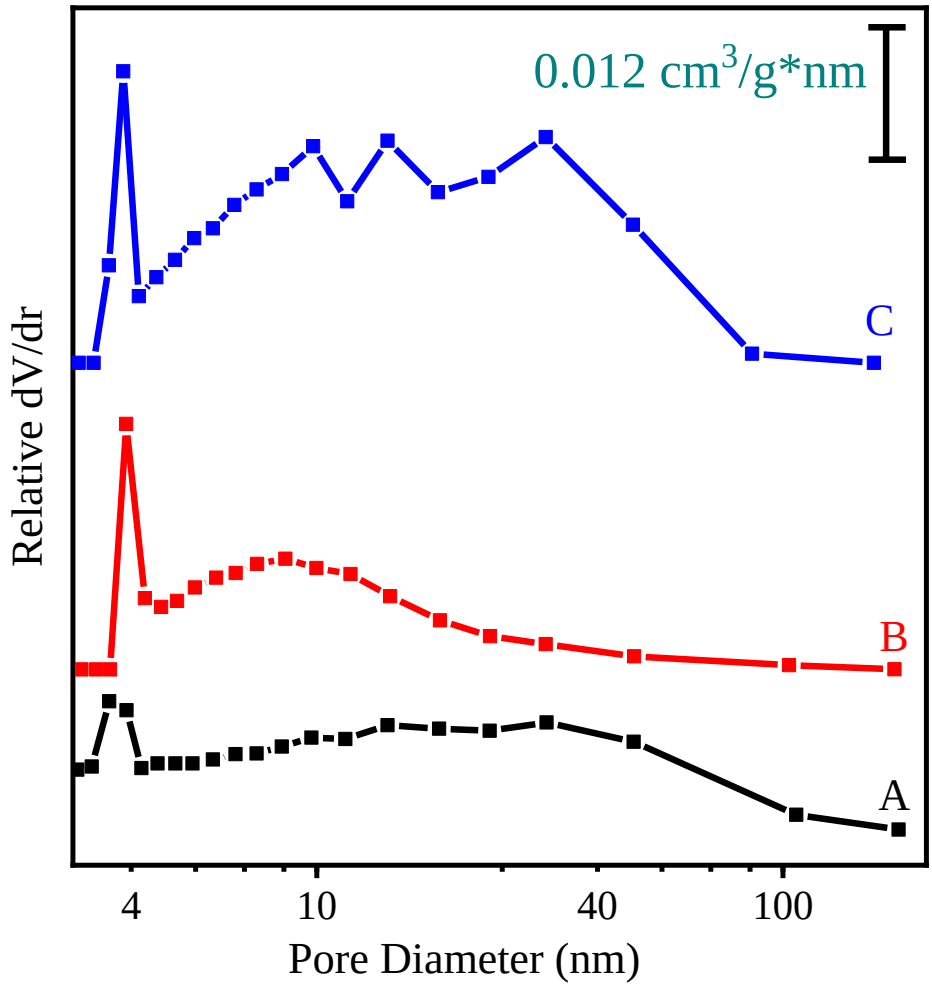

Figure 28. Pore diameter distribution of (A) LDH_3, (B) LDH_{10} and (C) LDH_{30}. The data were calculated from the desorption part of the sorption isotherms.[121]

These findings also prove that SDS adsorption and colloidal stability of the precursor materials play an important role in the formation of the final structure. The developed structures showed higher porosity and advantageous hierarchical structure if the feeding material for the calcination-rehydration process formed a stable dispersion. This can be clearly seen in case of SDS_{30}-LDH, where homogeneously distributed precursor particles of high negative charge were

present leading to the formation of novel material with the most beneficial properties for adsorbent applications.

5.3.2. Removal of anions from aqueous samples

A widespread application area for high specific surface area materials is their use as adsorbents in wastewater treatment.[29] The materials obtained in the present study were tested for the adsorption of nitrate and dichromate.

Removal of nitrate is important since in natural waters its presence leads to adverse effects of nitrification.[135] The materials showed remarkable nitrate adsorption capacity in all cases investigated. The adsorbed amount of nitrate was independent from the pore distribution and the surface area of the materials. The adsorption process was quantified in equilibrium with the following formula:

$$q_e = \frac{(c_0 - c_e)V}{m} \quad (7)$$

where c_0 is the initial mass concentration of anion in solution, c_e is the equilibrium concentration, q_e is the equilibrium sorption capacity, m is the mass of adsorbent and V is the volume of the solution.

The Langmuir model was used to fit the adsorption isotherms and to determine the maximum adsorbed amount of contaminant as follows:

$$\frac{c_e}{q_e} = \left(\frac{1}{K_L} q_m\right) + \left(\frac{c_e}{q_m}\right) \quad (8)$$

where q_m is the theoretical maximum monolayer sorption capacity and K_L is the Langmuir sorption constant.[136] 104 mg/g was the maximum amount of nitrate that could be absorbed on the LDH_{30} material (Figure 29).

For LDH_{30}, the sorption capacity was 749.7 mg/L, which is the highest ever reported value for single-phase LDH materials.[137,138,139,140,141]

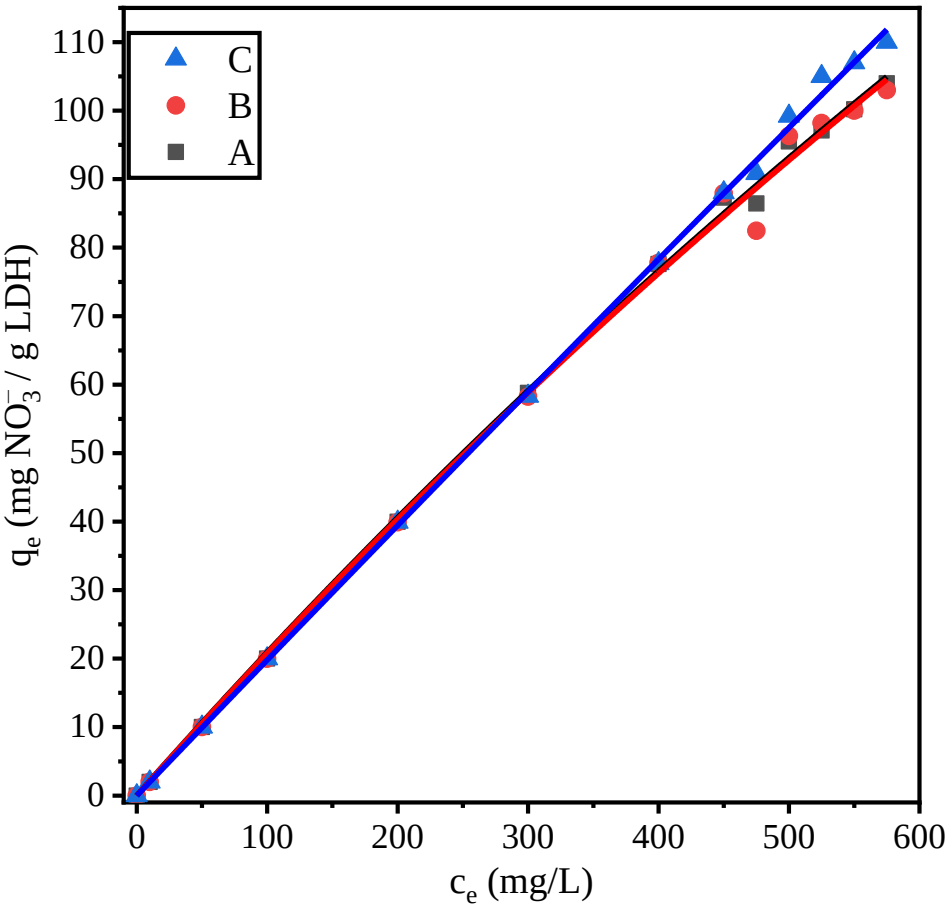

Figure 29. Nitrate ion adsorption isotherms of (A) LDH_3, (B) LDH_{10} and (C) LDH_{30}. The solid lines indicate the calculations using the Langmuir method.[121]

Such a high value can be explained by the XRD patterns recorded at various nitrate concentrations after the adsorption took place (Figure 30). The change in the peaks indicates a staging effect and the intercalation of the nitrate ions. In case of the pristine LDH, the typical LDH peaks can be observed. The shift in case of 200 mg/L refers to a two-phase material, in which probably some of the LDH is intercalated with nitrate, while a part still possesses the original structure. In case of 400 mg/L, only one shifted peak can be observed, all of the material went through ion exchange and intercalation by the nitrate ions. This proves that the nitrate not only adsorb on the porous outer surface of the LDH, but the adsorption of the nitrate is also enhanced by the intercalation.

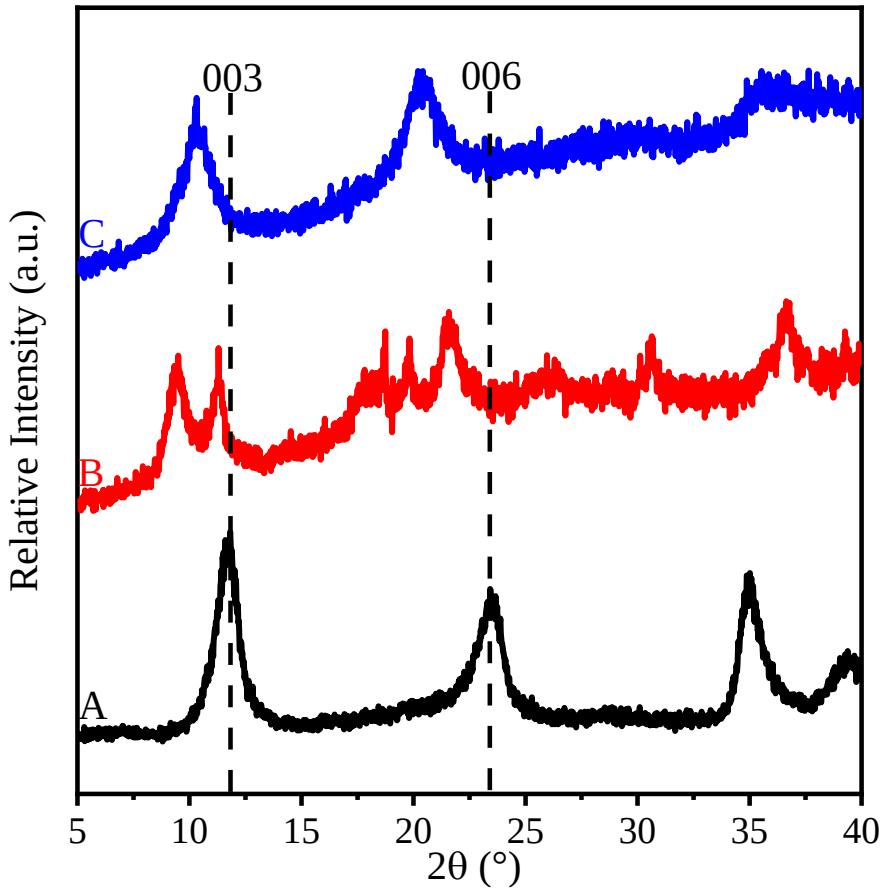

Figure 30. XRD patterns of LDH_{30} after nitrate adsorption experiments (nitrate concentrations were A: 0 mg/L, B: 200 mg/L and C: 400 mg/L).[121]

Dichromate ion was also studied to assess contaminant removal and adsorption capacity of the obtained materials. Dichromate is a well-known carcinogenic polluttant[142] and $Cr_2O_7^{2-}$ was the predominant species under the conditions applied. The adsorption capacities showed dependency on the specific surface area and the pore size distribution (Table 4 and 5). Higher surface area and larger pores led to a more efficient removal in case of LDH_{30} since its larger pores are more favourable for the dichromate ion adsorption. This effect can only be seen in case of dichromate since its hydrated size is bigger than in the case of nitrate ions and dichromate ions most likely cannot diffuse into the smaller pores.

Sorption isotherms were calculated for the dichromate adsorption process (Figure 31). Both Langmuir and Freundlich models were applied, however, the first method fitted better the experimental data (Table 5). LDH_{30} showed a capacity of 388.8 mg/L, what is the highest among

the published single-phase LDH compounds[84,143,144,145,146,147,148,22,149,150,151,152,153,154,155] and is comparable to industrially used adsorbent materials.[156,157,158,159,160,161]

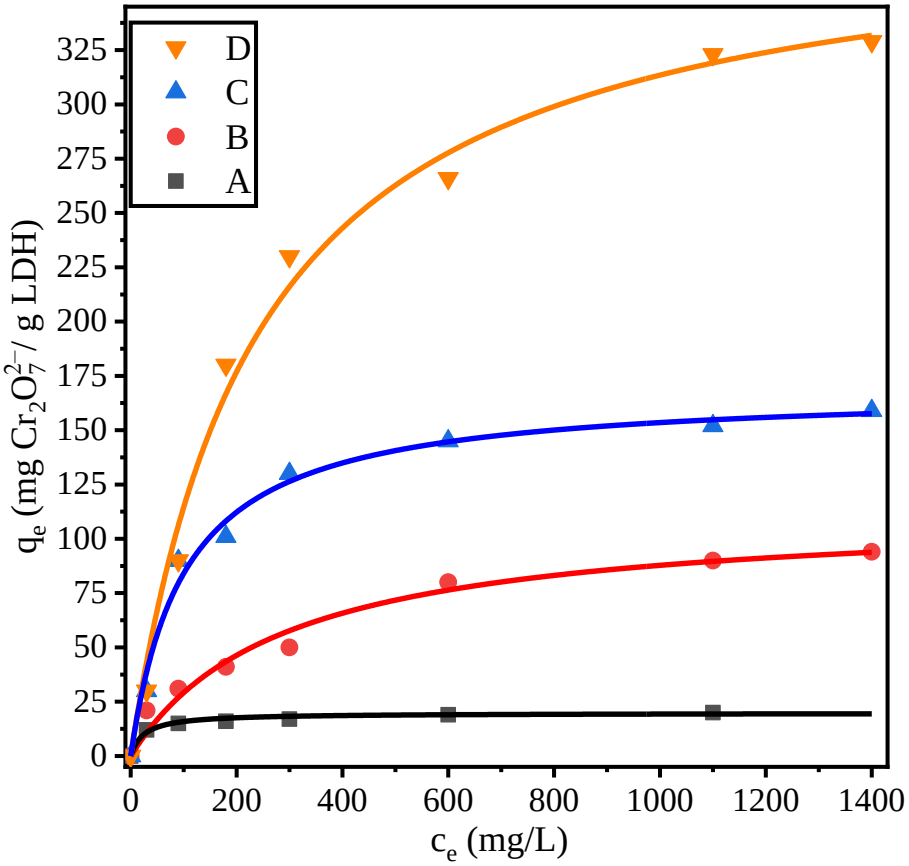

Figure 31. Dichromate ion adsorption isotherm of (A) MgAl–LDH, (B) LDH_3, (C) LDH_{10} and (D) LDH_{30}. The solid lines are fits using the Langmuir model.[121]

Table 5. The parameters of the isotherms for dichromate adsorption

	Langmuir		Freundlich	
Adsorbent	**q_m (mg/g)**	**K_L (10^{-3} L/mg)**	**n**	**K_F (L/g)**
MgAl–LDH	19.8	41.0	2.5	2.0
LDH_3	113.1	3.5	3.7	13.9
LDH_{10}	169.0	9.9	4.8	24.0
LDH_{30}	388.5	0.4	6.3	36.2

The XRD patterns were recorded also for the dichromate exchanged materials. They showed increased interlayer distances indicating the intercalation of the dichromate. The XRD patterns were recorded for the regenerated materials too, where the interlayer distance decreased back to the original value proving the successful elimination of dichromate upon regeneration. The crystallinity of the samples reduced after each reaction cycle, as indicated by the change in the sharpness of the peaks comparing both the pristine LDH with the regenerated LDH and comparing the chromate adsorbed LDH after the second and fifth reaction cycles (Figure 32).

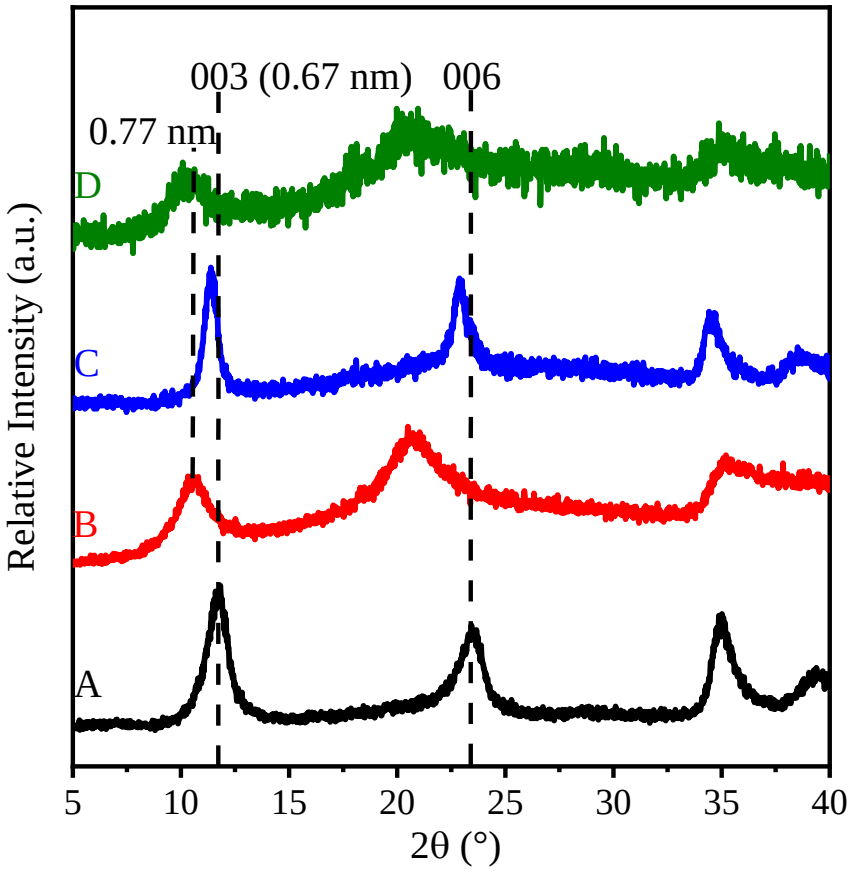

Figure 32. XRD patterns of (A) as-prepared LDH_{30}, (B) LDH_{30} after second use, (C) regenerated LDH_{30} after second use and (D) LDH_{30} after the fifth reaction cycle.[121]

As mentioned above, the recyclability of the materials was tested by regenerating after the dichromate adsorption in concentrated (3M) NaCl solution. The adsorption isotherms were recorded after the regeneration for comparison. After 5 cycles, only a small decrease was observed in the adsorption capacity showing good recyclability of the material (Figure 33).

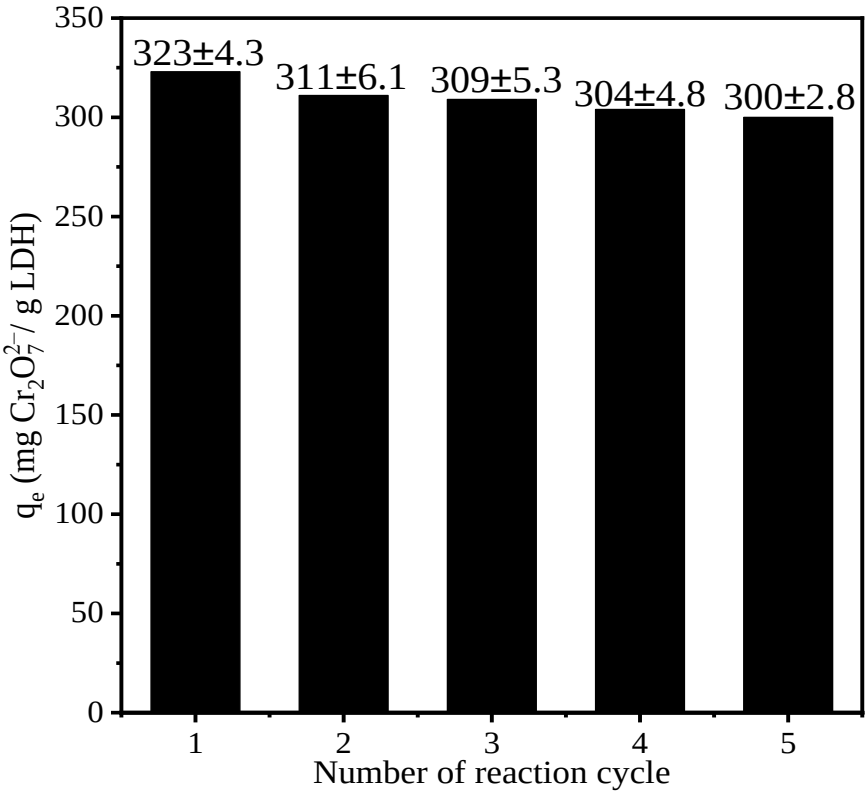

Figure 33. Regeneration of LDH_{30} adsorbent for 5 consecutive cycles indicated by the adsorption capacities for dichromate ions.[121]

Summarizing, a high specific surface area porous LDH material was developed with SDS treatment. The treatment to gain this material was based on experiments on the effect of SDS adsorption on the surface of the LDH particles and its effect on colloidal properties. The developed material was highly effective in removal of dichromate and nitrate ions from model solutions.

5.4. Wastewater treatment with LDH colloids

Removal of contaminants from wastewaters is a major challenge in environmental chemistry, as discussed also in the previous chapter. Maximising the recovery of treated water is a crucial point as well from both economic and environmental aspect. LDH-type materials have been investigated for a long time as adsorbent in wastewater treatment processes.[86] However, most studies were carried out in model systems instead of real wastewaters and the efficient separation of the LDH was not comprehensively studied in many reports. Since small particles and aggregates can be present after the remediation due to the fact that wastewater can be a suitable medium to form a stable dispersion.

In our work, *in* and *ex situ* LDHs were prepared both in model systems and in acidic mine wastewater received from Boddington Gold Mine, Australia as a cooperation with CSIRO. The removal of contaminants was investigated and separation of the LDH was carried out after the treatment.

5.4.1. Characterization

Samples

Four different samples were prepared and studied to examine them from the point of colloidal stability in order to gain better understanding of the behaviour LDH-like materials. Two types of LDH samples were formed with coprecipitation method in the treatment of an acidic mine water in an *in situ* way and two model LDH-like samples were prepared in an *ex situ* way and investigated. The preparation of samples is detailed in chapter 4.6. The samples were characterized with various techniques to gain structural information.

5.4.1.1. XRD analysis

The XRD patterns were recorded for all samples. In case of sample 1, the presence of brucite was dominant with minor presence of LDH forming (Figure 34 (a)). Sample 4 also formed in a model system, the gained material was quintinite, an LDH type material (Figure 34 (d)).[162] Sample 2 and 3 were both composed in acidic mine water. Sample 2 shows pure LDH phase (Figure 34 (b)), while in case of sample 3 both brucite and LDH are present indicating the added $Mg(OH)_2$ was only partially used in the LDH formation (Figure 34 (c)). Both sample 2 and 3 showed poor crystallinity.

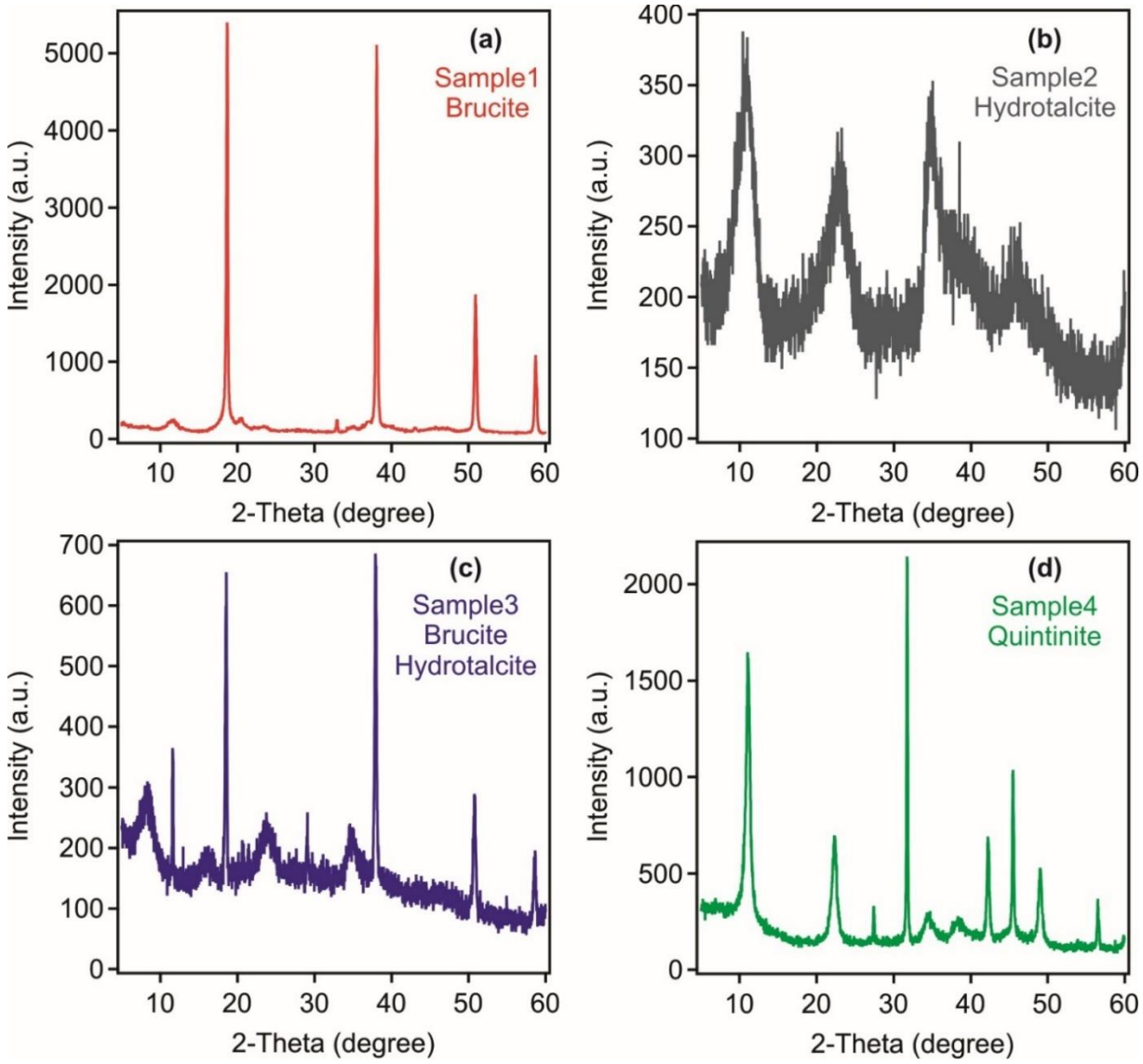

Figure 34. Powder XRD patterns of the solid materials obtained from (a) sample 1, (b) sample 2, (c) sample 3 and (d) sample 4.[163]

5.4.1.2. IR study

IR analysis was also carried out to gain information on the adsorbed and intercalated compounds. All samples showed the common peaks for LDH materials. Accordingly, the peak at 1365 cm^{-1} can be assigned to the asymmetric stretching of carbonate[123] in sample 1,2,3, while in sample 4 this is shifted towards higher wavenumbers (Figure 30 (a-d)). The peak around 1635 cm^{-1} corresponds to the scissor vibration of the interlayer located water.[123,124] At 3400 cm^{-1}, the band corresponds to the valence vibration of O-H groups of water molecules.[2,123,124] In sample 2 and 3 another peak can be observed around 1090 cm^{-1} corresponding to the sulfate symmetric stretching

vibrations,[124,125] which refers to the intercalation or adsorption of sulfate on the outer surface (Figure 30 (b,d)).

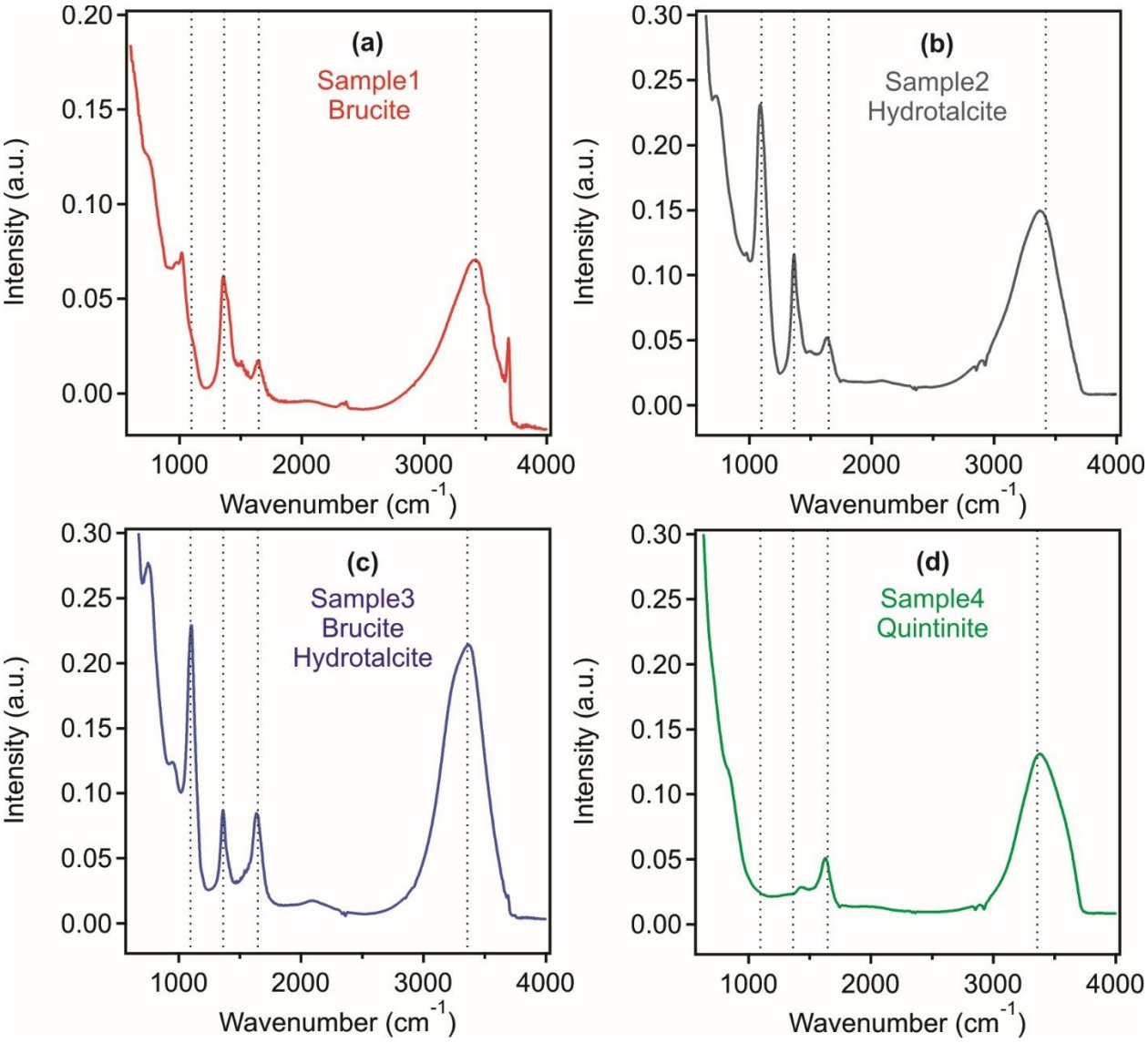

Figure 35. IR spectra of (a) sample 1, (b) sample 2, (c) sample 3 and (d) sample 4.[163]

5.4.1.3. Microscopy imaging

The morphology of the formed LDH materials was investigated with SEM. All samples contained primary particles of a few hundred nanometers in diameter forming bigger aggregates in the micron range (Figure 36 (a-d)). The particles showed irregular morphology, what is common in case of MgAl LDHs. In case of sample 3, crystals of different morphology were present in the material (Figure 36 (c)), which is in line with the XRD results that indicated the presence of both LDH and brucite.

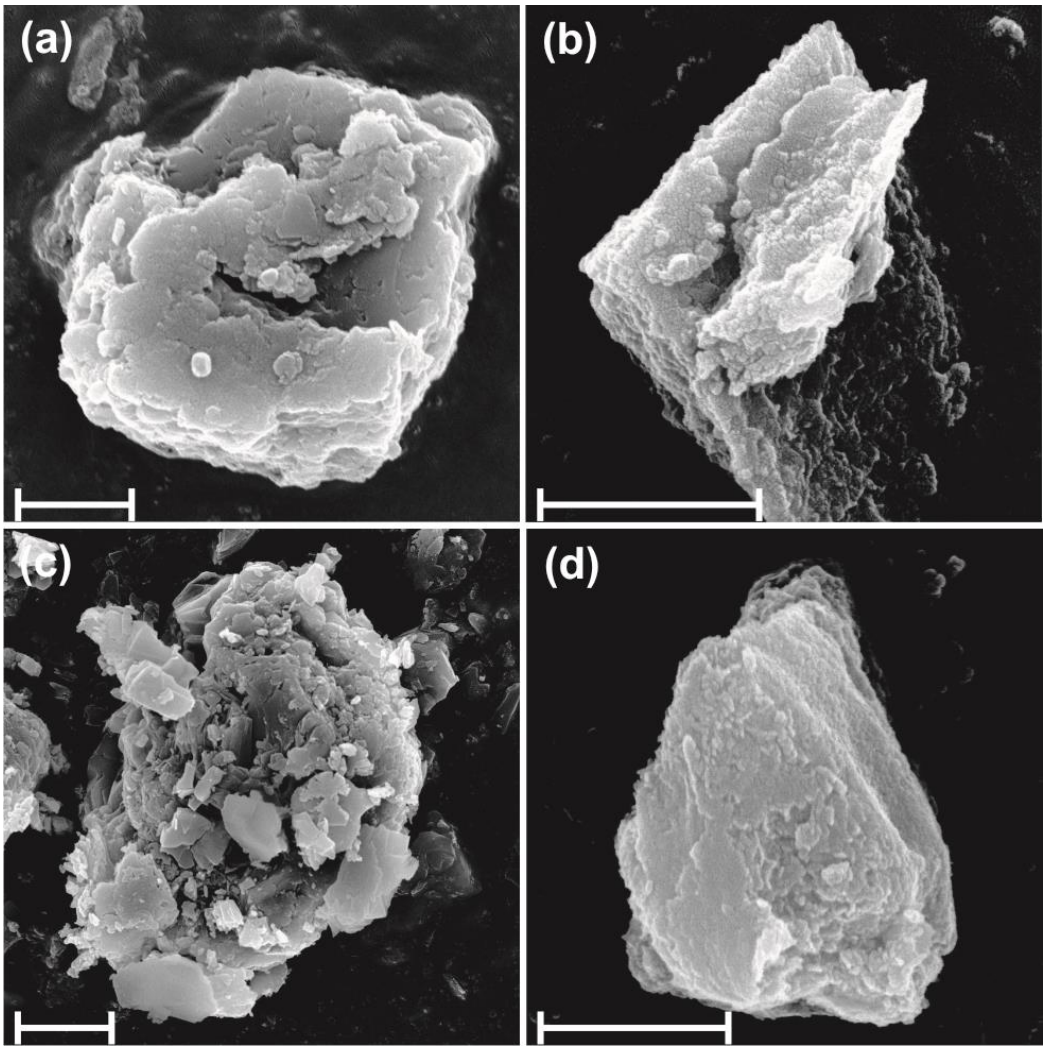

Figure 36. SEM images of (a) sample 1, (b) sample 2, (c) sample 3 and (d)sample 4. The scale bars indicate 1 micrometer dimension.[163]

SEM-EDX measurements were carried out to assess the composition of the materials (Figure 37). The size of the particles correlates with the sizes observed on the SEM images in the micrometer range as another proof of forming LDH aggregates. Uniform distribution of Mg, Al and O in the particles can be observed in all samples proving that all of our samples contain LDH phase. Analysis of sample 2 and 3 clearly indicated the presence of sulfate within the particle, which correlates to the IR results. The fact that the sulfate is concentrated in the particles is another proof that the *in situ* formation of LDH lead to the adsorption and removal of sulfate. In the *in situ* samples no other characteristic peak was observed other than sulfate and carbon, which is due to the adhesive material used to fix the samples. The adsorption of sulfate is specific from the

wastewater. In case of sample 4 the presence of chloride is owing to the interlayer chloride, which originates from the preparation of the material from metal-chloride salts.

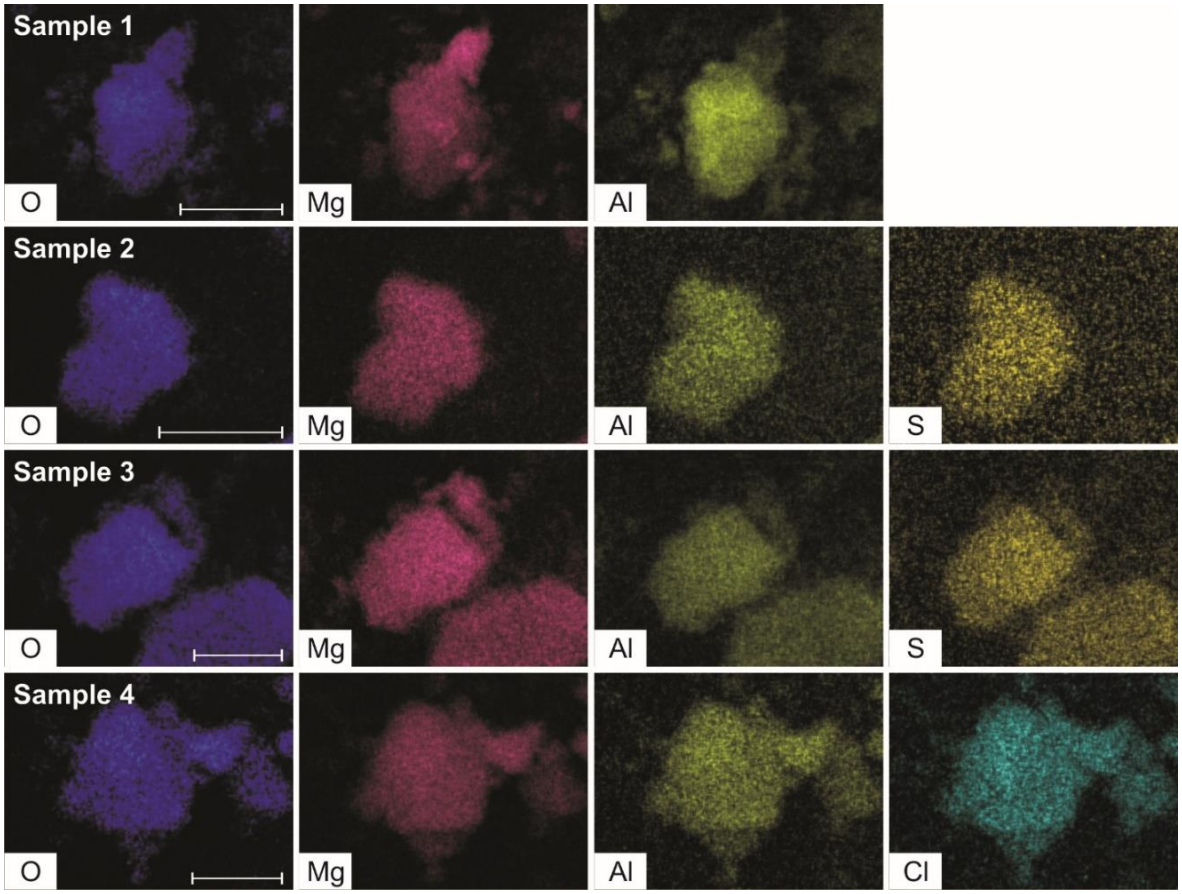

Figure 37. Elemental distribution images in sample 1-4 determined by SEM-EDX measurements. The scale bars refer to 3 µm distance.[163]

5.4.2. Separation of LDH materials by flocculation agents

Surface charging and aggregation processes are closely related according to DLVO theory.[39] Small particles of significant charge usually do not sediment out of the dispersion, but in case of bigger aggregated particles this is possible. Polyelectrolytes and multivalent ions have been used for influencing the charging properties in wastewater treatment as flocculation agents for long time.[49] Due to the structural positive charge of the LDH layers, negatively charged PSS, dextran sulfate (DXS) and phosphate ions were used in different concentrations to tune charging features and subsequently, to aggregate and sediment the solid materials in the treated wastewater.

First, electrophoretic mobility measurements were carried out at different polyelectrolyte and phosphate concentrations. Slightly positive mobility values were measured in case of sample 1 (Figure 38 (a)) and 3 at low doses (Figure 38 (c)), while in case of sample 2 and 4 the mobilities

were close to zero (Figure 38 (b,d)) even at low doses of the flocculants. Such low values are presumably the result of the high ionic strength (*ca.* 80 mM) leading to screening of the surface charge. The adsorption of the negatively charged species led to charge reversal of the solid materials through the IEP. The most effective charge reversal and most negative electrophoretic mobilities occurred in case of brucite containing samples (sample 1 and 3). Moreover, polyelectrolytes were more effective in tuning the charge compared to the phosphate ions.

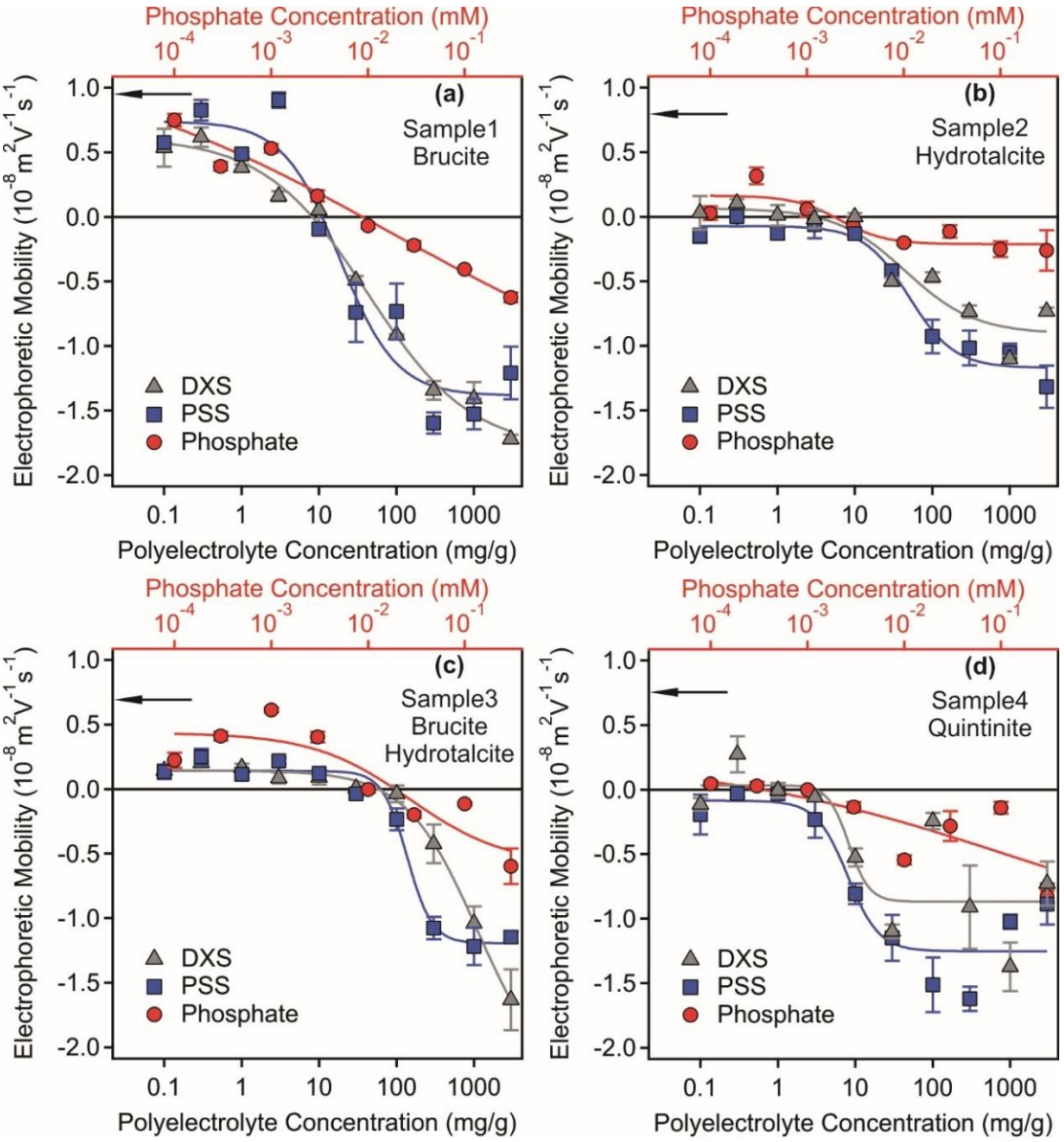

Figure 38. Electrophoretic mobilities of particles in samples 1–4 ((a) sample 1, (b) sample 2, (c) sample 3 and (d) sample 4) as a function of the polyelectrolyte (PSS and DXS) and phosphate concentration. The ionic strength (80 mM) was kept constant in the experiments. The solid lines are eye guides. The arrows indicate the mobilities of the bare particles.[163]

Dynamic light scattering measurements were carried out to follow possible particle aggregation and the sedimentation, however, both the size and the polydispersity of the particles were too high to explore such processes. The results proved that the dispersions are composed of larger aggregates, which are stable despite of their large size. This finding indicates the formation of a network of particles or aggregates. This phenomenon occurs in high particle concentration systems giving rise to a stable 3D network of the dispersed materials, which are interlinked through interstitial water molecules.[164,165]

Since DLS was not suitable for the proper characterization of the samples, another approach was taken. The absorbance of the samples was measured with UV-Vis spectroscopy as an indicator of the turbidity in a time-resolved manner at 450 nm wavelength. No specific adsorption was present at that wavelength for any of the samples and thus, the absorbance values provided good indication for the presence of solid materials in the laser path. The spectra were recorded for the samples for 60 minutes and all of them was confirmed to be stable colloid.

From the electrophoretic mobility curves, the IEP value was calculated and the correlating dose of polyelectrolyte or phosphate was applied (Table 6), but it had no effects on the stability of the systems, i.e., the colloid remained stable at the IEPs and no sedimentation occurred. This is a rather surprising result, since it was shown before that charge neutralized LDH particles tend to aggregate at the IEP. One can then assume that the stabilizing force between the solid particles is of non-electrostatic origin.

Table 6. Applied dose of the polyelectrolytes and phosphate to set the IEP.

	PSS (mg/g)	**DXS (mg/g)**	**Phosphate (mM)**
Sample 1	12	4.5	0.0084
Sample 2	0.4	6.8	0.0207
Sample 3	13.5	46.0	0.0096
Sample 4	0.9	1.1	0.0010

5.4.3. Sedimentation by dilution

The formation of particle networks, what is possibly responsible for the elevated stability of the samples occurs usually at high solid contents.[49,166] Therefore, dilution was applied on the samples and the absorbance was followed in time-resolved experiments. Sample 1 to 4 were all

diluted 10-fold with water having the same pH and ionic strength as in the original samples. Sample 1 showed rapid sedimentation after the dilution in 2 minutes (Figure 39 (a)). Sample 2 and 3 showed an increase in absorbance after a short time due to the phenomenon that aggregates concentrated in the laser path for a short period of time and sedimented after around 20 minutes (Figure 39 (b,c)). Absorbances in sample 4 decreased only slightly after the dilution indicating that the system remained rather stable (Figure 39 (d)).

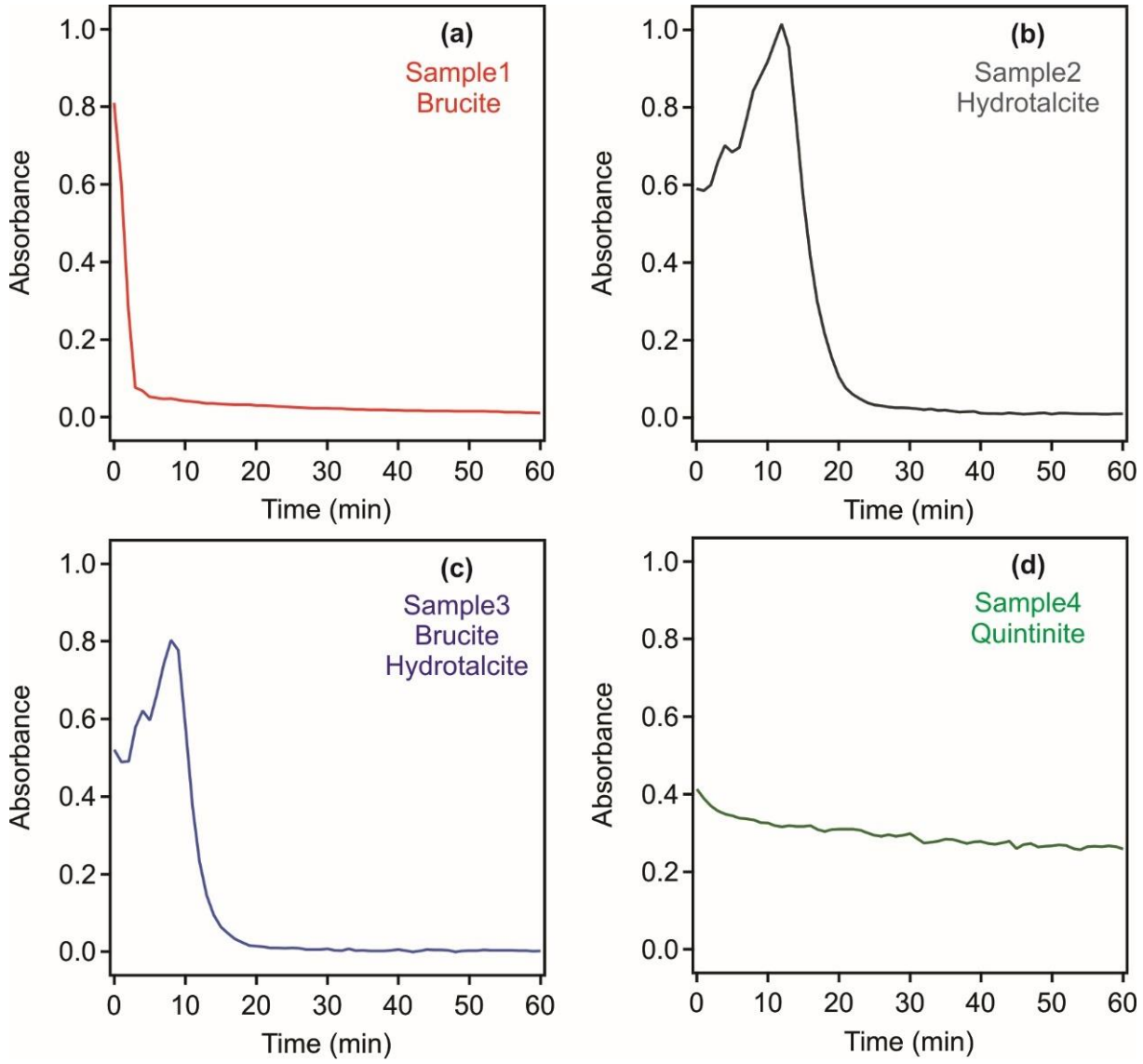

Figure 39. Time-resolved absorbance measurements performed at 450 nm for samples 1–4 ((a) sample 1, (b) sample 2, (c) sample 3 and (d) sample 4). The original samples were 10x diluted with water (pH and ionic strength was adjusted as per the original samples), which results in a solid content of about 1000 mg/L.[163]

Moreover, several dilution rates were applied in a similar time-resolved manner to gain further information on the effect of dilution. The time needed to reach 50% of the maximum absorbance (half time of sedimentation) was measured in all samples as a function of the dilution ratio. A typical example is shown in Figure 40.

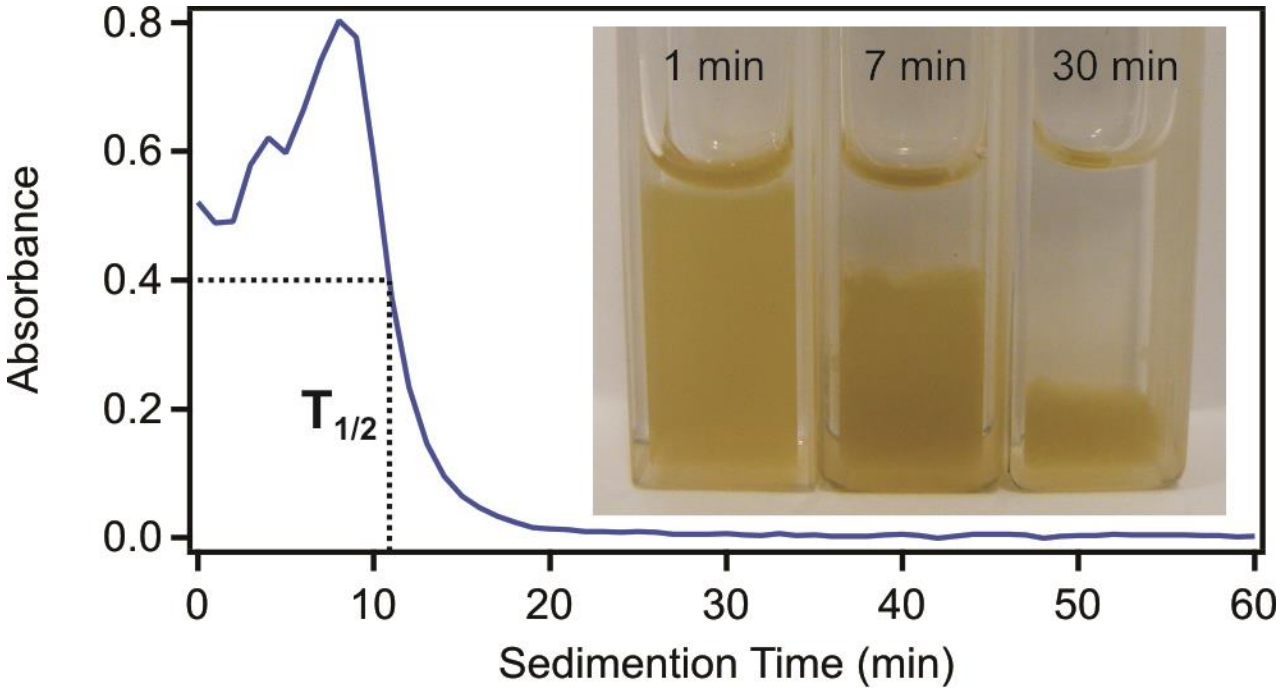

Figure 40. Illustration of the sedimentation of sample 2 over time with dilution and the absorbance change including the point of half time of sedimentation.[163]

Sample 4 showed no sign of sedimentation upon dilution. On the other hand, sample 1-3 sedimented after dilution with water of the same pH and ionic strength as the mine wastewater. Sample 1 sedimented most easily at the lowest dilution factor. Complete sedimentation occurred at 125 s. For sample 2 and 3, dilution factors were higher to achieve the full sedimentation in the range of 10 and 15-fold dilution, while minimum sedimentation times increased to 235 s for the former and 370 s for the latter one (Figure 41).

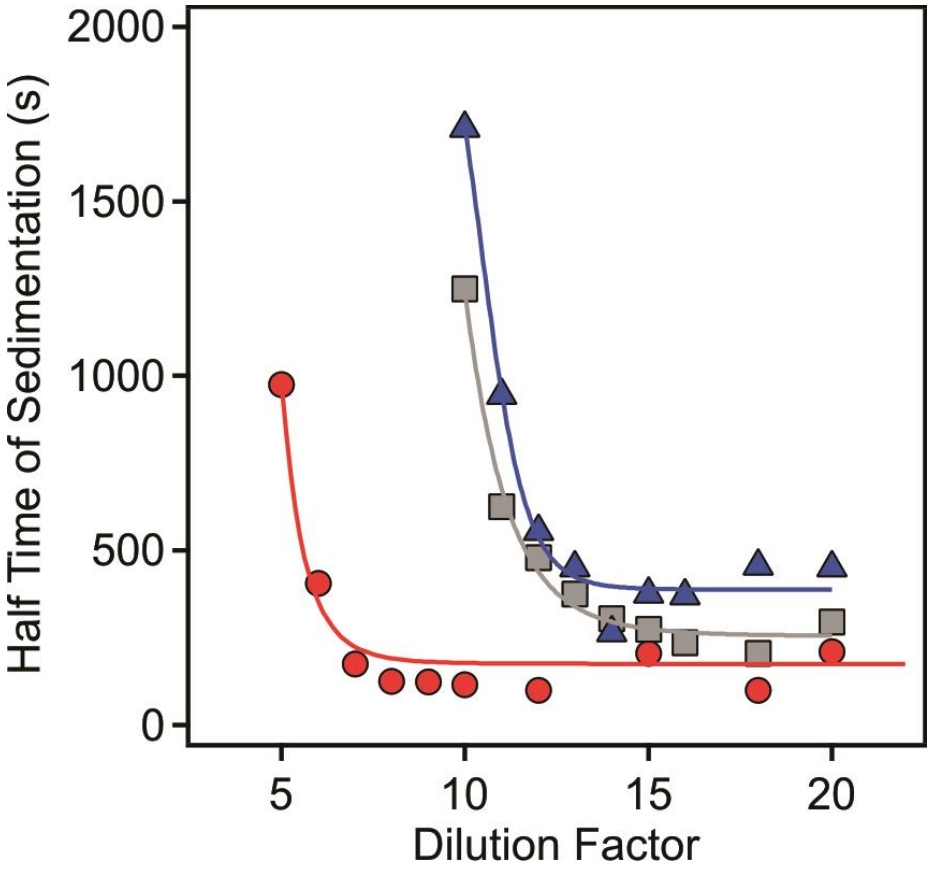

Figure 41. Half time of sedimentation as a function of the dilution factor for sample 1 (circles), sample 2 (squares) and sample 3 (triangles).[163]

As an overall experience with the measurements performed in mine wastewaters, the morphology and the composition of the LDH-like samples influenced the sedimentation. The particle network could not be broken with by tuning the charge due to the gel-like structure, however, it could be broken by dilution in most cases giving rise to sedimentation of the solid content. Sedimentation time of the samples depended on the composition. Sample 4, which was quintinite did not sediment at all. The sedimentation of sample 1, what was predominantly brucite was quick after dilution. The sedimentation of sample 2 containing LDH and sample 3 containing LDH and brucite were similar. It was rather surprising that sample 3, which was a mixture of brucite and LDH, sedimentation was quicker than the pure LDH phase in sample 2. Also, the samples formed in wastewater tend to adsorb some of the contaminants especially sulfate. This information might be helpful for development and usage of LDH colloids in water treatment applications.

6. Conclusions

The present work covers the design and application of LDH colloids in various fields. The particles involve composite and single phase LDH materials, which were developed in novel synthetic routes combining colloid and materials chemistry. The main conclusions made on the basis of the findings can be summarized as follows.

The results obtained considering polyelectrolyte and metal complex modified LDH nanoparticles led to better understanding of the build-up of such a novel composite structure. An additional stabilizing force by the PDADMAC layer in the bilayer hybrid material was identified. The developed dual polyelectrolyte-LDH compound showed high colloidal stability indicating the importance of the correct dose of polyelectrolytes applied. The hybrid served as a base material for immobilization of metal complexes with the sequential adsorption method. Similar complex material was not reported earlier in the literature. The antioxidant activity of the developed COMP was explored in various assays, however, high activity was only detected in the SOD test. Therefore, the COMP can be considered as a selective agent for dismutation of superoxide radicals. The composite was characterized with various methods leading to the conclusion that the high SOD activity is probably the result of the synergistic effect of the metal complexes embedded in the hybrid material. Moreover, it showed high colloidal stability against salt-induced aggregation proving that it can be applied in heterogeneous systems, which are the case in most of the industrial manufacturing processes.

The novel colloidal approach involving SDS modified LDH precursors led to the development of highly porous material of advantageous pore size distribution. The effect of SDS adsorption on the colloidal stability of LDH particles was investigated in detail determining both stability ratio and electrophoretic mobility values in a wide range of experimental conditions. The obtained information from these measurements allowed the selection of three regimes of SDS dose, where the charging and aggregation behaviour of the particles were considerably different. The chosen SDS doses corresponded to stable and unstable particles used for the final calcination-rehydration processes. The application of the sacrificial SDS template method gave rise to remarkably high porosity and capacity for the adsorption of dichromate and nitrate ions. The determined adsorption capacities are among the highest ones reported earlier for single phase LDHs in the literature. The gained results bring important information to the scientific community developing highly efficient LDH-based adsorbents for environmental processes for instance.

LDH materials were prepared *in situ* in acidic mine wastewater received from Boddington Gold Mine, Western Australia. During the *in situ* preparation, the forming material removed important contaminants such as sulfate ions from the wastewater, as revealed during structural characterization of the solid material after adsorption and/or intercalation took place. However, these LDH systems formed highly stable colloidal samples, which did not tend to sediment causing significant problem during water remediation. Such a separation of contaminant containing LDH particles from the treated aqueous phase was explored and a novel method was developed to solve this problem. The investigations led to the result that the stability of the system is not due to electrostatic interactions, but to formation of a gel-like structure consisting of LDH particles at high concentration. This gel-like structure was destabilized by dilution and the optimal dilution factors and sedimentation times were determined. It is foreseen that these results will be useful to our Australian partner while improving the existing water treatment processes.

In conclusions, the aims drawn up at the beginning of the doctoral work were accomplished. Accordingly, a hybrid material containing polyelectrolytes, enzyme mimicking metal complexes and LDH support proved as an efficient antioxidant agent of high colloidal and functional stability as well as of excellent selectivity for superoxide radical ions. Application of a colloid route during development of LDH-based adsorbents resulted in mesoporous materials of advantageous pore size distribution and specific surface area. Such compounds hold great promise in applications, wherever the goal is the removal of unwanted anions. Finally, a solution was provided for problems caused by the high colloidal stability of *in situ* formed LDHs during water remediation. The precise determination of dilution factors allows the separation of the solid phase containing the contaminants with a simple and economic method. We believe that the developed LDH colloid systems will attract considerable interest in the scientific and technological communities dealing with similar issues.

7. Acknowledgement

First of all, I would like to thank the help of my supervisor Dr. István Szilágyi. I am sincerely grateful for all the guidance, patience he showed towards me throughout my PhD. I would also like to thank my co-supervisor Dr. István Pálinkó. I am thankful for all the help and guidance I got from him and for initiating me on the road being a scientist, wish he could witness this. I am grateful for Szabolcs Muráth for helping me throughout my research and the supervising. I would also like to say thanks to Dr. Dániel Sebők for the XRD measurements, Dr. Nóra Nagy May for her help and immerse knowledge in the EPR measurements and evaluation of the results, Szilárd Sáringer for SEM and TEM measurements as well as Gábor Varga and Péter Nagy for the common work producing the results leading to this moment work. I would like to thank Dr. Grant Douglas for the corporation during my project. I would like to generally thank all my colleagues, the workers of the chemistry institute who helped my work. I would like to genuinely thank professor Dr. Ágota Tóth for letting me carry out my thesis in the Department of Physical Chemistry and Material Science. Last but not least I would like to say thank you for my family and my wonderful friends for the support I got all over the years to complete my work.

8. References

1. Rives, V., *Layered double hydroxides: Present and future*. Nova Science Publishers, Inc.: New York, 2001.
2. Rives, V.; Kannan, S., Layered double hydroxides with the hydrotalcite-type structure containing Cu^{2+}, Ni^{2+} and Al^{3+}. *J. Mater. Chem.* **2000,** *10* (2), 489-495.
3. Evans, D. G.; Slade, R. C. T., Structural aspects of layered double hydroxides. In *Layered Double Hydroxides*, Duan, X.; Evans, D. G., Eds. 2006; Vol. 119, pp 1-87.
4. Cavani, F.; Trifiro, F.; Vaccari, A., Hydrtalcite-type anionic clays: Preparation, properties and applications. *Catal. Today* **1991,** *11* (2), 173-301.
5. He, J.; Wei, M.; Li, B.; Kang, Y.; Evans, D. G.; Duan, X., Preparation of layered double hydroxides. In *Layered Double Hydroxides*, Duan, X.; Evans, D. G., Eds. 2006; Vol. 119, pp 89-119.
6. Das, N. N.; Konar, J.; Mohanta, M. K.; Srivastava, S. C., Adsorption of Cr(VI) and Se(IV) from their aqueous solutions onto Zr^{4+}-substituted ZnAl/MgAl-layered double hydroxides: effect of Zr^{4+} substitution in the layer. *J. Colloid Interface Sci.* **2004,** *270* (1), 1-8.
7. Mostafa, M. S.; Bakr, A. S. A.; El Naggar, A. M. A.; Sultan, E. S. A., Water decontamination via the removal of Pb (II) using a new generation of highly energetic surface nano-material: Co+2Mo+6 LDH. *J. Colloid Interface Sci.* **2016,** *461*, 261-272.
8. Shao, M. F.; Ning, F. Y.; Zhao, J. W.; Wei, M.; Evans, D. G.; Duan, X., Hierarchical layered double hydroxide microspheres with largely enhanced performance for ethanol electrooxidation. *Adv. Funct. Mater.* **2013,** *23* (28), 3513-3518.
9. Prevot, V.; Szczepaniak, C.; Jaber, M., Aerosol-assisted self-assembly of hybrid Layered Double Hydroxide particles into spherical architectures. *J. Colloid Interface Sci.* **2011,** *356* (2), 566-572.
10. Li, L.; Feng, Y. J.; Li, Y. S.; Zhao, W. R.; Shi, J. L., Fe_3O_4 core/layered double hydroxide shell nanocomposite: Versatile magnetic matrix for anionic functional materials. *Angew. Chem.-Int. Edit.* **2009,** *48* (32), 5888-5892.
11. Zhang, T.; Zhou, Y. M.; Fu, X. Q.; Li, S. W.; Rong, J.; Qiu, F. X., Facile Fabrication of Hierarchical Flower-Like BSA/Layered Double Hydroxide Hybrids. *Synth. React. Inorg. Met.-Org. Nano-Metal Chem.* **2016,** *46* (10), 1485-1488.
12. Zhang, J.; Xie, X. L.; Li, C. J.; Wang, H.; Wang, L. J., The role of soft colloidal templates in the shape evolution of flower-like MgAl-LDH hierarchical microstructures. *RSC Adv.* **2015,** *5* (38), 29757-29765.
13. Pavlovic, M.; Rouster, P.; Oncsik, T.; Szilagyi, I., Tuning colloidal stability of layered double hydroxides: from monovalent ions to polyelectrolytes. *ChemPlusChem* **2017,** *82*, 121-131.
14. Pavlovic, M.; Huber, R.; Adok-Sipiczki, M.; Nardin, C.; Szilagyi, I., Ion specific effects on the stability of layered double hydroxide colloids. *Soft Matter* **2016,** *12*, 4024-4033.
15. Parida, K.; Mohapatra, L.; Baliarsingh, N., Effect of Co2+ Substitution in the Framework of Carbonate Intercalated Cu/Cr LDH on Structural, Electronic, Optical, and Photocatalytic Properties. *J. Phys. Chem. C* **2012,** *116* (42), 22417-22424.
16. Geraud, E.; Rafqah, S.; Sarakha, M.; Forano, C.; Prevot, V.; Leroux, F., Three dimensionally ordered macroporous layered double hydroxides: Preparation by templated impregnation/coprecipitation and pattern stability upon calcination. *Chem. Mat.* **2008,** *20* (3), 1116-1125.

17. Yuan, Z. J.; Bak, S. M.; Li, P. S.; Jia, Y.; Zheng, L. R.; Zhou, Y.; Bai, L.; Hu, E. Y.; Yang, X. Q.; Cai, Z.; Sun, Y. M.; Sun, X. M., Activating layered double hydroxide with multivacancies by memory effect for energy-efficient hydrogen production at neutral pH. *ACS Energy Lett.* **2019,** *4* (6), 1412-1418.
18. Sun, G. B.; Sun, L. N.; Wen, H.; Jia, Z. Q.; Huang, K. L.; Hu, C. W., From layered double hydroxide to spinel nanostructures: Facile synthesis and characterization of nanoplatelets and nanorods. *J. Phys. Chem. B* **2006,** *110* (27), 13375-13380.
19. Abello, S.; Mitchell, S.; Santiago, M.; Stoica, G.; Perez-Ramirez, J., Perturbing the properties of layered double hydroxides by continuous coprecipitation with short residence time. *J. Mater. Chem.* **2010,** *20* (28), 5878-5887.
20. Xu, Z. P.; Lu, G. Q., Hydrothermal synthesis of layered double hydroxides (LDHs) from mixed MgO and Al2O3: LDH formation mechanism. *Chem. Mat.* **2005,** *17* (5), 1055-1062.
21. Sokol, D.; Vieira, D. E. L.; Zarkov, A.; Ferreira, M. G. S.; Beganskiene, A.; Rubanik, V. V.; Shilin, A. D.; Kareiva, A.; Salak, A. N., Sonication accelerated formation of Mg-Al-phosphate layered double hydroxide via sol-gel prepared mixed metal oxides. *Sci. Rep.* **2019,** *9*, 10419.
22. Jaiswal, A.; Mani, R.; Banerjee, S.; Gautam, R. K.; Chattopadhyaya, M. C., Synthesis of novel nano-layered double hydroxide by urea hydrolysis method and their application in removal of chromium(VI) from aqueous solution: Kinetic, thermodynamic and equilibrium studies. *J. Mol. Liq.* **2015,** *202*, 52-61.
23. Zheng, Y. L.; Chen, Y. H., Preparation of polypropylene/Mg-Al layered double hydroxides nanocomposites through wet pan-milling: formation of a second-staging structure in LDHs intercalates. *RSC Adv.* **2017,** *7* (3), 1520-1530.
24. Mousty, C.; Prevot, V., Hybrid and biohybrid layered double hydroxides for electrochemical analysis. *Anal. Bioanal. Chem.* **2013,** *405* (11), 3513-3523.
25. Nalawade, P.; Aware, B.; Kadam, V. J.; Hirlekar, R. S., Layered double hydroxides: A review. *J. Sci. Ind. Res.* **2009,** *68* (4), 267-272.
26. Forano, C.; Costantino, U.; Prevot, V.; Taviot Gueho, C., Layered double hydroxides (LDH). In *Handbook of Clay Science*, Bergaya, F.; Lagaly, G., Eds. Elsevier: Amsterdam, 2013; Vol. 5A, pp 745-782.
27. Jobbagy, M.; Regazzoni, A. E., Anion-exchange equilibrium and phase segregation in hydrotalcite systems: Intercalation of hexacyanoferrate(III) ions. *J. Phys. Chem. B* **2005,** *109* (1), 389-393.
28. Beres, A.; Palinko, I.; Bertrand, J. C.; Nagy, J. B.; Kiricsi, I., Dehydration-rehydration behaviour of layered double hydroxides: A study by X-ray diffractometry and MAS NMR spectroscopy. *J. Mol. Struct.* **1997,** *410*, 13-16.
29. Prevot, V.; Tokudome, Y., 3D hierarchical and porous layered double hydroxide structures: an overview of synthesis methods and applications. *J. Mater. Sci.* **2017,** *52* (19), 11229-11250.
30. Zhang, P.; Ouyang, S. D.; Li, P.; Huang, Y.; Frost, R. L., Enhanced removal of ionic dyes by hierarchical organic three-dimensional layered double hydroxide prepared via soft-template synthesis with mechanism study. *Chem. Eng. J.* **2019,** *360*, 1137-1149.
31. Tokudome, Y.; Morimoto, T.; Tarutani, N.; Vaz, P. D.; Nunes, C. D.; Prevot, V.; Stenning, G. B. G.; Takahashi, M., Layered double hydroxide nanoclusters: Aqueous, concentrated, stable, and catalytically active colloids toward green chemistry. *ACS Nano* **2016,** *10* (5), 5550-5559.

32. Wang, T.; Su, P.; Lin, F. Y.; Yang, Y., Self-sacrificial template synthesis of mixed-valence-state cobalt nanomaterials with high catalytic activities for colorimetric detection of glutathione. *Sens. Actuator B-Chem.* **2018,** *254*, 329-336.
33. Geraud, E.; Prevot, V.; Ghanbaja, J.; Leroux, F., Macroscopically ordered hydrotalcite-type materials using self-assembled colloidal crystal template. *Chem. Mat.* **2006,** *18* (2), 238-240.
34. Derjaguin, B.; Landau, L. D., Theory of the stability of strongly charged lyophobic sols and of the adhesion of strongly charged particles in solutions of electrolytes. *Acta Phys. Chim.* **1941,** *14* (6), 633-662.
35. Verwey, E. J. W.; Overbeek, J. T. G., *Theory of stability of lyophobic colloids*. Elsevier: Amsterdam, 1948.
36. Cao, T. C.; Sugimoto, T.; Szilagyi, I.; Trefalt, G.; Borkovec, M., Heteroaggregation of oppositely charged particles in the presence of multivalent ions. *Phys. Chem. Chem. Phys.* **2017,** *19* (23), 15160-15171.
37. Delgado, A. V.; Gonzalez-Caballero, F.; Hunter, R. J.; Koopal, L. K.; Lyklema, J., Measurement and interpretation of electrokinetic phenomena. *J. Colloid Interface Sci.* **2007,** *309* (2), 194-224.
38. Faraudo, J.; Martin-Molina, A., Competing forces in the interaction of polyelectrolytes with charged interfaces. *Curr. Opin. Colloid Interface Sci.* **2013,** *18* (6), 517-523.
39. Missana, T.; Adell, A., On the applicability of DLVO theory to the prediction of clay colloids stability. *J. Colloid Interface Sci.* **2000,** *230* (1), 150-156.
40. Elimelech, M.; Gregory, J.; Jia, X.; Williams, R. A., *Particle deposition and aggregation: Measurement, modeling, and simulation*. Butterworth-Heinemann Ltd.: Oxford, 1995.
41. Holthoff, H.; Egelhaaf, S. U.; Borkovec, M.; Schurtenberger, P.; Sticher, H., Coagulation rate measurements of colloidal particles by simultaneous static and dynamic light scattering. *Langmuir* **1996,** *12* (23), 5541-5549.
42. Dautzenberg, H.; Jaeger, W.; Kotz, J.; Philipp, B.; Seidel, C.; Stscherbina, D., *Polyelectrolytes: Formation, characterization and application*. Hanser Publishers: New York, 1994.
43. Koetz, J.; Kosmella, S., *Polyelectrolytes and nanoparticles*. Springer: Berlin, 2007.
44. Hornok, V.; Erdohelyi, A.; Dekany, I., Preparation of ultrathin membranes by layer-by-layer deposition of layered double hydroxide (LDH) and polystyrene sulfonate (PSS). *Colloid Polym. Sci.* **2005,** *283* (10), 1050-1055.
45. Peng, F.; Wang, D. H.; Zhang, D. D.; Yan, B. C.; Cao, H. L.; Qiao, Y. Q.; Liu, X. Y., PEO/Mg-Zn-Al LDH composite coating on Mg alloy as a Zn/Mg ion-release platform with multifunctions: Enhanced corrosion resistance, osteogenic, and antibacterial activities. *ACS Biomater. Sci. Eng.* **2018,** *4* (12), 4112-4121.
46. Shchukin, D. G.; Lamaka, S. V.; Yasakau, K. A.; Zheludkevich, M. L.; Ferreira, M. G. S.; Mohwald, H., Active anticorrosion coatings with halloysite nanocontainers. *J. Phys. Chem. C* **2008,** *112* (4), 958-964.
47. Miao, Y. E.; Zhu, H.; Chen, D.; Wang, R. Y.; Tjiu, W. W.; Liu, T. X., Electrospun fibers of layered double hydroxide/biopolymer nanocomposites as effective drug delivery systems. *Mater. Chem. Phys.* **2012,** *134* (2-3), 623-630.
48. Szilagyi, I.; Trefalt, G.; Tiraferri, A.; Maroni, P.; Borkovec, M., Polyelectrolyte adsorption, interparticle forces, and colloidal aggregation. *Soft Matter* **2014,** *10* (15), 2479-2502.
49. Bolto, B.; Gregory, J., Organic polyelectrolytes in water treatment. *Water Res.* **2007,** *41* (11), 2301-2324.

50. Leong, Y. K., Interparticle forces arising from an adsorbed strong polyelectrolyte in colloidal dispersions: charged patch attraction. *Colloid Polym. Sci.* **1999,** *277* (4), 299-305.
51. Layrac, G.; Destarac, M.; Gerardin, C.; Tichit, D., Highly Stable Layered Double Hydroxide Colloids: A Direct Aqueous Synthesis Route from Hybrid Polyion Complex Micelles. *Langmuir* **2014,** *30* (32), 9663-9671.
52. Xu, Z. P.; Stevenson, G.; Lu, C. Q.; Lu, G. Q., Dispersion and size control of layered double hydroxide nanoparticles in aqueous solutions. *J. Phys. Chem. B* **2006,** *110* (34), 16923-16929.
53. Letaief, S.; Martin-Luengo, M. A.; Aranda, P.; Ruiz-Hitzky, E., A colloidal route for delamination of layered solids: Novel porous-clay nanocomposites. *Adv. Funct. Mater.* **2006,** *16* (3), 401-409.
54. Choi, G.; Piao, H.; Kim, M. H.; Choy, J. H., Enabling nanohybrid drug discovery through the soft chemistry telescope. *Ind. Eng. Chem. Res.* **2016,** *55* (43), 11211-11224.
55. Chibwe, K.; Jones, W., Intercalation of organic and inorganc anions into layered double hydroxides. *J. Chem. Soc.-Chem. Commun.* **1989,** (14), 926-927.
56. Brenneisen, P.; Reichert, A. S., Nanotherapy and reactive oxygen species (ROS) in cancer: A novel perspective. *Antioxidants* **2018,** *7* (2), 31.
57. Nimse, S. B.; Pal, D., Free radicals, natural antioxidants, and their reaction mechanisms. *RSC Adv.* **2015,** *5* (35), 27986-28006.
58. Valko, M.; Rhodes, C. J.; Moncol, J.; Izakovic, M.; Mazur, M., Free radicals, metals and antioxidants in oxidative stress-induced cancer. *Chem.-Biol. Interact.* **2006,** *160* (1), 1-40.
59. Finley, J. W.; Kong, A. N.; Hintze, K. J.; Jeffery, E. H.; Ji, L. L.; Lei, X. G., Antioxidants in foods: State of the science important to the food industry. *J. Agric. Food Chem.* **2011,** *59* (13), 6837-6846.
60. Nirmala, C.; Bisht, M. S.; Bajwa, H. K.; Santosh, O., Bamboo: A rich source of natural antioxidants and its applications in the food and pharmaceutical industry. *Trends Food Sci. Technol.* **2018,** *77*, 91-99.
61. Gupta, K. M.; Das, S.; Chow, P. S.; Macbeath, C., Encapsulation of ferulic acid in lipid nanoparticles as antioxidant for skin: Mechanistic understanding through experiment and molecular simulation. *ACS Appl. Nano Mater.* **2020,** *3* (6), 5351-5361.
62. Ames, B. N.; Shigenaga, M. K.; Hagen, T. M., Oxidants, antioxidants, and the degenerative diseases of aging. *Proc. Natl. Acad. Sci. U. S. A.* **1993,** *90* (17), 7915-7922.
63. Belle, C.; Pierre, J. L., Asymmetry in bridged binuclear metalloenzymes: Lessons for the chemist. *Eur. J. Inorg. Chem.* **2003,** (23), 4137-4146.
64. Zhou, J. X.; Chen, Y.; Lan, L. T.; Zhang, C.; Pan, M. X.; Wang, Y. Y.; Han, B. K.; Wang, Z. H.; Jiao, J.; Chen, Q., A novel catalase mimicking nanocomposite of Mn(II)-poly-L-histidine-carboxylated multi walled carbon nanotubes and the application to hydrogen peroxide sensing. *Anal. Biochem.* **2019,** *567*, 51-62.
65. Pavlovic, M.; Murath, S.; Katona, X.; Alsharif, N. B.; Rouster, P.; Maleth, J.; Szilagyi, I., Nanocomposite-based dual enzyme system for broad-spectrum scavenging of reactive oxygen species. *Sci Rep* **2021,** *11* (1), 4321.
66. Beaucham, C.; Fridovich, I., Superoxide dismutase - improved assays and an assay applicable to acrylamide gels. *Anal. Biochem.* **1971,** *44* (1), 276-287.
67. Katsube, T.; Tabata, H.; Ohta, Y.; Yamasaki, Y.; Anuurad, E.; Shiwaku, K.; Yamane, Y., Screening for antioxidant activity in edible plant products: Comparison of low-density lipoprotein oxidation assay, DPPH radical scavenging assay, and Folin-Ciocalteu assay. *J. Agric. Food Chem.* **2004,** *52* (8), 2391-2396.

68. Apak, R.; Guclu, K.; Ozyurek, M.; Karademir, S. E., Novel total antioxidant capacity index for dietary polyphenols and vitamins C and E, using their cupric ion reducing capability in the presence of neocuproine: CUPRAC method. *J. Agric. Food Chem.* **2004,** *52* (26), 7970-7981.
69. Murath, S.; Alsharif, N. B.; Saringer, S.; Katana, B.; Somosi, Z.; Szilagyi, I., Antioxidant materials based on 2D nanostructures: A review on recent progresses. *Crystals* **2020,** *10* (3), 148.
70. Ansy, K. M.; Lee, J. H.; Piao, H.; Choi, G.; Choy, J. H., Stabilization of antioxidant gallate in layered double hydroxide by exfoliation and reassembling reaction. *Solid State Sci.* **2018,** *80*, 65-71.
71. Kong, X. G.; Jin, L.; Wei, M.; Duan, X., Antioxidant drugs intercalated into layered double hydroxide: Structure and in vitro release. *Appl. Clay Sci.* **2010,** *49* (3), 324-329.
72. Murath, S.; Szerlauth, S.; Sebok, D.; Szilagyi, I., Layered double hydroxide nanoparticles to overcome the hydrophobicity of ellagic acid: An antioxidant hybrid material. *Antioxidants* **2020,** *9* (2), 153.
73. Pontes-Neto, J. G.; Fontes, D. A. F.; de Lyra, M. A. M.; de Brito, M. D. M.; Chaves, L. L.; Rolim-Neto, P. J.; Soares, M. F. D.; Quintans, L. J.; de Freitas, R. M.; Soares-Sobrinho, J. L., Evaluation of antioxidant potencial of novel CaAl and NiAl layered double hydroxides loaded with olanzapine. *Life Sci.* **2018,** *207*, 246-252.
74. Pavlovic, M.; Nafradi, M.; Rouster, P.; Murath, S.; Szilagyi, I., Highly stable enzyme-mimicking nanocomposite of antioxidant activity. *J. Colloid Interface Sci.* **2019,** *543*, 174-182.
75. Qiao, F. M.; Shi, W. J.; Dong, J.; Lv, W.; Ai, S. Y., Functional hybrids of layered double hydroxides with hemin: synergistic effect for peroxynitrite-scavenging activity. *RSC Adv.* **2014,** *4* (84), 44614-44620.
76. Pavlovic, M.; Rouster, P.; Somosi, Z.; Szilagyi, I., Horseradish peroxidase-nanoclay hybrid particles of high functional and colloidal stability. *J. Colloid Interface Sci.* **2018,** *524*, 114-121.
77. Wei, H.; Wang, E. K., Nanomaterials with enzyme-like characteristics (nanozymes): next-generation artificial enzymes. *Chem. Soc. Rev.* **2013,** *42* (14), 6060-6093.
78. Zhang, Y. W.; Tian, J. Q.; Liu, S.; Wang, L.; Qin, X. Y.; Lu, W. B.; Chang, G. H.; Luo, Y. L.; Asiri, A. M.; Al-Youbi, A. O.; Sun, X. P., Novel application of CoFe layered double hydroxide nanoplates for colorimetric detection of H_2O_2 and glucose. *Analyst* **2012,** *137* (6), 1325-1328.
79. Wu, L. H.; Wan, G. P.; Shi, S. H.; He, Z. Y.; Xu, X. F.; Tang, Y. L.; Hao, C. C.; Wang, G. Z., Atomic layer deposition-assisted growth of CuAl LDH on carbon fiber as a peroxidase mimic for colorimetric determination of H_2O_2 and glucose. *New J. Chem.* **2019,** *43* (15), 5826-5832.
80. Wu, Y. Y.; Chi, Y.; Bai, H. M.; Qian, G. R.; Cao, Y. L.; Zhou, J. Z.; Xu, Y. F.; Lu, Q.; Xu, Z. P.; Qiao, S. Z., Effective removal of selenate from aqueous solutions by the Friedel phase. *J. Hazard. Mater.* **2010,** *176* (1-3), 193-198.
81. Mandel, K.; Drenkova-Tuhtan, A.; Hutter, F.; Gellermann, C.; Steinmetz, H.; Sextl, G., Layered double hydroxide ion exchangers on superparamagnetic microparticles for recovery of phosphate from waste water. *J. Mater. Chem. A* **2013,** *1* (5), 1840-1848.
82. Shen, Y. M.; Liu, D. B.; Li, S. F.; Fan, L. H.; Chen, S.; Haque, M. A., Removal of lead from aqueous solution on glutamate intercalated layered double hydroxide. *Arab. J. Chem.* **2017,** *10*, S2295-S2301.

83. Zhao, P. W.; Liu, X. H.; Tian, W. L.; Yan, D. P.; Sun, X. M.; Lei, X. D., Adsolubilization of 2,4,6-trichlorophenol from aqueous solution by surfactant intercalated ZnAl layered double hydroxides. *Chem. Eng. J.* **2015,** *279*, 597-604.
84. Tian, W. L.; Kong, X. G.; Jiang, M. H.; Lei, X. D.; Duan, X., Hierarchical layered double hydroxide epitaxially grown on vermiculite for Cr(VI) removal. *Mater. Lett.* **2016,** *175*, 110-113.
85. Shan, R. R.; Yan, L. G.; Yang, K.; Yu, S. J.; Hao, Y. F.; Yu, H. Q.; Du, B., Magnetic Fe_3O_4/MgAl-LDH composite for effective removal of three red dyes from aqueous solution. *Chem. Eng. J.* **2014,** *252*, 38-46.
86. Zubair, M.; Daud, M.; McKay, G.; Shehzad, F.; Al-Harthi, M. A., Recent progress in layered double hydroxides (LDH)-containing hybrids as adsorbents for water remediation. *Appl. Clay Sci.* **2017,** *143*, 279-292.
87. Goh, K. H.; Lim, T. T.; Dong, Z., Application of layered double hydroxides for removal of oxyanions: A review. *Water Res.* **2008,** *42* (6-7), 1343-1368.
88. Alekseeva, T.; Prevot, V.; Sancelme, M.; Forano, C.; Besse-Hoggan, P., Enhancing atrazine biodegradation by Pseudomonas sp strain ADP adsorption to Layered Double Hydroxide bionanocomposites. *J. Hazard. Mater.* **2011,** *191* (1-3), 126-135.
89. Halma, M.; Mousty, C.; Forano, C.; Sancelme, M.; Besse-Hoggan, P.; Prevot, V., Bacteria encapsulated in layered double hydroxides: Towards an efficient bionanohybrid for pollutant degradation. *Colloid Surf. B* **2015,** *126*, 344-350.
90. Wang, Q. W.; Lin, Q. H.; Li, Q. Z.; Li, K. Z.; Wu, L. Y.; Li, S. M.; Liu, H., As(III) removal from wastewater and direct stabilization by in-situ formation of Zn-Fe layered double hydroxides. *J. Hazard. Mater.* **2021,** *403*.
91. Peligro, F. R.; Pavlovic, I.; Rojas, R.; Barriga, C., Removal of heavy metals from simulated wastewater by in situ formation of layered double hydroxides. *Chem. Eng. J.* **2016,** *306*, 1035-1040.
92. Rahman, M. T.; Kameda, T.; Miura, T.; Kumagai, S.; Yoshioka, T., Facile method for treating Zn, Cd, and Pb in mining wastewater by the formation of Mg-Al layered double hydroxide. *Int. J. Environ. Sci. Technol.* **2020,** *17* (5), 3023-3032.
93. Xu, Z. P.; Stevenson, G. S.; Lu, C. Q.; Lu, G. Q. M.; Bartlett, P. F.; Gray, P. P., Stable suspension of layered double hydroxide nanoparticles in aqueous solution. *J. Am. Chem. Soc.* **2006,** *128* (1), 36-37.
94. Rockenbauer, A.; Korecz, L., Automatic computer simulations of ESR spectra. *Appl. Magn. Reson.* **1996,** *10* (1-3), 29-43.
95. Hassan, P. A.; Rana, S.; Verma, G., Making sense of Brownian motion: Colloid characterization by dynamic light scattering. *Langmuir* **2015,** *31* (1), 3-12.
96. Evans, D. F.; Wennerstrom, H., *The colloidal domain*. John Wiley: New York, 1999.
97. Trefalt, G.; Szilagyi, I.; Oncsik, T.; Sadeghpour, A.; Borkovec, M., Probing colloidal particle aggregation by light scattering. *Chimia* **2013,** *67* (11), 772-776.
98. Murath, S.; Somosi, Z.; Toth, I. Y.; Tombacz, E.; Sipos, P.; Palinko, I., Delaminating and restacking MgAl-layered double hydroxide monitored and characterized by a range of instrumental methods. *J. Mol. Struct.* **2017,** *1140*, 77-82.
99. Bragg, W. H.; Bragg, W. L., The reflection of X-rays by crystals. *Proc. R. soc. Lond. Ser. A-Contain. Pap. Math. Phys. Character* **1913,** *88* (605), 428-438.
100. Somosi, Z.; Pavlovic, M.; Palinko, I.; Szilagyi, I., Effect of polyelectrolyte mono- and bilayer formation on the colloidal stability of layered double hydroxide nanoparticles. *Nanomaterials* **2018,** *8* (12), 986.

101. Decher, G., Fuzzy nanoassemblies: Toward layered polymeric multicomposites. *Science* **1997,** *277* (5330), 1232-1237.
102. Hierrezuelo, J.; Sadeghpour, A.; Szilagyi, I.; Vaccaro, A.; Borkovec, M., Electrostatic stabilization of charged colloidal particles with adsorbed polyelectrolytes of opposite charge. *Langmuir* **2010,** *26* (19), 15109-15111.
103. Manning, G. S., Limiting laws and counterion condensation in polyelectrolyte solutions 1. Colligative properties. *J. Chem. Phys.* **1969,** *51* (3), 924-933.
104. Fuchs, A.; Killmann, E., Adsorption of polyelectrolytes on colloidal latex particles, electrostatic interactions and stability behaviour. *Colloid Polym. Sci.* **1998,** *279* (1), 53-60.
105. Hierrezuelo, J.; Vaccaro, A.; Borkovec, M., Stability of negatively charged latex particles in the presence of a strong cationic polyelectrolyte at elevated ionic strengths. *J. Colloid Interface Sci.* **2010,** *347*, 202-208.
106. Hierrezuelo, J.; Szilagyi, I.; Vaccaro, A.; Borkovec, M., Probing nanometer-thick polyelectrolyte layers adsorbed on oppositely charged particles by dynamic light scattering. *Macromolecules* **2010,** *43* (21), 9108-9116.
107. Meng, Z. Y.; Hashmi, S. M.; Elimelech, M., Aggregation rate and fractal dimension of fullerene nanoparticles via simultaneous multiangle static and dynamic light scattering measurement. *J. Colloid Interface Sci.* **2013,** *392*, 27-33.
108. Fritz, G.; Schadler, V.; Willenbacher, N.; Wagner, N. J., Electrosteric stabilization of colloidal dispersions. *Langmuir* **2002,** *18* (16), 6381-6390.
109. Somosi, Z.; May, N. V.; Sebok, D.; Palinko, I.; Szilagyi, I., Catalytic antioxidant nanocomposites based on sequential adsorption of redox active metal complexes and polyelectrolytes on nanoclay particles. *Dalton Trans.* **2021,** *50* (7), 2426-2435.
110. Martin, R. B., Citrate binding of Al^{3+} and Fe^{3+}. *J. Inorg. Biochem.* **1986,** *28* (2-3), 181-187.
111. Shweky, I.; Bino, A.; Goldberg, D. P.; Lippard, S. J., Syntheses, structures, and magnetic-properties of 2 dinuclear iron(III) citrate complexes. *Inorg. Chem.* **1994,** *33* (23), 5161-5162.
112. Cao, Z. B.; Li, B.; Sun, L. Y.; Li, L.; Xu, Z. P.; Gu, Z., 2D layered double hydroxide nanoparticles: Recent progress toward preclinical/clinical nanomedicine. *Small Methods* **2019,** *4* (2), 1900343.
113. Garribba, E.; Micera, G.; Sanna, D.; Strinna-Erre, L., The Cu(II)-2,2 '-bipyridine system revisited. *Inorg. Chim. Acta* **2000,** *299* (2), 253-261.
114. El-Missiry, M. A., *Antioxidant enzyme*. InTech: Rijeka, 2012.
115. Pavlovic, M.; Rouster, P.; Szilagyi, I., Synthesis and formulation of functional bionanomaterials with superoxide dismutase activity. *Nanoscale* **2017,** *9* (1), 369-379.
116. Ozyurek, M.; Guclu, K.; Tutem, E.; Baskan, K. S.; Ercag, E.; Celik, S. E.; Baki, S.; Yildiz, L.; Karaman, S.; Apak, R., A comprehensive review of CUPRAC methodology. *Anal. Methods* **2011,** *3* (11), 2439-2453.
117. Taviot-Gueho, C.; Prevot, V.; Forano, C.; Renaudin, G.; Mousty, C.; Leroux, F., Tailoring hybrid layered double hydroxides for the development of innovative applications. *Adv. Funct. Mater.* **2018,** *28* (27), 1703868.
118. Fernandez, L.; Ledezma, I.; Borras, C.; Martinez, L. A.; Carrero, H., Horseradish peroxidase modified electrode based on a film of Co-Al layered double hydroxide modified with sodium dodecylbenzenesulfonate for determination of 2-chlorophenol. *Sens. Actuator B-Chem.* **2013,** *182*, 625-632.

119. Deng, L.; Zeng, H. X.; Shi, Z.; Zhang, W.; Luo, J. M., Sodium dodecyl sulfate intercalated and acrylamide anchored layered double hydroxides: A multifunctional adsorbent for highly efficient removal of Congo red. *J. Colloid Interface Sci.* **2018,** *521*, 172-182.
120. Trefalt, G.; Szilagyi, I.; Borkovec, M., Poisson-Boltzmann description of interaction forces and aggregation rates involving charged colloidal particles in asymmetric electrolytes. *J. Colloid Interface Sci.* **2013,** *406*, 111-120.
121. Varga, G.; Somosi, Z.; Kukovecz, A.; Konya, Z.; Palinko, I.; Szilagyi, I., A colloid chemistry route for the preparation of hierarchically ordered mesoporous layered double hydroxides using surfactants as sacrificial templates. *J. Colloid Interface Sci.* **2021,** *581*, 928-938.
122. Pavan, P. C.; Crepaldi, E. L.; Gomes, G. D.; Valim, J. B., Adsorption of sodium dodecylsulfate on a hydrotalcite-like compound. Effect of temperature, pH and ionic strength. *Colloid Surf. A* **1999,** *154* (3), 399-410.
123. Iyi, N.; Matsumoto, T.; Kaneko, Y.; Kitamura, K., Deintercalation of carbonate ions from a hydrotalcite-like compound: Enhanced decarbonation using acid-salt mixed solution. *Chem. Mat.* **2004,** *16* (15), 2926-2932.
124. Sun, Y.; Zhou, Y.; Ye, X.; Chen, J.; Wang, Z., Fabrication and infrared emissivity study of hybrid materials based on immobilization of collagen onto exfoliated LDH. *Mater. Lett.* **2008,** *62* (17–18), 2943-2946.
125. Zhang, P.; Qian, G. R.; Xu, Z. P.; Shi, H. S.; Ruan, X. X.; Yang, J.; Frost, R. L., Effective adsorption of sodium dodecylsulfate (SDS) by hydrocalumite (CaAl-LDH-Cl) induced by self-dissolution and re-precipitation mechanism. *J. Colloid Interface Sci.* **2012,** *367*, 264-271.
126. Kloprogge, J. T.; Wharton, D.; Hickey, L.; Frost, R. L., Infrared and Raman study of interlayer anions CO_3^{2-}, NO_3^-, SO_4^{2-} and ClO_4^- in Mg/Al hydrotalcite. *Am. Miner.* **2002,** *87* (5-6), 623-629.
127. Suo, H. R.; Duan, H. H.; Chen, C. P.; Buffet, J. C.; O'Hare, D., Bifunctional acid-base mesoporous silica@aqueous miscible organic-layered double hydroxides. *RSC Adv.* **2019,** *9* (7), 3749-3754.
128. Wang, Q.; O'Hare, D., Large-scale synthesis of highly dispersed layered double hydroxide powders containing delaminated single layer nanosheets. *Chem. Commun.* **2013,** *49* (56), 6301-6303.
129. Shami, Z.; Amininasab, S. M.; Shakeri, P., Structure-property relationships of nanosheeted 3D hierarchical roughness MgAl-layered double hydroxide branched to an electrospun porous nanomembrane: A superior oil-removing nanofabric. *ACS Appl. Mater. Interfaces* **2016,** *8* (42), 28964-28973.
130. Pourfaraj, R.; Fatemi, S. J.; Kazemi, S. Y.; Biparva, P., Synthesis of hexagonal mesoporous MgAl LDH nanoplatelets adsorbent for the effective adsorption of Brilliant Yellow. *J. Colloid Interface Sci.* **2017,** *508*, 65-74.
131. Chen, C. P.; Wangriya, A.; Buffet, J. C.; O'Hare, D., Tuneable ultra high specific surface area Mg/Al-CO_3 layered double hydroxides. *Dalton Trans.* **2015,** *44* (37), 16392-16398.
132. Touati, S.; Mansouri, H.; Benguedach, A.; de Roy, A.; Forano, C.; Prevot, V., Nanostructured layered double hydroxide aerogels with enhanced adsorption properties. *Chem. Commun.* **2012,** *48* (57), 7197-7199.
133. Tokudome, Y.; Tarutani, N.; Nakanishi, K.; Takahashi, M., Layered double hydroxide (LDH)-based monolith with interconnected hierarchical channels: enhanced sorption affinity for anionic species. *J. Mater. Chem. A* **2013,** *1* (26), 7702-7708.

134. Tarutani, N.; Tokudome, Y.; Fukui, M.; Nakanishi, K.; Takahashi, M., Fabrication of hierarchically porous monolithic layered double hydroxide composites with tunable microcages for effective oxyanion adsorption. *RSC Adv.* **2015,** *5* (70), 57187-57192.
135. Cheng, K. Y.; Kaksonen, A. H.; Douglas, G. B., Sequential in situ hydrotalcite precipitation and biological denitrification for the treatment of high-nitrate industrial effluent. *Bioresour. Technol.* **2014,** *172*, 373-381.
136. Langmuir, I., The adsorption of gases on plane surfaces of glass, mica and platinum. *J. Am. Chem. Soc.* **1918,** *40* (9), 1361-1403.
137. Halajnia, A.; Oustan, S.; Najafi, N.; Khataee, A. R.; Lakzian, A., Adsorption-desorption characteristics of nitrate, phosphate and sulfate on Mg-Al layered double hydroxide. *Appl. Clay Sci.* **2013,** *80-81*, 305-312.
138. Sasai, R.; Norimatsu, W.; Matsumoto, Y., Nitrate-ion-selective exchange ability of layered double hydroxide consisting of Mg-II and Fe-II. *J. Hazard. Mater.* **2012,** *215*, 311-314.
139. Torres-Dorante, L. O.; Lammel, J.; Kuhlmann, H.; Witzke, T.; Olfs, H. W., Capacity, selectivity, and reversibility for nitrate exchange of a layered double-hydroxide (LDH) mineral in simulated soil solutions and in soil. *J. Plant Nutr. Soil Sci.* **2008,** *171* (5), 777-784.
140. Islam, M.; Patel, R., Synthesis and physicochemical characterization of Zn/Al chloride layered double hydroxide and evaluation of its nitrate removal efficiency. *Desalination* **2010,** *256* (1-3), 120-128.
141. Ivanova, D.; Albert, P.; Kavulicova, J., Nitrate removal from model aqueous solutions and real water by calcined Mg/Al layered double hydroxides. *Appl. Clay Sci.* **2018,** *152*, 65-72.
142. Manna, J.; Shilpa, N.; Bandarapu, A. K.; Rana, R. K., Oxyanion-binding in a bioinspired nanoparticle-assembled hybrid microsphere structure: Effective removal of arsenate/chromate from water. *ACS Appl. Nano Mater.* **2019,** *2* (3), 1525-1532.
143. Chao, H. P.; Wang, Y. C.; Tran, H. N., Removal of hexavalent chromium from groundwater by Mg/Al-layered double hydroxides using characteristics of in-situ synthesis. *Environ. Pollut.* **2018,** *243*, 620-629.
144. He, S.; Zhao, Y. F.; Wei, M.; Evans, D. G.; Duan, X., Fabrication of hierarchical layered double hydroxide framework on aluminum foam as a structured adsorbent for water treatment. *Ind. Eng. Chem. Res.* **2012,** *51* (1), 285-291.
145. Zhang, B.; Luan, L. Y.; Gao, R. T.; Li, F.; Li, Y. J.; Wu, T., Rapid and effective removal of Cr(VI) from aqueous solution using exfoliated LDH nanosheets. *Colloid Surf. A-Physicochem. Eng. Asp.* **2017,** *520*, 399-408.
146. Eshaq, G.; Rabie, A. M.; Bakr, A. A.; Mady, A. H.; ElMetwally, A. E., Cr(VI) adsorption from aqueous solutions onto Mg-Zn-Al LDH and its corresponding oxide. *Desalin. Water Treat.* **2016,** *57* (43), 20377-20387.
147. Ruiz-Huerta, E. A.; Varelal, A. D.; Gomez-Bernal, J. M.; Castillo, F.; Avalos-Borja, M.; SenGupta, B.; Martinez-Villegas, N., Arsenic contamination in irrigation water, agricultural soil and maize crop from an abandoned smelter site in Matehuala, Mexico. *J. Hazard. Mater.* **2017,** *339*, 330-339.
148. Asiabi, H.; Yamini, Y.; Shamsayei, M., Highly selective and efficient removal of arsenic(V), chromium(VI) and selenium(VI) oxyanions by layered double hydroxide intercalated with zwitterionic glycine. *J. Hazard. Mater.* **2017,** *339*, 239-247.
149. Wang, W. W.; Zhou, J. B.; Achari, G.; Yu, J. G.; Cai, W. Q., Cr(VI) removal from aqueous solutions by hydrothermal synthetic layered double hydroxides: Adsorption performance,

coexisting anions and regeneration studies. *Colloid Surf. A-Physicochem. Eng. Asp.* **2014,** *457*, 33-40.
150. Zhao, S.; Gao, B. Y.; Yue, Q. Y.; Wang, Y., Effect of Enteromorpha polysaccharides on coagulation performance and kinetics for dye removal. *Colloid Surf. A-Physicochem. Eng. Asp.* **2014,** *456*, 253-260.
151. Ait Bentaleb, K.; El Khattabi, E.; Lakraimi, M.; Benaziz, L.; Sabbar, E.; Berraho, M.; Legrouri, A., Removal of Cr(VI) from wastewater by anionic clays. *J. Mater. Environ. Sci.* **2016,** *7* (8), 2886-2896.
152. Otgonjargal, E.; Nyamsuren, B.; Surenjav, E.; Burmaa, G.; Temuujin, J.; Khasbaatar, D., Removal of chromium from aqueous solution by thermally treated MgAl layered double hydroxide. *Ann. Civil Environ. Eng.* **2017,** *1*, 1-8.
153. Hu, H. J.; Liu, J. Y.; Xu, Z. H.; Zhang, L. Y.; Cheng, B.; Ho, W. K., Hierarchical porous Ni/Co-LDH hollow dodecahedron with excellent adsorption property for Congo red and Cr(VI) ions. *Appl. Surf. Sci.* **2019,** *478*, 981-990.
154. Lazaridis, N. K.; Pandi, T. A.; Matis, K. A., Chromium(VI) removal from aqueous solutions by Mg-Al-CO_3 hydrotalcite: Sorption-desorption kinetic and equilibrium studies. *Ind. Eng. Chem. Res.* **2004,** *43* (9), 2209-2215.
155. Wang, X. J.; Zhu, X. P.; Lan, L. M.; Zuo, H. B., Removal of chromium from laboratory wastewater using preparation-adsorption technology with a Mg/Al/Cr layered compound. *RSC Adv.* **2016,** *6* (88), 85595-85602.
156. Boddu, V. M.; Abburi, K.; Talbott, J. L.; Smith, E. D., Removal of hexavalent chromium from wastewater using a new composite chitosan biosorbent. *Environ. Sci. Technol.* **2003,** *37* (19), 4449-4456.
157. Zhu, L.; Liu, Y.; Chen, J., Synthesis of N-methylimidazolium functionalized strongly basic anion exchange resins for adsorption of Cr(VI). *Ind. Eng. Chem. Res.* **2009,** *48* (7), 3261-3267.
158. Srivastava, H. C. P.; Mathur, R. P.; Mehrotra, I., Removal of chromium from industrial effluents by adsorption on sawdust. **1986,** *7* (1), 55-63.
159. Sharma, D. C.; Forster, C. F., Removal of hexavalent chromium using sphagnum moss peat. *Water Res.* **1993,** *27* (7), 1201-1208.
160. Perezcandela, M.; Martinmartinez, J. M.; Torregrosamacia, R., Chromium(VI) removal with activated carbons. *Water Res.* **1995,** *29* (9), 2174-2180.
161. Aboutorabi, L.; Morsali, A.; Tahmasebi, E.; Buyukgungor, O., Metal-organic framework based on isonicotinate N-oxide for fast and highly efficient aqueous phase Cr(VI) adsorption. *Inorg. Chem.* **2016,** *55* (11), 5507-5513.
162. Zhitova, E. S.; Yakovenchuk, V. N.; Krivovichev, S. V.; Zolotarev, A. A.; Pakhomovsky, Y. A.; Ivanyuk, G. Y., Crystal chemistry of natural layered double hydroxides. 3. The crystal structure of Mg,Al-disordered quintinite-2H. *Mineral. Mag.* **2010,** *74* (5), 841-848.
163. Somosi, Z.; Murath, S.; Nagy, P.; Sebok, D.; Szilagyi, I.; Douglas, G., Contaminant removal by efficient separation of in situ formed layered double hydroxide compounds from mine wastewaters. *Environ. Sci.-Wat. Res. Technol.* **2019,** *5* (12), 2251-2259.
164. Sandkuhler, P.; Sefcik, J.; Morbidelli, M., Kinetics of aggregation and gel formation in concentrated polystyrene colloids. *J. Phys. Chem. B* **2004,** *108* (52), 20105-20121.
165. Gisler, T.; Ball, R. C.; Weitz, D. A., Strain hardening of fractal colloidal gels. *Phys. Rev. Lett.* **1999,** *82*, 1064-1067.
166. Kobayashi, M.; Yuki, S.; Adachi, Y., Effect of anionic surfactants on the stability ratio and electrophoretic mobility of colloidal hematite particles. *Colloid Surf. A* **2016,** *510*, 190-197.

9. Summary

Layered double hydroxides are lamellar anionic clays. The layers are generally composed of divalent and trivalent cations leading to a net positive charge, which is compensated by interlayer anions. The interlayer space raises the opportunity to apply these compounds in various processes as drug carrier, anion exchanger, catalyst support, etc. However, the outer surface of the material can be utilized as adsorption site as well. Throughout the study, LDH colloids were synthetized with various compositions and sizes. In general, colloid systems play an important role in various fields including industrial processes like manufacturing of cosmetics or water treatment and pharmaceutical applications. Using LDH colloids can be advantageous due to their ease to synthetize, low cost and biocompatibility.

In the first part of the dissertation Mg_2Al-LDH nanoparticles were prepared and dispersed into aqueous solutions. The LDH particles were characterized with XRD and IR spectroscopy. The colloidal stability of the system was extensively investigated as it is a crucial point in the majority of the applications. For instance, unstable dispersions are unfavourable due to particle aggregation and loss of active sites. The colloidal stability of the prepared LDH particles was very limited, i.e., the particles aggregated already at small concentration of electrolytes. The goal was to increase the colloidal stability of the LDH. This was achieved with the adsorption of charged macromolecules (polyelectrolytes), which strongly adsorbed on the oppositely charged surfaces leading to a variation in the surfaces charge of the particles. This is important since according to the DLVO theory aggregation of colloidal particles is influenced by electrostatic forces, which can be tuned with the charge of the particles.

The first layer applied was PSS, a negatively charged polyelectrolyte, which adsorbed strongly on the oppositely charged LDH particles. The aggregation properties were followed with a time-resolved DLS method. The colloid dispersions were stable at low PSS doses, while increasing the dose, charge neutralization occurred at the IEP, where the dispersion was unstable. Further increase in the polyelectrolyte dose led to charge reversal and subsequent surface saturation at the onset of the ASP. Further added polyelectrolytes remained dissolved in the bulk phase. At the onset of ASP, the particles possessed highly negative charge and the dispersions were fairly stable and thus, this was the chosen loading of PSS for further studies. A second layer was also built-up on the LDH-PSS using PDADMAC, a positively charged polyelectrolyte. The same phenomena took place as in the case of PSS including charge neutralization at the IEP and

subsequent charge reversal at higher doses. Moreover, at the onset of the ASP, a stable LDH-PSS-PDADMAC hybrid was obtained, which showed atypical behaviour in salt-induced aggregation measurements. While in general at high salt concentrations dispersions become unstable, the bilayer hybrid kept some of its stability, which is rather unusual and not predicted by the DLVO theory. Most likely steric stabilization effects are responsible for this unexpected behaviour meaning that adsorbed polyelectrolyte chains overlap and extra (non-DLVO) stabilizing forces evolve.

On the basis of the above bilayer material, a nanocomposite was developed by adsorbing metal complexes ($[Cu(Bpy)_2]$ and $[Fe(Cit)_2]$) on the LDH-polyelectrolyte surfaces. The final COMP hybrid was built-up with the sequential adsorption method. The first layer was exactly the same PSS as mentioned above. The following adsorbed layer was $[Cu(Bpy)_2]$, a complex possessing overall positive charge. The $[Cu(Bpy)_2]$ had limited solubility and thus, the dose required for charge reversal could not be reached. The final dose in COMP was chosen as the composite still possessed negative overall charge and was considerably stable. On the negatively charged LDH-PSS-$Cu(Bpy)_2$ particles, PDADMAC was adsorbed. The process was similar as the one above, however, shifts in electrophoretic mobility and stability ratio values were observed proving the successful immobilization of the metal complex in the previous step. The final layer was $[Fe(Cit)_2]$ a negatively charged metal complex, which was immobilized on the LDH-PSS-$Cu(Bpy)_2$-PDADMAC composite. The adsorption of $[Fe(Cit)_2]$ induced charge reversal and surface saturation occurred at appropriate doses. The chosen loading dose of $[Fe(Cit)_2]$ in COMP was the same as for the other metal complex. Resistance against salt-induced aggregation was assessed. The composite had overall high negative charge and possessed higher colloidal stability than the bare LDH particle indicated by the higher CCC value. The structure of COMP was characterized with SEM and EPR. The EPR measurements provided valuable information on the structure of the metal complexes in solution and on the surface. The results shed light on that a mixed ligand system formed, in which copper(II) was coordinated with both bipyridine nitrogen and citrate oxygen.

The above metal complexes were immobilized with the purpose to mimic antioxidant enzyme's function. To test the enzymatic/antioxidant activity of the composite, different assays were carried out. In SOD assays, the activity of COMP was found to be similar to the one of the native enzymes, once the efficiency was expressed in mass concentration. The composite was also

tested in other assays including the reduction of DPPH radical, CUPRAC and horseradish peroxidase assays. In DPPH probe, moderate activity was assessed and in the case of the latter two, no significant activities were measured. These results pointed out that the composite material is selective for dismutation of superoxide radical ions. Moreover, it possesses high colloidal stability making it a promising candidate in industrial application, in which electrolytes are present.

In the next part of the dissertation, the effect of SDS surfactant on the charge and aggregation of LDH particles was studied to optimize preparation conditions for mesoporous adsorbent materials. SDS is widely used in such preparation processes, however, no systematic studies were carried out to investigate the relation between the adsorption features and colloidal stability of the dispersions. The charge reversal with increased SDS dose occurred above the IEP. By optimizing the SDS concentration, the experimental procedure was tuned that stable colloids were obtained for the further steps, in which calcination and rehydration processes were involved. Characterization of all materials were carried out with various methods. The XRD results showed that with increasing SDS dose intercalation occurs. However, after the calcination-rehydration process, the LDH structure was regained and no sign of SDS was present. Similar findings were obtained in case of IR spectroscopy. After the SDS treatment, characteristic IR peaks of SDS could be observed, while after the calcination-rehydration process, these peaks disappeared proving the final materials were free of SDS template. Transmission electron microscopy images of the final materials were recorded and it could be clearly observed that with increasing SDS dose, holes appeared on the surface leading to formation of the porous structure. This was confirmed by BET measurements, which determined the porosity of the materials. Both the specific surface area and the porosity increased with increasing the SDS dose. The materials were hierarchically mesoporous and a clear connection was discovered between the colloidal stability of the precursor SDS-LDH hybrids and the features of the final material.

The adsorption capacity of the most advantageous LDH structure was tested for two anions, namely, dichromate and nitrate. The adsorption of the anions was followed by UV-Vis spectroscopy. The sorption capacity of nitrate was quantified with the Langmuir isotherm and the measured data were the highest among the single-phase LDH materials reported in the literature. The sorption capacity of dichromate was also calculated from the Langmuir model, which was also the highest among single-phase LDH materials making it a value adsorbent to be used in industrial and environmental processes. The porous LDH was regenerated five times with no significant loss

in the activity. Summarily, a template and organic material free highly porous LDH-based adsorbent was developed with great sorption properties.

Finally, potential environmental application of LDH colloids was explored. LDH and LDH-like materials were synthesised both in *ex* and *in situ* systems. Overall, 4 samples, 2 *ex situ* and 2 *in situ*, were prepared. The *in situ* LDHs were formed in acidic mine wastewater with the addition of base allowing the LDH formation with the ions in the wastewater. The goal of the study was to characterize the LDH samples and, since they showed high colloidal stability and no sign of sedimentation, to destabilize their colloids. The samples were characterized with various techniques. XRD results gave us information about the structure of the materials. One of the *ex situ* sample was pure brucite (sample 1) and the other was an LDH-like material called quintinite (sample 4). The *in situ* prepared samples were LDH (sample 2) and LDH-brucite mixture (sample 3). On the IR spectra, peaks typical for LDH-type materials appeared in all samples, however, in the case of *in situ* prepared samples a peak appeared as a sign of sulfate content. This was in good agreement with the SEM-EDX results, which proved the sulfur content in the *in situ* prepared samples and that the *in situ* formation removed some of the sulfur content of the wastewater.

Adsorbing contaminants is just one part of wastewater treatment, on the other hand, removal of the solid content is equally important. The formed LDHs could not be removed from the wastewater due to their high colloidal stability. At first, PSS, dextran-sulfate and phosphate anions were adsorbed on the slightly positive LDH particles to reach the IEP, where particle aggregation and subsequent sedimentation were expected on the basis of previous results obtained with LDH dispersions. Surprisingly, no sedimentation occurred. It was realized that the reason behind the high stability is not due to electrostatic stabilizing forces, but rather due to the formation of interlinked aggregates, i.e., a stable colloidal network. It was observed that this system can be destabilized with dilution. In case of sample 1, 2 and 3, the dilution factors were optimized to quickly sediment the solid material from the samples. The required time for complete sedimentation was determined. In case of sample 4, no sedimentation occurred. These results can be useful in the application of LDH colloids in water remediation processes.

10. Tartalmi összefoglaló

A réteges kettős hidroxidok (LDH) anionos agyagásványok réteges szerkezettel. A rétegeket általánosan két- és háromszorosan töltött kationok alkotják, melynek következtében a lamellák pozitív töltéssel rendelkeznek, melyet a rétegközi anionok egyenlítenek ki. A rétegközi tér lehetőséget ad, hogy az anyagot gyógyszerhatóanyag hordozóként, anioncserélőként és még számos egyéb módon hasznosítsuk, azonban az anyag felülete is hasznosítható, mint adszorpciós hely. Az LDH-k változatos szerkezettel és méretben állíthatók elő. A jelen tanulmányban az LDH kolloidokat vizsgáltuk. A kolloid rendszerek számos ipar területen fontos szerepet játszanak, mint például a kozmetikai vagy textilipar, szennyvízkezelés, illetve gyógyszeripari folyamatok. Az LDH kolloidok alkalmazása előnyös, egyszerű és alacsony költségű előállításuk, illetve biokompatibilitásuk miatt.

A disszertáció első részében Mg_2Al-LDH nanorészecskék lettek előállítva és diszpergálva vizes kolloid rendszerré. Az LDH részecskék szerkezeti jellemzése porröntgen diffraktometriával (XRD) és infravörös spektroszkópiával (IR) zajlott. Vizsgáltuk a kolloid stabilitását a rendszernek, minthogy ezen tulajdonság lényeges a kolloid rendszerek alkalmazása szempontjából. Az ipari alkalmazások során a nem stabilis diszperziókban ugyanis aggregáció lép fel, mely következtében az aktív felület lecsökken, mely hátrányos az alkalmazásban. Az LDH részecskék kolloid stabilitása alacsony, emiatt a kolloid stabilitás növelése volt a cél, hogy későbbi kísérletekben ideális kiindulási anyag legyen. A kolloid stabilitás növelését polielektrolitokkal értük el, ezen töltéssel rendelkező makromolekulák erősen adszorbeálódnak az ellentétes töltésű felülethez és módosítják a töltését. Ez lényeges, minthogy a DLVO elmélet alapján a kolloid részecskék aggregációja a van der Waals erők és elektrosztatikus erők következménye, melyekből az utóbbi befolyásolható a részecskék töltésén keresztül.

Az első polielektrolit, melyet adszorbeáltunk az LDH részecskék felületén a polisztirol-szulfonát (PSS) volt, mely negatív töltéssel rendelkezik. Az aggregációs tulajdonságokat és a felületi töltést fényszórás technikákkal mértük meg. A kolloid diszperzió stabilis volt alacsony PSS koncentrációnál, a koncentrációt növelve a felületi töltés pozitívből negatívra váltott az izoelektromos ponton keresztül (IEP), amely pont közelében a diszperzió instabilis. A polelektrolit koncentráció tovább növelve elérhetjük az adszorpciós maximumot (ASP), ahol már nem tud több polielektrolit a felületre adszorbeálódni. PSS adszorpciója esetén elérve az ASP-t, a felület nagy negatív töltéssel rendelkezett és nagy stabilitással. Erre adszorbeáltuk a következő réteget, ami

pozitív töltésű polielektrolit poli(dimetil-diallil-ammónium-klorid) (PDADMAC) volt. A PSS esetéhez hasonlóan, az adszorpció a töltés áttöltődését okozta, magas PDADMAC koncentrációnál egy stabilis LDH-PSS-PDADMAC hibrid jött létre. Ez a hibrid atipikus viselkedést mutatott a sófüggő aggregációs mérések során. Magas sókoncentráció mellett a rendszer instabilissá válik, ám a hibrid ezen körülmények között is megőrizte stabilitásának egy részét. Ennek az lehet az oka, hogy a polielektrolitok oldalláncai egymással átfednek, ezáltal sztérikus stabilizációt okoznak.

Ezen eredmények alapján egy kompozit (COMP) lett kifejlesztve fémkomplexek ([$Cu(Bpy)_2$] és [$Fe(Cit)_2$]) immobilizálásával az LDH-polielektrolit felületekre. Az első réteg továbbra is PSS volt, melyet [$Cu(Bpy)_2$] követett, mely komplex pozitív töltésűnek tekinthető az alkalmazott kísérleti körülmények között. A [$Cu(Bpy)_2$] oldhatósága limitált, így az áttöltési tartományt nem tudtuk elérni, ezért alacsonyabb adszorpciós koncentrációt választottunk, melyen a kompozit még negatív töltésű és megőrzi stabilitását. A negatív töltésű LDH-PSS-$Cu(Bpy)_2$ részecskékre PDADMAC-ot adszorbeáltunk. Hasonló folyamat volt megfigyelhető, mint mikor közvetlenül a PSS rétegre adszorbeáltuk, ám eltolódás történt mind az elektroforetikus mobilitás, mind a stabilitási arányokban, mely alapján arra lehet következtetni, hogy a fémkomplex adszorpciója sikeres volt az előző lépésben. A megváltozott tulajdonságok miatt alacsonyabb PDADMAC koncentráció is elegendő volt az ASP eléréséhez, mint a az LDH-PSS-PDADMAC hibrid esetében. Az utolsó adszorbeált réteg a [$Fe(Cit)_2$], egy negatívan töltött fémkomplex volt. A fémkomplex adszorpciója követte polielektrolitoknál tapasztalt trendeket. Az ASP meghatározása után kiválasztottuk a végső COMP anyagban alkalmazott koncentrációt. A sófüggő aggregációval szembeni kolloid stabilitást meghatároztuk a COMP (LDH-PSS-$Cu(Bpy)_2$-PDADMAC-$Fe(Cit)_2$) esetében. A végső kompozit negatív töltéssel rendelkezett és kolloid stabilitása magasabb volt, mint az eredeti LDH részecskéknek. A szerkezetét pásztázó elektron mikroszkópiával (SEM) és elektron paramágneses rezonancia spektroszkópiával (EPR) vizsgáltuk. Az EPR mérések az immobilizált fémkomplexek szerkezetéről adott információt, ez alapján a réz(II) vegyes komplexet képez a bipiridinnel és a citráttal.

A fémkomplexeket azzal a céllal immobilizáltuk, hogy a fémcentrum az irodalom alapján képes lehet enzim utánzó tulajdonságra. Az enzematikus/antioxidáns hatás mérésére különböző teszteket végeztünk el UV-Vis spektroszkópia segítségével. Az oxigén szabadgyökök problémát jelentenek mind egészségünkben, ha szintjük túl magas, illetve az iparban is alacsonyabb minőségű termékekhez vezetve. A kompozit esetében mért szuperoxid gyök dizmutáló aktivitás hasonló volt

a természetes SOD enziméhez. A kompozitot egyéb antioxidáns/enzimatikus tesztekben is vizsgáltuk, ám ezekben nem mutatott jelentős aktivitást, így kijelenthető, hogy a kompozitunk specifikus a szuperoxid gyökök bontására. Összességében az előállított anyag tulajdonságai alapján ígéretes, alapjául szolgálhat ipari alkalmazásra felhasználható antioxidáns kompozitoknak.

Az nátrium-dodecil-szulfonát (SDS) hatását vizsgáltuk LDH részecskék kolloid tulajdonságaira a disszertáció további részében. Az SDS-t elterjedten használják az LDH-kkal kapcsolatos kutatásokban, azonban átfogó tanulmány még nem készült az SDS adszorpciójának az LDH részecskék töltésére és kolloid stabilitására gyakorolt hatását illetően. Az SDS koncentrációjának növekedésével áttöltődés valósult meg az IEP-n keresztül. A mérések alapján három különböző SDS koncentráció lett kiválasztva, mellyel kezeltük az LDH-t a szintézis során, a legalacsonyabb az IEP körüli értéknek felelt meg, egy a kritikus koagulációs koncentrációnál, míg a legnagyobb koncentrációnál, 30 mM-nál a részecskék nagy negatív töltéssel rendelkeztek és rendkívül stabilisak voltak. Ezeken az SDS koncentrációkon kevertettük, majd kiégettük és rehidratáltuk az LDH-kat a termékekhez jutva. Ezen anyagokat szerkezet vizsgáló módszereknek vetettük alá. Az XRD mérések alapján az SDS dózis növekedésével interkaláció lép fel, azonban a kiégetés után az eredeti LDH szerkezet visszaáll, nincs nyoma a tenzidnek. Ezt a tapasztalatot alátámasztották az IR mérések is, mely során a felületaktív anyaggal való kezelés után megjelentek a karakterisztikus csúcsok a spektrumokon, ám a kiégetés-rehidratálás után ezek eltűntek, ez alapján az anyag SDS mentes. Transzmissziós elektron mikroszkópiával is vizsgálva voltak az anyagok, ez alapján az SDS koncentráció növekedésének következtében a végső anyag felületén egyre nagyobb mennyiségben lyukak jelentek meg, az anyag porózusabb lett. Ezt alátámasztották a BET mérések, melyekkel meghatároztuk a porozitást. Mind a fajlagos felület, mind a porozitás megnőtt a kezelés során alkalmazott SDS koncentrációval. Az anyagok hierarchikus pórusszerkezetű, mezopórusosak voltak. Egyértelmű összefüggés felfedezhető az SDS-LDH prekurzor kolloid stabilitása és a végső porozitás között.

Minthogy a 30 mM SDS-sel kezelt LDH fajlagos felülete az irodalomban található egyéb LDH-k között is számottevő, további kísérleteket végeztünk, hogy vizsgáljuk, mint lehetséges adszorbenst. Ennek során két anion adszorpcióját vizsgáltuk UV-Vis spektroszkópiával, melyek a dikromát és a nitrát voltak. A szorpciós kapacitást az adatokra illesztett Langmuir függvényből számoltuk, mely mindkét esetben az irodalomban fellelhető legmagasabb adat az egyfázisos LDH-kra tudomásunk szerint. Az LDH-t öt cikluson keresztül használtuk és regeneráltuk, mely során

csak minimális aktivitás vesztést mutatott. Összességében létrehoztunk egy szerves anyag és templát mentes nagy fajlagos felületű anion adszorbenst.

A disszertáció utolsó részében az LDH kolloidok környezeti alkalmazását vizsgáltam. LDH és LDH-szerű anyagok lettek előállítva. Összesen 4 minta, 2 *ex situ* és 2 *in situ* módon. Az *in situ* készült LDH-k egy savas bányavízmintában készültek, mely során lúgot adtunk hozzá és a szennyvíz iontartalmával alkotott LDH-t. A mintákat a boddingtoni aranybányában, Ausztráliában készítették. A kutatás célja az volt, hogy az LDH mintákat szerkezetileg vizsgáljuk, illetve minthogy magas kolloid stabilitást mutattak és emiatt nem ülepedtek, az ülepedés elősegítése volt, mely előnyös a későbbi szennyvízkezelési folyamatok szempontjából. A minták XRD-vel való vizsgálata során az *ex situ* minták esetén az egyik tiszta brucit fázis volt (sample 1), míg a másik egy LDH-szerű ásvány quintinite (sample 4). Az *in situ* minták esetén az egyik tiszta hidrotalcit volt (sample 2), míg a másik hidrotalcit és brucit keveréke (sample 3). Az IR spektrumokon az LDH-kra jellemző csúcsok megjelentek, ám az *in situ* minták esetén megjelent a szulfátra jellemző csúcs is. Ezt alátámasztották a SEM-EDX mérések, melyek kimutatták a kén tartalmat, ezzel bizonyítva, hogy az *in situ* képződő minták megkötik a szulfátot, mely pozitív tulajdonság a vízkezelés szempontjából.

A szennyezők megkötése LDH-ként azonban csak egy része a kezelésnek, ha nem távolítjuk el azt a rendszerünkből, a szennyezők továbbra is a vízben maradnak. A létrejött LDH-kat azonban nem lehetett a szennyvízből eltávolítani, minthogy kolloid stabilitásuk túl nagy volt és így nem ülepedtek ki. PSS, dextrán-szulfát és foszfát anionok lettek adszorbeáltatva a kis pozitív töltéssel rendelkező LDH részecskékre, hogy az IEP-t beállítsuk, ahol a DLVO elmélet szerint a rendszer instabilis, aggregálódik és a részecskék ki tudnak ülepedni. Azonban ez nem történt meg az IEP-nek megfelelő koncentrációknál, ami arra engedett következtetni, hogy a stabilitásnak nem elektrosztatikus okai vannak. Magas részecske koncentrációjú kolloid rendszereknél egy hálózat alakulhat ki az aggregátumokból, mely rendkívül stabilis gél-szerű struktúrához vezet. Megfigyeltük, hogy ez a hálózat hígítással megtörhető. Az 1,2,3-as minta esetén meghatároztuk az optimális víz mennyiségét, amely szükséges a hígításhoz és kiülepedéshez. Az ülepedéshez szükséges időt meghatároztuk. A 4-es minta esetén nem történt kiülepedés. Ezen eredmények hasznosak lehetnek az LDH kolloidok szennyvízkezelésben való alkalmazása szempontjából.